Aus dem Max-Planck-Institut für Kolloid- und
Grenzflächenforschung

Superpara- and paramagnetic polymer colloids by miniemulsion processes

Dissertation
zur Erlangung des akademischen Grades
„doctor rerum naturalium“
(Dr. rer. nat.)
in der Wissenschaftdisziplin Physikalische Chemie

eingereicht an der
Mathemathisch-Naturwissenschaftlichen Fakultät
der Universität Potsdam

von
Liliana Patricia Ramírez Ríos

Potsdam, Februar 2004

„Jedenfalls liebt der Magnetstein das Eisen.

Wenn er es nur sieht und berührt, zieht er es zu sich, als wenn er in sich Liebesfeuer hätte“

Achileus Tatios aus Alexandrien (zit. nach A. Kross, *Geschichte des Magnetismus*, 1994)[1]

To Gunnar Jochen Weimann

TABLE OF CONTENTS

LIST OF FIGURES

LIST OF TABLES

ABBREVIATIONS AND SYMBOLS

SDS	Sodium Dodecyl Sulfate
PEO-PMAA	Poly(ethylene oxide)-*b*-poly(methacrylic acid)
HEMA	2-hydroxyethylmethacrylate
MAA	Methacrylic acid
DTPA	Diethylenetriamine penta-acetic acid
Gd-DTPA	Gadolinium-(diethylenetriamine penta-acetic acid)
Gd-DOTA	Gadolinium-(1,4,7,10-tetraazacyclododecan N, N', N", N'"-tetraacetic acid)
PEO-PMAA	Poly(ethylene oxide)-*b*-poly(methacrylic acid)
KPS	Potassium peroxodisulfate
tmhd	2,2,6,6, tetramethyl-3,5-heptandionate
DTA	Differential thermal analysis
TGA	Thermogravimetric analysis
DSC	Differential scanning calorimetry
TEM	Transmission electron microscopy
WAXS	Wide angle X-ray
SAXS	Small angle X-ray
FTIR	Fourier transform infrared spectroscopy
IPC	Iron pentacarbonyl
BA	Butyl acrylate
PBA	Poly(butyl acrylate)
AA	Acryl acid
LMA	Lauryl methacrylate
ΔG	Free Gibbs energy difference

γ	Surface/interfacial tension
ΔA	Newly formed interface
i	Current
r_{loop}	Loop radius
M	Magnetization
v	Volume of the material
μ	Magnetic dipole moment
μ_{total}	Net magnetic dipole moment
B	Magnetic induction
C_m	Magnetization constant
B_{ext}	Strength of the external magnetic field
μ_0	Permeability of the free space, $4\pi\ 10^{-7}\ T{\cdot}m{\cdot}A^{-1}$
H	Magnetic field strength
χ	Mass magnetic susceptibility of the material
M_s	Saturation magnetization
M_r	Remanence
H_{ci}	Intrinsic coercivity
T	Temperature (K)
d_{mp}	Diameter of the magnetic particle
d_s	A critical diameter below which the particles become *single domains*
d_p	A diameter below which the particles are *superparamagnetic*
m_s	Saturation magnetization of the bulk material per volume
V	Volume of a spherical particle
k	Boltzmann constant

$\chi_{H\to 0}$	Initial mass magnetic susceptibility in emu·Oe^{-1}
$\sigma_{H\to\infty}$	Specific saturation magnetization (σ, values extrapolated to $H\to\infty$) in emu·g^{-1} latex
T_1	Spin-lattice relaxation time or longitudinal relaxation time
γ	Proton gyromagnetic ratio
S	Electron spin quantum number
g	Electronic g factor
β	Bohr magneton
ω_I	Larmor frequencies for nuclear
ω_S	Larmor frequencies for electron spins
r_{in}	Ion-nucleus distance
$A/\hbar$	Electron-nuclear hyperfine coupling constant
τ_c	Correlation times for dipolar
τ_e	Correlation times for scalar interactions
$[M]$	Concentration of the paramagnetic species
R_1	Relaxivity in M^{-1}·s^{-1} or mM^{-1}·s^{-1}
P_M	Mole fraction of metal ion
q_w	Number of water molecules bound per metal ion
T_{1M}	Relaxation time of the bound water protons
τ_M	Residence lifetime of the bound water
C	Numerical constant
N_S	Number of metal ions per cubic centimeter
d_a	Distance of closest approach of the solvent molecule to the metal complex
$\hbar$	Dirac constant

τ_D	Relative translational diffusion
D_I	Diffusional coefficients of water
D_S	Diffusional coefficients of the metal complex
ρ	Resolution for TEM
λ	Wavelength
α	Angle of the incoming beam in TEM
h	Planck constant
m_e	Mass of an electron
v_e	Electron velocity
d	Separation between the planes for X-ray diffraction
θ	Angle of incidence
n	Order of the reflection (n= 1, 2,…) for X-ray diffraction
	Turns of the coil for magnetometry
I	Scattering intensity
S	Inverse of the separation between the planes for X-ray diffraction ($S = d^{-1}$)
$I_{t'}$	Number of photons arriving at the detector at the time interval t'
t	Delay time for X-ray diffraction
Γ	Cumulant
D	Diffusion coefficient
q	Norm of the scattering vector
n_0	Refraction index for a pure solvent
b	An instrumental constant
η	Viscosity of the solvent
D_z	z-average diffusion coefficient

m_i	Total mass of the of the *i* particles
M_i	Molecular weight of the *i* particles
G	Centrifugal force
F_b	Buoyant force
F_f	Frictional force
ω	Angular velocity, rad·s^{-1}
r	Centrifugal radius, cm
m_p	Mass of the particle
$\bar{v}$	Partial specific volume of the particle
ρ_s	Density of solvent
N_A	Avogadro's number
f	Frictional coefficient of a single particle
a	Radius of the spherical particles
$\frac{dr}{dt}$	Velocity of the particles
r_Θ	Radial coordinate of the isopycnic point of the zone which corresponds to the maximal concentration (c_r, Θ) of the particles
c_r	Concentration at radius *r*
R	Gas constant
Emf	Electro-motive force
n_c	Turn in a coil
ϕ	Magnetic flux through the loop

1 Introduction

Magnetisches Pulver hat die Fähigkeit,

„dicken Schleim abzuführen, wenn es mit Honig gemischt verabreicht wird".

Psellus von Anazerba (zit. nach A. Kross, *Geschichte des Magnetismus*, 1994)[1]

Magnetism has always been conceived as something mysterious and mystic. During the process of understanding of this phenomenon an extensive range of medical and technical applications have emerged. Until today, magnetism continues to be in the focus of research predominantly as regards finding new and powerful applications.

Magnetite is the oldest and most common iron oxide compound in the earth. Its natural form was called lodestone by the ancients. Natural research has revealed that a large number of species, from bacteria to humans, can produce magnetite. In the case of *magnetotactic bacteria*,[2] the magnetite allows the bacteria to find their way downwards into areas of poor oxygen conditions –their habitat medium- by the orientation they gain from the magnetic field of the earth. Magnetite has also been found in animals that navigate by compass direction, such as bees,[3] birds,[4] and fishes.[5] A very controversial paper was published by Kirschvink[6] demonstrating the existence of magnetite crystals in the human brain. This raises the question as to the usefulness of magnetite even in the human body. Research has not yet found an answer to this question, but what this finding clearly demonstrates is that magnetism is an essential phenomenon of the life that surrounds us and that, at present, the range of its potential applications is only becoming apparent from a distance.

On the other hand, there is no doubt that *nanotechnology* has gained great relevance in the last two decades due to the great variety of real and feasible applications in *multidisciplinary* fields such as chemistry, physics, medicine, engineering, biology, pharmacy, among others.

Nanotechnology is making great steps forward in the improvement of existing materials and the creation of innovative materials in the colloidal range based on both inorganic and polymeric materials as well as nanocomposites consisting of a mixture of both of them.

According to the IUPAC,[7] the term *colloid* refers to a state of subdivision, implying that the molecules or polymolecular particles dispersed in a medium have at least in one direction a dimension roughly between 1 nm and 1 μm. In nature and daily life, it exists a great variety of colloidal systems, such as fog, mist, smoke, aerosols, milk, mayonnaise, creams, soaps, blood, bones, etc., to enumerate just some typical examples. Colloids can be produced by different techniques. One of the best positioned techniques is the miniemulsion process. Miniemulsions are described as stable emulsions of oil or water droplets having a size between 50-500 nm prepared by shearing a system containing oil, water, a surfactant, and a highly water insoluble compound, the so-called hydrophobe which suppresses Ostwald ripening of the droplets.[8, 9] The fusion/fission process and the low amount of surfactant used during the miniemulsion process turn the miniemulsion into a very suitable technique for the encapsulation process and the generation of novel colloids having amazing properties.

Combining the magnetic properties of a given material with the tremendous advantages of colloids can exponentially increase the advantages of both systems. This thesis deals with the field of *magnetic nanotechnology*, thus it is that, the design and characterization of new magnetic colloids with fascinating properties compared with the bulk materials is presented.

Ferrofluids are referred to either as water or organic stable dispersions of superparamagnetic nanoparticles which respond to the application of an external magnetic field but lose their magnetization in the absence of a magnetic field. This kind of magnetism is called superparamagnetism or paramagnetism depending on several parameters such as particle size, electronic configuration, chemical composition, among others. In section 4.1, a three-step synthesis for the fabrication of a novel *water-based ferrofluid* is presented. The encapsulation of high amounts of magnetite into polystyrene particles can efficiently be achieved by a new

process including two miniemulsion processes. The ferrofluids consist of novel magnetite polystyrene nanoparticles dispersed in water which are obtained by three-step process including coprecipitation of magnetite, its hydrophobization and further surfactant coating to enable the redispersion in water and the posterior encapsulation into polystyrene by miniemulsion polymerization.

The formulation and application of polymer particles and hybrid particles composed of polymeric and magnetic material is of high interest for biomedical applications. Ferrofluids can for instance be used in medicine for cancer therapy and magnetic resonance imaging.[10, 11] For such applications, it is necessary that the materials or especially the surface of the particles are biocompatible, non-toxic and sometimes also biodegradable. It is a desire to take advantage of a potential thermodynamic control for the design of nanoparticles, and the concept of "nanoreactors"[12] where the essential ingredients for the formation of the nanoparticles are already in the beginning. It is the topic of this section to describe a recent development where the availability of high shear devices such as ultrasound decrease the droplet or nanoreactor diameter down to 30-100 nm and allows to formulate magnetite hybrid particles for biomedical applications. Superparamagnetic or paramagnetic colloids containing iron or gadolinium are also being used as magnetic resonance imaging contrast agent, for example as a important tool in the diagnostic of cancer, since they enhance the relaxation of the water of the neighbouring zones. New *nanostructured composites* by the thermal decomposition of iron pentacarbonyl in the monomer phase and thereafter the formation of paramagnetic nanocomposites by miniemulsion polymerization is discussed in section 4.2. In order to obtain the confined paramagnetic nanocomposites a two-step process was used. In the first step, the thermal decomposition of the iron pentacarbonyl was obtained in the monomer phase using oleic acid as stabilizer. In the second step this iron containing monomer dispersion was used for making a miniemulsion polymerization thereof.

The addition of lanthanide complexes to ester-containing monomers such as butyl acrylate and subsequent polymerization leading to the spontaneous formation of highly organized *layered nanocomposites*, is presented in section 4.3. By an one-step miniemulsion process, the formation of lamellar structure within the polymer nanoparticles is developed. The magnetization and the NMR relaxation measurements have shown these new layered nanocomposites to be very apt for application as contrast agent in magnetic resonance imaging.

2 Theoretical Section

2.1 Miniemulsions and miniemulsion polymerization

Emulsions are metastable heterogeneous system of two immiscible liquids, in which small droplets of one fluid (disperse phase) are dispersed in the other fluid (continuous phase) by means of shaking, mechanical agitation or ultrasound. Depending on which compound is forming the continuous phase, the emulsions can be classified as *direct*, oil in water (O/W), and *inverse*, water in oil (W/O).

The emulsions are divided in macroemulsions, miniemulsions or microemulsions, depending on the droplet size and the stabilization mechanism. The droplet size goes usually from about 100 nm to several μm for macroemulsions, between 50 and 500 nm for miniemulsions and between 1 and 100 nm for microemulsions, approximately.

An emulsion tends to break over time because the system tries to be in the state of minimum energy, to go back to his original state, it means, lower surface and interface tension and larger volume. The principal, instabilization mechanisms are the coalescence and the Ostwald ripening. Coalescence is the process of aggregation of two droplets to form one larger droplet through collision, while Ostwald ripening is the process whereby large droplets grow at the expense of smaller ones due to the transport of dispersed phase molecules from the smaller to the larger droplets through the continuous phase.

The classification by size is more or less ambiguous and thus it is that they are also classified depending on the stability mechanisms, amount of surfactant, etc. The predominant difference between emulsions lies in their respective stability. Macroemulsions are kinetic stable, microemulsions are thermodynamic stable and miniemulsions are stable against molecular diffusion (Ostwald ripening) and against coalescence (for more details, see next section).

2.1.1 Miniemulsions

Miniemulsions[13] are emulsions wherein the droplets are stabilized against molecular diffusion degradation (Ostwald ripening, a unimolecular process or τ_1 mechanism) and against coalescence by collisions (a bimolecular process or τ_2 mechanism).

Stabilization against coalescence can be obtained in colloidal chemistry by means of the addition of suitable surfactants which can act as steric, electrostatic, or electrosteric stabilizer agents.

When an emulsion is prepared, a distribution of the droplet size is obtained. Even when the surfactant provides the droplets with sufficient colloidal stability, the outcome of this size distribution is determined by their droplet or Laplace pressures, which increase with decreasing droplet size, resulting in a net mass flux by diffusion between the droplets. If the droplets are not stabilized against diffusional degradation, small ones will disappear increasing the average droplet size (Ostwald ripening).[8]

The addition of a small amount of a third component that is almost completely insoluble in the continuous phase and is trapped within the droplets can stop the Ostwald ripening in the system. The pioneer in the concept that unstable droplets of aerosols or fog can be stabilized by the presence of a non-volatile third component was Köhler in 1922.[14] Higuschi and Misra [15] were the first to report the use of small amounts of a component insoluble in the disperse medium but distributed in the disperse in order to stop the Ostwald ripening.

This stabilization effect was described theoretically by Webster and Cates.[16] They considered an emulsion whose droplets contain a trapped species (insoluble in the continuous phase) and studied the emulsion's stability via the Lifshitz-Slyozov model[17] (based on Ostwald ripening). Webster and Cates extended the work of Kabalnov and coworkers[18] and derived general conditions regarding the mean initial droplet volume, which ensures stability in both size and composition of the initial droplets, even when arbitrary polydispersity is present. They

distinguished nucleated coarsening, which requires either fluctuations in the mean-field equations or a tail in the initial droplet size distribution, from spinodal coarsening in which a typical droplet is locally unstable. A weaker condition for stability, previously suggested by Kabalnov and coworkers, is sufficient only to prevent spinodal coarsening and is best viewed as a condition for meta-stability. The coarsening of unstable emulsions after long times is considered and shown to resemble that of ordinary emulsions with no trapped species, but with a reduced value of the initial volume fraction of the dispersed phase. The evolution of the emulsion is driven by the competition between the osmotic pressure of the trapped species and the Laplace pressure of the droplets.

The rate of Ostwald ripening depends on the droplet size, polydispersity and solubility of the dispersed phase in the continuous phase. This means that an already hydrophobic oil dispersed in small droplets of low polydispersity shows low diffusion. But by adding an "ultrahydrophobe", the stability can even be increased by additionally building up an osmotic pressure. It was used a small amount of perfluorodimorphinopropane to blood substitutes to hinder the molecular diffusion, and therefore increase the stability.[19, 20]

Davis and coworkers[21] investigated the effect of various added third components such as hexadecane and perfluorocarbon oil, in the stabilization against Ostwald ripening of hexane emulsions stabilized by sodium dodecyl sulfate. Small droplets have higher solubilities (or vapor pressures) than larger droplets or the bulk material and therefore smaller droplets tend to diffuse in the medium, from the small droplets to the large droplets in order to reach a state of equilibrium. Because of this mass transport, the difference of the solubility (vapor pressure) between the small and the large droplets will increase and Ostwald ripening will be enhanced. When small quantities of a third component, which has lower vapor pressure (solubility) than the disperse phase, are present in the disperse phase, the loss of the oil within the small droplet will cause an increment in the mole fraction of the third component in these small droplets and therefore the small droplets will have now a more reduced pressure vapor than the larger

droplets. It is by this means that the increase of the Laplace pressure (size difference) will be balanced by the decrease in the osmotic pressure (concentration difference). As a result, the mean droplet size of the emulsion will change slightly before stability of Ostwald ripening is reached. David and coworkers explained that with the addition of a small quantity of an insoluble oil to the disperse phase in an O/W emulsion, stabilized by sodium dodecyl sulfate, the Ostwald ripening is prevented.

The ripening inhibitors are called "ultrahydrophobe" or "hydrophobe" in O/W miniemulsions and "lipophobe" and in W/O miniemulsions.

2.1.1.1 Preparation and homogenization of miniemulsions

Homogenization of the emulsions to obtain miniemulsions can be achieved by different methods. In the first articles published, simple stirring was used. The use of an omnimixer and ultra-turrax was also described in early articles. However, the shear obtained by these techniques is not sufficient in order to obtain small and homogeneously distributed droplets.[22]

A much higher energy, with respect of the thermodynamic part ($\Delta G = \gamma \Delta A$ with ΔG - free Gibbs energy difference, γ - surface/interfacial tension and ΔA - the newly formed interface) is required, since the comminution of large droplets into smaller ones involves additional forces, so that the viscous resistance during agitation absorbs most of the energy.[23, 24] The excess energy is dissipated as heat. Nowadays, ultrasonication is used especially for the homogenzation of small quantities, whereas the microfluidizer or high pressure homogenizers are necessary for the emulsification of larger quantities.

Power ultrasound is one means among others for mechanically producing emulsions. Ultrasound emulsification was first reported in 1927.[25] There are several possible mechanisms of droplet formation and disruption under the influence of ultrasound. [26-28]

Acoustic cavitation in liquids is a phenomenon of the formation of cavities or gas/vapor bubbles cause by the rupture of the liquid by high intensity acoustic fields. The bubble collapse implies

drastic temperature and pressure conditions inside the bubbles. These "hot spots" have temperatures of about 5000 °K, and pressures of about 1000 atm and heating and cooling rates above 10^{10} $K \cdot s^{-1}$.[29] Parameters having a positive influence on cavitation in liquids, generally speaking, improve emulsification in terms of a smaller droplet size of the dispersed phase right after disruption. Imploding cavitation bubbles cause intensive shock waves in the surrounding liquid and the formation of liquid jets of high liquid velocity.[30] This may cause droplet disruption in the vicinity of the collapsing bubble. However, the exact process of droplet disruption due to ultrasound as a result of cavitation is not yet fully understood. At constant energy density during homogenization, droplet size decreases when adding stabilizers, whereas the viscosity of the oil in w/o emulsions has no effect.[31] In monomeric miniemulsions, the droplet size is in turn determined by monomer and water density, monomer solubility, level of surfactant, level of hydrophobe, and volume fraction of the phases. It is found for monomeric miniemulsions that the droplet size initially is a function of the amount of shear.[32] Monomer droplets also change quite rapidly in size during sonication in order to approach a pseudo-steady state. However, once this state is reached, the size of the monomer droplet no longer appears to be a function of the amount of shear, assuming a required minimum is used. In the beginning of homogenization, the polydispersity of the droplets is still quite high, but by constant fusion and fission processes, polydispersity decreases. The miniemulsion then reaches a steady state (see Fig. 2.1).[33]

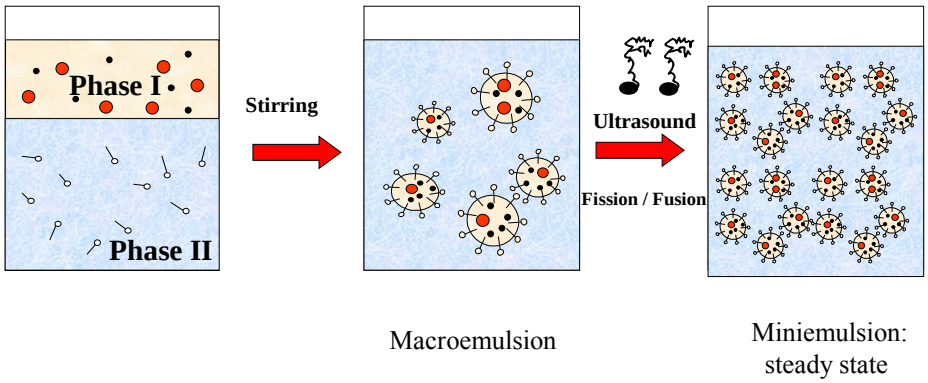

Fig. 2.1: Scheme of the miniemulsion process

With increasing time of ultrasonication the droplet size decreases and, therefore, the entire interface oil/water increases as well. The constant amount of surfactant now has to be distributed at a larger interface. Since there is always an equilibrium between the surfactant at the interfaces water/oil and water/air, the surface tension increases if the droplets are not fully covered by surfactant molecules. For miniemulsion polymerization, it was proved that the surface tension reaches a value close to 70 $mN \cdot m^{-1}$ indicating that the coverage of droplets is indeed very low. The value corresponds to a coverage of the droplets with surfactant molecules of 10 %. This value depends on the size of the droplets. The smaller the droplets are the higher the coverage is in order to obtain stable droplets, but in any case, full coverage is usually not obtained.[8]

The majority of the recipes described in the literature are based on the anionic sodium dodecyl sulfate (SDS) as a model system. The possibility of using cationic surfactants such as octadecyl pyridinium bromide for the preparation of miniemulsions was first exploited in 1976. However, the emulsions were prepared by stirring and the resulting emulsions showed broadly distributed droplet sizes.[34, 35] Recent work on steady-state miniemulsions showed that cationic and

nonionic surfactants form well-defined miniemulsions for further miniemulsion polymerization processes, resulting in narrow size distributed stable cationic and nonionic latex particles. Nonionic miniemulsions can be made by using 3-5 % of a poly(ethylene oxide) derivate as surfactant, resulting in larger, but also very well defined latexes.[36]

Lecithin can be used in an efficient way as biocompatible surfactant for the preparation of miniemulsions. Lecithin is usually used as synonym for phosphatidylcholine, which is the major component of a phosphatide fraction which is frequently isolated from either egg yolk, or soy beans. The structure of lecithin which is given in Fig. 2.2a is variable and dependent on fatty acid substitution. Compared with its synthetic alternatives, lecithin can be totally biodegraded and metabolized, since it is an integral part of biological membranes, making it virtually non-toxic, whereas other emulsifiers can only be excreted via the kidneys. The natural origin of lecithin produces, however, a rather complex composition, although in pharmacy in general well-defined singular excipients are favored. Lecithin is regarded as a well tolerated and non-toxic compound, making it suitable for long-term and large-dose infusion. As an emulsifier of intravenously administered fat emulsions, its composition and behavior determine the structure and stability of the emulsion in a decisive way. The salt of the cholic acid (3α,7α,12α trihydroxy-5β-cholan-24 acid) can also excellently be used for the formulation of miniemulsions. Cholic acid is composed of a steroid unit with a carboxylic acid group and three hydroxyl groups, which are all located at one side of the steroid nucleus (Fig. 2.2b). Cholic acid is one of the bile acids and its salt is found as natural constituent of the bile. The nucleus of the bile acids is closely related to cholesterol, from which they are formed in the liver, and this conversion depends on their relative concentrations. Due to their amphiphilic character, bile salts affect the absorption of fats, fat-soluble vitamins, and various ions. Tween 80 (polyethoxysorbitan monooleate) is a non-ionic surfactant comprised of a sorbitan ring and about 20 ethylene oxide units (Fig. 2.2c). The surfactant can be excellently used for the

formulation of miniemulsions. The surfactant is known as a non-toxic surfactant with excellent physiological properties and is widely used in biochemical applications including emulsifying and dispersing substances for pharmaceutics, cosmetics and food products.[37, 38]

a) b)

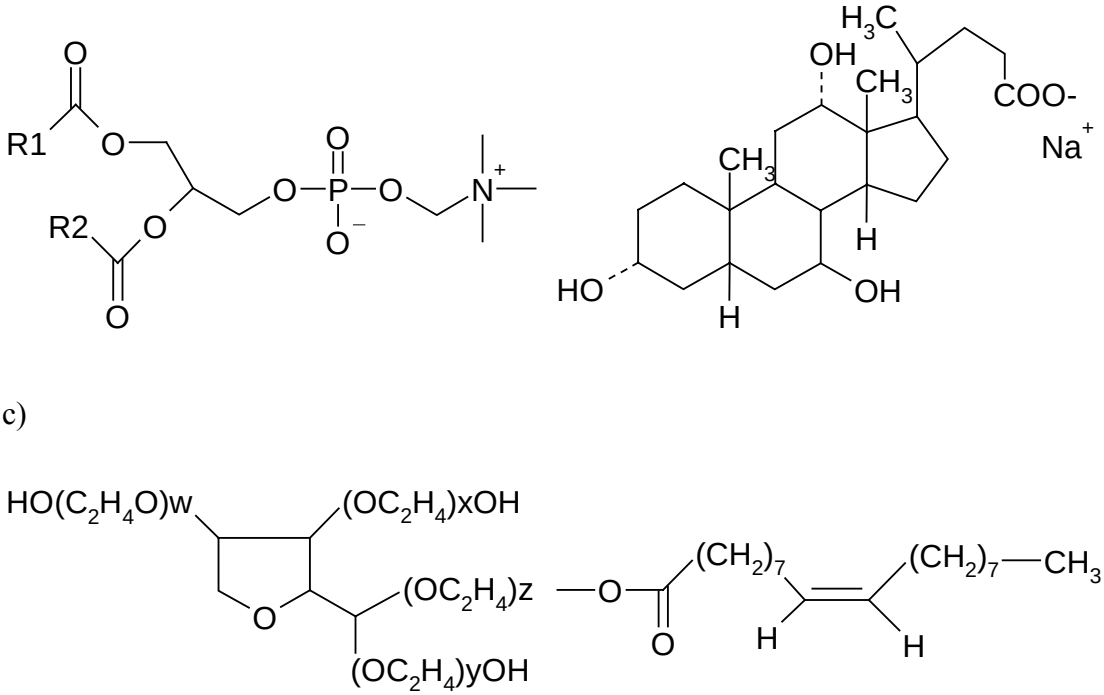

c)

Fig. 2.2: Chemical structure of a) lecithin; R1, R2: typically linear aliphatic rests with 15 or 17 carbon atoms with up to 4 cis double bonds, b) the sodium salt of cholic acid; c) Tween 80, sum of w,x,y,z = 20

2.1.1.2 Miniemulsion polymerization

The process of miniemulsion polymerization is schematically summarized in Fig. 2.3. Small droplets homogeneous in size are created by ultrasound-induced fission processes. Right after the miniemulsification process, there is no pressure balance in the droplets, but the osmotic pressure is usually smaller than the Laplace pressure. In order to gain their pressure equilibrium, the droplets tend to grow. The droplets seem not to grow because of Ostwald ripening, but because of collisions only. In miniemulsions, the monomer droplets stabilized against Ostwald ripening become predominantly the locus of the particle nucleation. The idea of miniemulsion polymerization is to initiate the polymerization in each of the small stabilized droplets, without

major secondary nucleation or mass transport processes involved. Preservation of the particle number and particle identity is therefore a key issue. Miniemulsion polymerization of methyl methacrylate using lauroyl peroxide as initiator as well as cosurfactant has been carried out by Reimers and Schork.[39] Diffusional stability was reduced to the point where nucleation in the monomer droplets and polymerization could be carried out before significant diffusional degradation took place. Ugelstad and coworkers[40] first published results where droplets with sizes of less than 0.7 μm were nucleated leading to polystyrene polymer particles. A continuation of this early work showed that the addition of cetyl alcohol increases the stability of the droplets.[41] Usually, the growth of minidroplets is slower than the polymerization time, and a situation very close to a 1:1 copying of the monomer droplets to polymer particles is obtained, freezing the critically stabilized state (Fig. 2.3). The identity in size before and after polymerization was recently proven by means of SANS measurements.[42] The pressure balance can also be obtained by intentionally adding an adequate amount of surfactant to the system (poststabilization). The growth of the droplets by collisions is then effectively suppressed (Fig. 2.3).

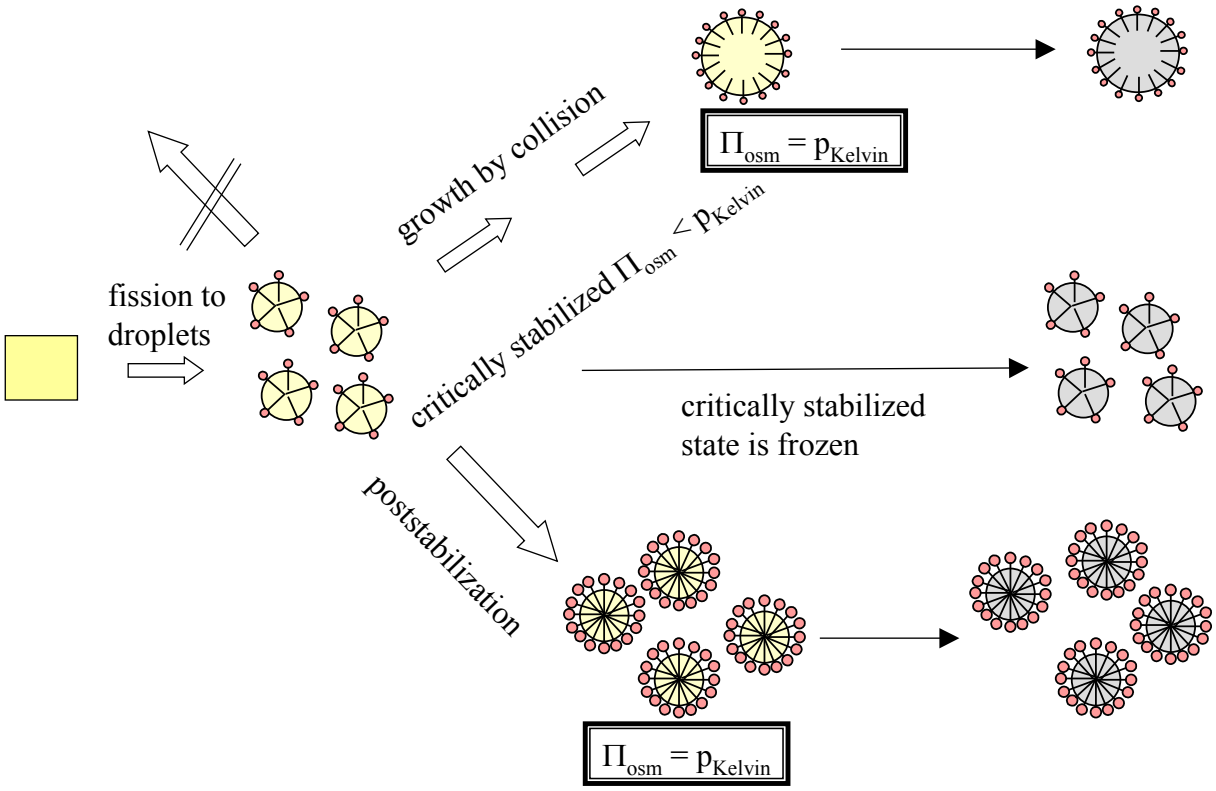

Fig. 2.3: Schematic summary of the process of miniemulsion polymerization

2.1.1.3 Encapsulations by miniemulsion polymerization

Polymerization in direct miniemulsion can be used for the efficient encapsulation of water-insoluble materials in hydrophobic polymers to obtain hybrid particles which are homogenous in their size and their inorganic material content as shown recently for the encapsulation of hydrophobized $CaCO_3$[43] and TiO_2.[44] For these encapsulation processes, the encapsulating material is dispersed in the monomer phase prior to miniemulsification. Another approach was developed for the encapsulation of high amounts of carbon black: Both monomer and carbon black were independently dispersed in water using SDS as a surfactant and mixed afterwards in any ratio between the monomer and carbon. Then, this mixture was cosonicated, and the controlled fusion/fission process characteristic for miniemulsification destroyed all aggregates and liquid droplets, and only hybrid particles being composed of carbon black and monomer remained due to their higher stability.[45]

Thus, it is plausible the encapsulation of magnetic components through the miniemulsion process.

2.2 Magnetism

Magnetic field origins from the movement of electric charges. An electrical current in a wire produces a magnetic field that curls around the wire. A current loop surrounding an area πr_{loop}^2 and carrying a current *i,* creates what is called *magnetic dipole moment* μ whose magnitude is $i\pi r_{loop}^2$ and has units of A·m^2 in SI or emu (electromagnetic unit of magnetic moment) in cgs.

Atoms have magnetic dipole moments, which are produced both for electron spin and for the rotation of electrons around the nucleus. The nucleus has a small magnetic moment, which, nevertheless is negligible compared to the one of the electrons. Electrons can be imagined as tiny circuits and carrying tiny magnetic dipole moments. They respond to external magnetic fields and give rise to a magnetization (*M*) that is defined as the net magnetic dipole moment (μ_{total}) per unit volume in the material (*v*):

$$M = \frac{\mu_{total}}{v} \qquad \text{Eq. 1}$$

The total magnetic field inside such a material (the magnetic induction *B*) is a function of the applied external field and the magnetization

$$B = B_{ext} + \mu_0 M \qquad \text{Eq. 2}$$

where B_{ext} is the strength of the external magnetic field and μ_0 is the permeability of the free space, $4\pi\ 10^{-7}$ T·m·A^{-1}.

The magnetic field strength *H* depend only on the strength of the external magnetic field:

$$H = \frac{B_{ext}}{\mu_0} \qquad \text{Eq. 3}$$

and replacing Eq. 3 in Eq. 2, it results

$$B = \mu_0 (H + M) \qquad \text{Eq. 4}$$

The relationship between M in the material and the external field H is defined as:

$$M = \chi H \qquad \text{Eq. 5}$$

where the proportional constant χ is the mass magnetic susceptibility of the material.

The typical curves of M against H are called magnetization curves as shown in the Fig. 2.4.

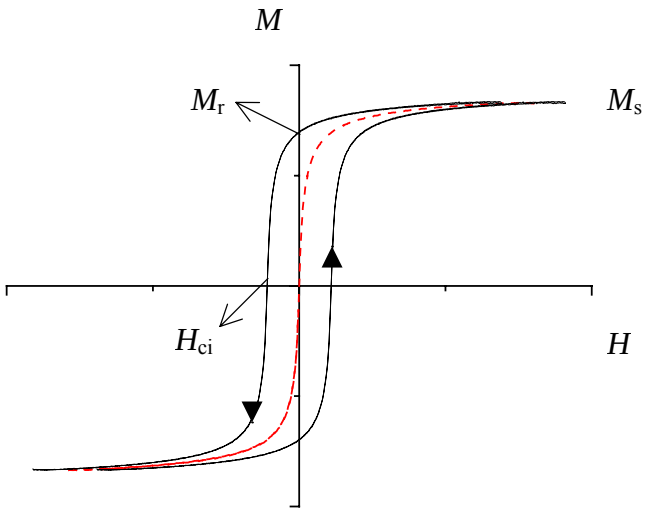

Fig. 2.4: Typical magnetization curve and hysteresis loop

Saturation magnetization M_s: at strong magnetic field, the magnetization becomes constant at its saturation value

Remanence M_r: is the magnetization value, when H is reduced to zero after saturation has been reached.

Intrinsic coercivity H_{ci}: is the negative (reverse) applied field required to decrease the magnetization to zero.

2.2.1 Magnetism in materials

Materials can be classified by appropriate measurements in different types such as ferromagnetic, diamagnetic, paramagnetic, superparamagnetic, antiferromagnetic, ferromagnetic, etc, depending on the their response to an external applied magnetic field.

2.2.1.1 Ferromagnetism

In order to understand ferromagnetism, the Weiss theory has to be considered. A ferromagnetic in the demagnetized state is divided into a number of small regions called *domains.* Each domain is spontaneously magnetized to the saturation value M_s, but the directions of magnetization of the various domains are such that the specimen as a whole has no net magnetization. The process of magnetization is explained by converting the specimen from a multi-domain state into a state in which it is a single domain magnetized in the same direction as the applied flied.[46] The Weiss theory, therefore, contains two important postulates: spontaneous magnetization and division into domains.

The atoms in a ferromagnetic material have magnetic dipole moments that tend to align parallel within a domain throughout the bulk material. When an external magnetic field is applied, the magnetic domains are aligned with the external field. When the external field is removed, the domains maintain the alignment and the magnetism remains. The magnetic material has "magnetic memory" (hysteresis loop in the Fig. 2.4). Iron, cobalt and nickel are typical materials which exhibit ferromagnetism at room temperature.

2.2.1.2 Diamagnetism

When diamagnetic materials are placed in a strong magnetic field, the magnetic dipole moment appears oppositely to the direction of the magnetic field. The susceptibilities of such materials are negative and small, for this reason diamagnetism sometimes is called “negative magnetism”. The electron shells in these materials are completely filled and there are no unpaired electrons. He, Ne, H_2, N_2, some compounds formed with covalent bonding as NaCl, etc. are diamagnetics.

2.2.1.3 Paramagnetism

A paramagnetic material consists of atoms or molecules in which there is no cancellation of the moments of the electrons and therefore there is a net magnetic moment in the atom. In the absence of an applied field, these atomic moments are randomly aligned and cancelled one another so that the magnetization of the material is zero. When an external magnetic field is applied, there is a tendency for each atomic moment to turn toward the direction of the field, but the thermal motion of the atoms opposes this tendency, hindering the perfect alignment and favoring the random one. The result is only a partial alignment in the field direction and, therefore, a small positive susceptibility.

These materials are magnetic as long as the external magnetic field is present. Once the magnetic field is removed, the magnetization is lost.

Paramagnetic materials obey the Curie's law, which predicts that the magnetization varies inversely with the absolute temperature:

$$M = C_{\mathrm{m}}\left(\frac{B_{\mathrm{ext}}}{T}\right) \qquad \text{Eq. 6}$$

where C_{m} is a constant that depends on the material, T is the temperature (K) and B_{ext} is the applied magnetic field.

All other forms of magnetism have a critical temperature or Curie temperature, above which magnetic material becomes paramagnetic as a result of thermal agitation.

These substances are composed of atoms with unpaired electrons in inner shells such as rare earth chelates, which are very strongly paramagnetic.

2.2.1.4 Superparamagnetism

The coercivity is a magnetic property that depends on the particle size. As the particle size is reduced, it is found that the coercivity increases, goes through a maximum, and then tends toward zero as shown in the Fig. 2.5.

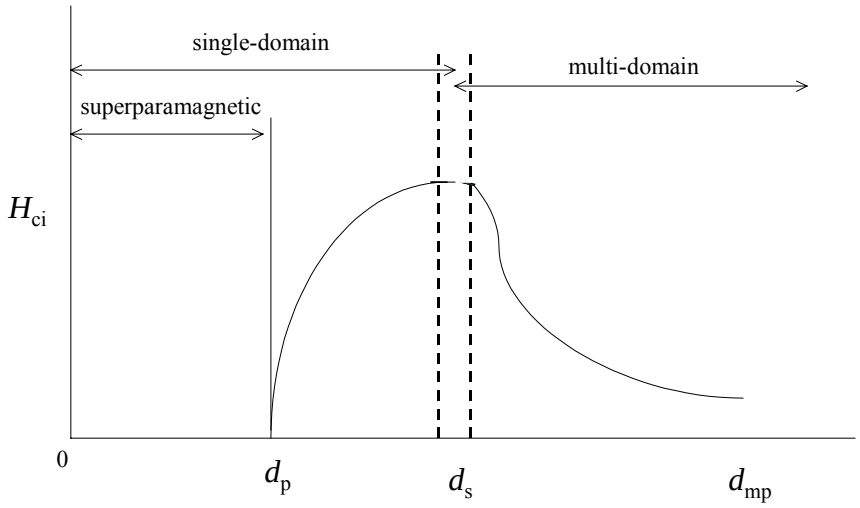

Fig. 2.5: Variation of the intrinsic coercivity H_{ci} with the particle diameter d_{mp}

Beginning at large sizes, we can distinguish the following regions:

1. *Multi-domain*. The interface between regions, in which the spontaneous magnetization has different directions, is called domain wall. The magnetization changes by domain wall motion. In this region the coercivity varies inversely with the diameter of the particles.

2. *Single-domain*. Below a critical diameter, d_s, the particles become single domains, and in this size range the coercivity reaches a maximum. At particles sizes lower than d_s, the coercivity decreases, because of thermal effects. Below a critical diameter, d_p, the coercivity is zero, again because of thermal effects, which are now strong enough to spontaneously demagnetize a previous saturated assembly of particles. Such particles are called *"superparamagnetic"*. The magnetic moment per atom or ion in a normal paramagnetic material is only a few Bohr magnetons. But a spherical particle contains thousands of atoms and therefore has a "super" moment, hence the name superparamagnetism.

Typical superparamagnetic behavior is shown in the Fig. 2.4 (red dashed line). In the superparamagnetic behavior there is no hysteresis. Both remanence and coercivity are zero. This means, when an external magnetic field is applied to the superparamagnetic particles, the moments tend to align in direction of the applied magnetic field, but the alignment is imperfect due to the thermal effects. When the magnetic field is removed, the superparamagnetic particles do not remember that they were magnetized and they lose the magnetization.

2.2.1.5 Antiferromagnetism

These materials have a strong tendency toward an antiparallel alignment of magnetic moments in the absence of an applied magnetic field, in special at lower temperatures where the thermal effect is too low to allow random alignment. Thus, in the crystal it forms two sublattices having opposed moments, which compensate each other.

2.2.1.6 Ferrimagnetism

The word "ferrimagnetism" is due to the certain oxides of iron called ferrites. Ferrites have the general formula $MO \cdot Fe_2O_3$ where M is a divalent metal ion. One of the most widely known ferrite, is the magnetite $Fe^{3+}[Fe^{2+}\,Fe^{3+}]O_4$ (or $FeO \cdot Fe_2O_3$). Ferrites have a spinel structure and it is so-called because the structure is closed to the structure of the mineral spinel $MgO \cdot Al_2O_3$. Spinel lattice consist of face centred cubic arrangements of oxygen atoms with cations localized in the center of tetrahedron and octahedron. In the mineral spinel, the Mg^{2+} ions are in the tetrahedral sites (A) and the Al^{3+} ions are in octahedral sites (B), so-called *normal spinel structure*. Other ferrites have the inverse spinel structure, in which the divalent ions are in the octahedral sites and the trivalent ions are equally divided between tetrahedral and octahedral positions. Magnetite has the *inverse spinel structure*, which it means the tetrahedral positions (A) are filled by Fe^{3+} cations and octahedral positions (B) are equally filled by Fe^{3+} and Fe^{2+}. Ferrimagnetic substances exhibit a similar behavior as the ferromagnetics, but have an antiparallel alignment of the magnetic moments as in the case of antiferromagnetism with the

difference that they do not compensate each other. There are AB, AA and BB interactions but the strongest is AB so that all the A moments are parallel to one another and antiparallel to the B moments but they do not cancel each other.[ ] Ferrimagnetism can be imagined as an "imperfect antiferromagnetism".

2.2.2 Diameter determination from the magnetization measurements

If the particles in a ferrofluid are highly monodisperse, the diameter of the particle can be determinated from the magnetization curve and the magnetic behavior can be described by the Langevin function:[47]

$$M = \coth\left(\frac{m_s VH}{kT}\right) - \left(\frac{kT}{m_s VH}\right) \qquad \text{Eq. 7}$$

where m_s is the saturation magnetization of the bulk material per volume (e.g. 480 emu·cm^{-3} for magnetite[ ]), V is the volume of a spherical particle, k is the Boltzmann constant and T the temperature. For low values of H, the Eq. 7 can be solved for V,

$$V = \frac{3kT\chi_{H\to 0}}{m_s \sigma_{H\to\infty}} \qquad \text{Eq. 8}$$

where $\chi_{H\to 0}$ is the initial mass magnetic susceptibility, it means, the magnetic susceptibility at magnetic field strength nearby zero and $\sigma_{H\to\infty}$ is the specific saturation magnetization (σ, values extrapolated to $H\to\infty$). Solving for d_p in nm, the following equation is obtained

$$d_p = 78.8 \sqrt[3]{\frac{\chi_{H\to 0}}{\sigma_{H\to\infty}}} \qquad \text{Eq. 9}$$

Where $\chi_{H\to 0}$ and $\sigma_{(H\to\infty)}$ are in units of emu·Oe^{-1} and emu·g^{-1} latex, respectively.

2.3 Ferrofluids

Ferrofluids or magnetic fluids or magnetic colloids are stable dispersions of ultrafine ferro- or ferrimagnetic particles or encapsulated ferro- or ferrimagnetic particles in an organic or aqueous carrier medium. The stabilization of these particles is achieved through a surfactant which hinders the particles from flocculation or sedimentation. Ideally, these particles remain uniformly dispersed in the carrier medium although they are or have been exposed to magnetic fields. Due to their small size, ferrofluids contain a single magnetic domain and although they are either ferro- or ferrimagnetic in the molecular scale, they are like paramagnetic components on the colloidal scale with magnetic moments which are much larger than the moments in a paramagnet. Thus, ferrofluids commonly show a superparamagnetic behavior.

In early publications, magnetic fluids were produced by grinding magnetite with heptane or long chain hydrocarbon and a grinding agent, e.g. oleic acid.[48] Later, magnetic fluids were produced by precipitation of an aqueous Fe^{3+} / Fe^{2+} solution with a base, coating these particles with an adsorbed layer of oleic acid and then dispersing them in a non-aqueous fluid.[49] Both processes result in tiny magnetite particles, a surfactant coating these magnetite particles and a non-aqueous liquid carrier in which the hydrophobic magnetite particles will be dispersed. Obviously, the latter process is more feasible to apply in the production of more homogeneous magnetite particles.

Other applications of ferrofluids rely on water as the continuous phase. Kelley[50] produced an aqueous magnetic material suspension by the conversion of iron compounds to magnetic iron oxide in the aqueous medium under controlled pH conditions in presence of a petroleum sulfonate dispersant. Shimoiizaka and coworkers[51] developed a water-based ferrofluid from the oleic acid coated magnetite particles dispersed by an anionic or nonionic surfactant solution, which is suitable to form a second surfactant layer.

Polymer covered magnetic particles can also be produced by an in situ precipitation of magnetic materials in the presence of polymer which acts as a stabilizer. In this way, magnetic polymer

nanoparticles are produced in presence of the water-soluble dextran,[52] poly(ethylene imine),[53] poly(vinyl alcohol),[54] poly(ethylene glycol),[55] sodium poly(oxyalkylene di-phosphonates),[56] and amylose starch.[57] In all cases, the magnetic particles are surrounded by a hydrophilic polymer shell.

Another method to produce magnetic polymer particles consists of the synthesis of magnetic particles and polymer particles separately and then mixing them together to enable either physical or chemical adsorption of the polymer onto the material magnetic. The polymer material can be produced by different ways, for instance by emulsion or precipitation polymerization.[58]

It is also possible to use a strategy comprising the polymerization in heterophase in the presence of magnetic particles. The magnetic material preferably having a surfactant layer is embedded into a polymer using processes such as the suspension, the emulsion, or the precipitation polymerization. Magnetic particles were encapsulated in hydrophilic polyglutaraldehyde by suspension polymerization resulting in particles with an average diameter of 100 nm.[53] Magnetite containing nanoparticles of 150 to 200 nm were also synthesized by seed precipitation polymerization of methacrylic acid and hydroxyethyl methacrylate in presence of magnetite particles containing tris(hydroxy methyl)aminomethane hydroxide in ethyl acetate medium.[59] Polymethacrylate/poly(hydroxy methacrylate) coated magnetite particles could be also prepared by a single inverse microemulsion process, leading to particles with a narrow size distribution, but only with a magnetite content of 3.3 wt.-%.[60]

Daniel and coworkers[61] obtained magnetic polymer particles by dispersing a magnetic material in an organic phase which consists of an organo-soluble initiator, vinyl aromatic monomers and/or a water insoluble compound. The mixture was emulsified in water by using an emulsifier and then polymerization took place in order to obtain polymer particles with a magnetite content between 0.5 and 35 wt.-% with respect to the polymer. However the resulting particle size distribution was rather broad (between 30-5000 nm). Charmot and Vidil[62] used a similar

method to produce magnetizable composite microspheres of a hydrophobic crosslinked vinylaromatic polymer, but they obtained a mixture of magnetizable particles and non-magnetizable blank microspheres.

Ugelstad and coworkers were the pioneers to obtain monodisperse magnetic polymer microparticles by in situ precipitation of magnetic oxides inside preformed porous mono-sized polymer particles, taking into account that the microparticles used as seed (0.5–1 μm) contain metal-binding groups.[63] Magnetic polymer microparticles (0.5–100 μm) with a high degree of monodispersity and up to 35 % of iron as magnetic oxides were obtained. It is important to stress that Ugelstad's work has to be considered as a great contribution in the magnetic carrier technology. Nevertheless, his work was emphasized to produce microparticles whereas our focus is addressed to the production of nano-sized magnetic polymer particles (50–500 nm).

2.3.1 Ferrofluids by miniemulsion polymerization

Wormuth[64] used the inverse miniemulsion process[65] to encapsulate magnetic particles by a hydrophilic polymer. The dispersion of magnetic iron oxide into hydrophilic monomers, followed by the inverse miniemulsion and a further polymerization process was carried out. The magnetite was precipitated from an aqueous poly(ethylene oxide)-*b*-poly(methacrylic acid) dispersion in short denoted as (PEO-PMAA) dispersion, containing iron III and II salts, by means of the addition of a concentrated ammonium solution. After dialysis and drying, the PEO-PMAA-magnetite wax-like solids were redispersed in a mixture of HEMA and MAA monomers. After inverse miniemulsion polymerization, a magnetite latex dispersion was obtained. With regard to the stabilization of the final dispersion, after certain time some sediment was observed.

The strategy of dispersing the material being encapsulated into the monomer phase prior to miniemulsification was also used for the encapsulation of hydrophilic magnetite into the hydrophobic polystyrene as shown schematically in the Fig. 2.6. To obtain a successful

encapsulation, the magnetite aggregates have to be hydrophobized (e.g. by oleoyl sarcosine acid) in order to make them dispersable in hydrophobic monomers such as styrene. Oleic acid, nitrobenzoic acid, catanionic mixtures and zwitterionic emulsifiers did not show efficient stabilization process. A mixture of magnetite particles in styrene containing oleoyl sarcosine acid as a surfactant was miniemulsified in water and after polymerization, polymer encapsulated magnetite particles were obtained.[66] However, the distribution of the magnetite in the polystyrene nanoparticles was still inhomogeneous, and the magnetite content in the polystyrene matrix was limited to 15 wt.-%.

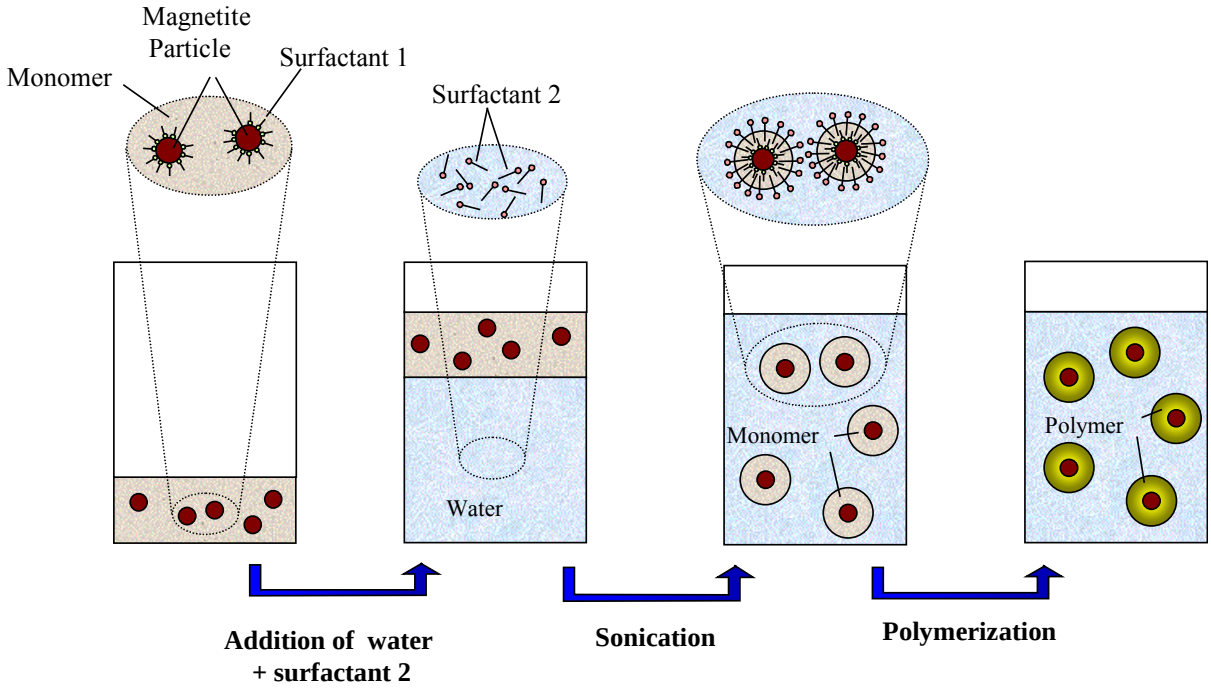

Fig. 2.6: Scheme of the encapsulation of magnetite into polystyrene by Hoffmann's process

2.3.2 Applications of ferrofluids

Magnetic polymer nanoparticles, which are usually dispersed in a carrier liquid (ferrofluid), can be tailor made depending on the final application.[67, 68] Several kinds of magnetic polymer nanoparticles have been produced from both natural and synthetic polymers with the intention

to incorporate groups on the surface or to treat their surface to perform, for instance, selective separations. In particular, magnetic nanoparticles with or without polymer encapsulation can be used for magnetic drug targeting,[69, 70] tissue engineering,[71] magnetic resonance imaging,[72] and hyperthermia.[73] There are also several applications for mechanical and electrical devices which take advantage of the magneto-rheological properties of ferrofluids, e. g. in loudspeakers, seals, sensors, dampers, etc.[74, 75]

Within the framework of the Deutsche Forschungsgemeinschaft (DFG) funded ferrofluid program (SPP1104), several and promising applications of ferrofluids can be found in the technical and medicine field. Ferrofluids used in the gap between the acting magnets in electric machines can enhance the forces in these motors.[76] Abel-Keilhack and Hesselbach[77] showed a comparison of the experimental and simulation of the hydrostatic bearing with magnetic fluids and the calculation of the payload capacity from the flow simulation of magnetic fluids.

Magnetic drug targeting is a drug delivery system using ferrofluids for chemotherapeutics in locoregional cancer treatment. Ferrofluids containing anthracendion-derivative mitoxantrone are injected into the tumor while an external magnetic field is applied on the tumor. In this way, the magnetic particles and mitoxantrone complex is concentrated in the tumor area in order to minimize the undesirable side effects in the organism. In this investigation it was revealed that the incorporation mechanism of the iron containing nanoparticles in the cells is the endocytosis.[78]

Hyperthermia is one of the four principal therapies used against cancer, in line with surgery, radiotherapy and chemotherapy. The principle of hyperthermia consists in the elevation of the temperature within a tumor with the purpose of destructing the cancer cells. The magnetic hyperthermia using ferrofluids is based on the generation of the heat by means of the interaction between alternating magnetic fields and magnetic materials. One of the advantages of using magnetic fluids is the possibility to increase the temperature within tumors without any effect in the surrounding healthy tissues.[79, 80]

Magnetic polymer nanoparticles should fulfill some criteria to fit further biomedical application: no sedimentation, uniform size and size distribution, high and uniform magnetic content, superparamagnetic behavior, no toxicity, no iron leaking, high selectivity in case that these particles are used for hyperthermia purposes, and sufficient heat generation at lower frequencies to enhance selective heating.[81] Therefore, magnetite particles homogeneously encapsulated in a hydrophobic polymer which keep away water-soluble components from contacting the magnetite particles are of high interest. Another important condition in order to implement the ferrofluids in the biomedicine is the use of biosurfactant in their synthesis, increasing their biocompatibility. There are several reasons to use polystyrene as hydrophobic encapsulation material in biomedical applications,[82] e.g. it is inexpensive and it is a hydrophobic polymer which allows physical adsorption of antibodies or proteins, it can also be functionalized e.g. by carboxylic groups which enables covalent binding of antibodies, proteins, or cells.

2.4 Nanostructured composites from iron pentacarbonyl decomposition

For the preparation of magnetic particles in the nanoscale many different approaches are known. Among them, the solution-phase metal salt reduction has the advantage to produce high amounts of colloids which can be further handled for different purposes. However, the reductant, as well as the counter-ion, is often an additional contamination source of the final metal.[83, 84] The decomposition of metal carbonyl complexes is thus a nice alternative, which has been used since many years to produce various metals (mainly Fe, Ni, Co).[85] Metal carbonyls e.g. iron carbonyl are compounds in which carbon monoxide is coordinated to the central metal atom. They act as intermediates in transition-metal catalysis, in which they largely control the course of the reaction.[86] Of the iron carbonyls, iron pentacarbonyl $Fe(CO)_5$, is the most widely used.

The decomposition of the metal carbonyls can be carried out by thermal decomposition (pyrolysis)[87] and sonochemical decomposition.[88] Pyrolysis allows the formation of crystalline solids[89], while the ultrasonic procedure often produces amorphous materials.[90-92]The most common method to obtain iron nanoparticles is by thermal decomposition of iron pentacarbonyl using a solvent in presence of either surfactants, such as oleic acid, or a polymer as stabilizer such as vinyl polymers[93] to avoid the sedimentation of the iron nanoparticles and to enable their stabilization.

The presence of organic and polymeric material during the thermal decomposition allow the formation of nanocomposite materials with the possibility to control the type and size of the metallic particle and the composition. Burke and coworkers[94] prepared nanocomposites consisting of polystyrene-coated iron nanoparticles by thermal decomposition of iron pentacarbonyl in the presence of polystyrene-tetraethylene-pentamine dispersants (PS-TEPA) using 1-methylnaphthalene as solvent. Pathmamanoharan and coworkers[95] used polyisobutene and oleic acid as stabilizer for the decomposition of iron pentacarbonyl in decalin; iron particles of approximately 10 nm were obtained. Using 3-mercaptopropyltrimethoxysilane as stabilizer leads to a combination of spherical and rodlike iron oxide colloids, however the obtained dispersions were not stable.

Hyeon and coworkers[96] reported the production of highly monodisperse maghemite particles from the thermal decomposition of iron pentacarbonyl in a mixture of oleic acid and octyl ether and further oxidation using trimethyl amine oxide. By changing the molar ratio of iron pentacarbonyl and oleic acid (from 1:1 to 1:4) a very good control of the particle size between 4 and 16 nm was achieved. Tannenbaum and coworkers[97] obtained polymer metal nanopyramides by thermal decomposition and simultaneous film formation of a mixture consisting of iron pentacarbonyl and poly(vinylidene difluoride) which is dissolved in dimethylformamide. The presence of solvent during the film formation allows the mobility of

the polymer chains and therefore an efficient adsorption of these chains on the surface of the forming iron oxide particles.

2.5 Gadolinium-based nanoparticles

Gadolinium is a lanthanide with seven unpaired electrons and therefore it has a large magnetic moment (7.9 Bohr magneton). Due to the toxicity of gadolinium as metal or ion, it is only used as complexes. The most important application of gadolinium complexes is in nuclear magnetic resonance as shift reagents[98] and imaging contrast agent,[99] but they can be also used as gadolinium neutron capture therapy agent.[100]

The most common and simplest gadolinium hydrophilic complexes used are Gd-DTPA [gadolinium-(diethylenetriamine penta-acetic acid)][101] and Gd-DOTA [gadolinium-(1,4,7,10-tetraazacyclododecan N, N', N", N'"-tetraacetic acid)].[102] Both of them are water-soluble and have a low molecular weight. To overcome the low molecular weight (and therefore the problem of osmotic pressure), the gadolinium as ion or metal chelator can be coupled directly to synthetic or natural macromolecules such as copolymers of polyethyleneglycol amine derivates,[103] starch,[104] dextran,[105, 106] chitosan,[107] albumin,[108] cholesterol,[109] synthetic polyaminoacid,[110] homopolypeptid,[111] dendrimers,[112] liposomes,[113] polyaminocarboxilate,[114] polyester,[115] protein,[116] human and rat red blood cells.[117] One of the advantages of the complexation of gadolinium to a macromolecule is the possibility of attach multiple paramagnetic ions to one large molecule, therefore the molar dose of the contrast agent can be reduced and hence its toxicity.

The macromolecular carrier can be either a fluid, particulate material, spherical particle or a colloid. Compared with other forms of carriers, a colloid, which is the main focus of this work, is well known to have a major surface area and hence a larger concentration of paramagnetic ions on the surface. Thus, a higher relaxation time can be achieved. Braybrook and Hall[118] synthesized particulate ion-exchange resins containing paramagnetic ions bound to their

surfaces with a water-soluble coating. The sulphonated or imino-diacetic acid cross-linked polystyrene resins (45-170 μm) were stirred in solutions of metal salts and, after rinsing and drying, metal-loaded resins were obtained. These particles are coated with a layer of cellulose acetate butyrate or cellulose acetate phthalate by using a phase separation technique.

Another type of gadolinium-loaded nanoparticles is reported by Reynolds and coworkers.[119] They synthesized metal-loaded core-shell nanoparticles of 120 nm by a three-step method. The polymer core consists of acidic methacrylic acid, which forms a strong complex with gadolinium, and is made using emulsion polymerization. Further, gadolinium nitrate is added to load these particles with gadolinium. In the final step, these metal-loaded polymer cores are encapsulated with a porous polymer shell by a second emulsion polymerization. The gadolinium-loaded emulsion polymer had a loading of 0.045 g Gd per gram resin. The final gadolinium-loaded core–shell nanoparticles consisted of 0.031 g Gd/g polymer.

Gadolinium oxide magnetoliposomes are synthesized from both lauric acid coated gadolinium oxide nanoparticles (20 nm) and fluorescein labelled liposomes (70 nm). They are mixed with and subjected to agitation for 24 h for favoring the formation of a bilayer membrane around the gadolinium oxide particles.[113] Gadolinium oxide liposomes, which are paramagnetic, are obtained, but an optimization of the synthesis were suggested to improve reproducibility.

Most of the polymeric gadolinium contrast agents are based on water soluble chelates, e. g. DTPA. A water soluble functionalized polymer is commonly used for favoring the conjugate process. Gd-DTPA has been covalently attached to epichlorohydrin cross-linked hydrolyzed potato starch microspheres. These particles have a mean particle diameter of 1.50 μm and a gadolinium content between 1.1 and 12.2 %.[104] Gadolinium-containing lipid emulsions with a particle size between 78 and 280 nm were prepared by a thin-film hydratation method using a bath-sonicator. The emulsions comprised soy bean oil, water, Gd-DTPA-disteraylamide, hydrogenated egg yolk phosphatidylcholine as a surfactant and/or an appropriate co-surfactant to reduce the particle size. The gadolinium content was 3.0 mg/ml.[120] Tournier and

coworkers[121] obtained gadolinium-containing micelles, mixing an amphiphilic gadolinium chelate, phospholipids and/or non-ionic surfactant(s) (e.g. Tween). The amphiphilic gadolinium chelate was obtained by esterification or amidation between DTPA and alcohols or amines. The mean diameter of the micelles prepared was between 30 and 100 nm. In these two approaches, the gadolinium chelate was emulsified but the molecular weight was not increased. Tokumitsu and coworkers[107] have reported the preparation of gadolinium-loaded chitosan particulate for cancer neutron capture therapy. Both glutaraldehyde cross-linked and non-crosslinked gadolinium-loaded chitosan particulate system were synthesized. They demonstrated that the use of glutaraldehyde as crosslinking agent reduced the loading amount of Gd-DTPA. The non-crosslinked gadolinium-loaded chitosan nanoparticles were produced by the emulsion-droplet coalescence technique. This technique involves the precipitation of chitosan in an aqueous acidic Gd-DTPA solution by neutralization with an emulsion of sodium hydroxide. A gadolinium content of up to 13.0 % and with a particle size of 452 nm was obtained.

As far as we can see, most of these approaches used water based polymers for the conjugation the gadolinium ion or the metal chelator to the macromolecules. It seems reasonable to envisage the encapsulation of chelates directly in a heterophase polymerization process to produce hydrophobic polymeric nanoparticles containing gadolinium chelate. The chelate should be compatible with the monomer in order to get better encapsulation.

2.5.1 Lanthanide shift reagents for nuclear magnetic resonance

Lanthanide materials have, due to their very special electronic structure, a number of extraordinary properties, including their optical, electronic and magnetic behavior. However, pure lanthanide compounds are usually crystalline and non-ductile and have low material performance. This is why compounding or composite formation with a polymer would be highly profitable, bringing in the potential for solvent processing, cohesive films, flexible coating, plus some mechanical advantages.

A class of easily available lanthanide compounds which dissolve in organic solvents are lanthanide NMR shift reagents. Here, different trivalent lanthanide ions (Dy, Er, Eu, Gd, Ho, La, Pr, Yb) are complexed/Coulomb-bounded with three monocharged bidentate ligands (usually 2,2,6,6, tetramethyl-3,5-heptandionate, tmhd-, and 1,1,1,2,2,3,3-heptafluoro-4,6-octandionate, fod), forming a stable, neutral complex. These two ligands are so tightly bound that the compounds can be regarded as stable under most practical circumstances. A typical structure is depicted in Fig. 2.7.

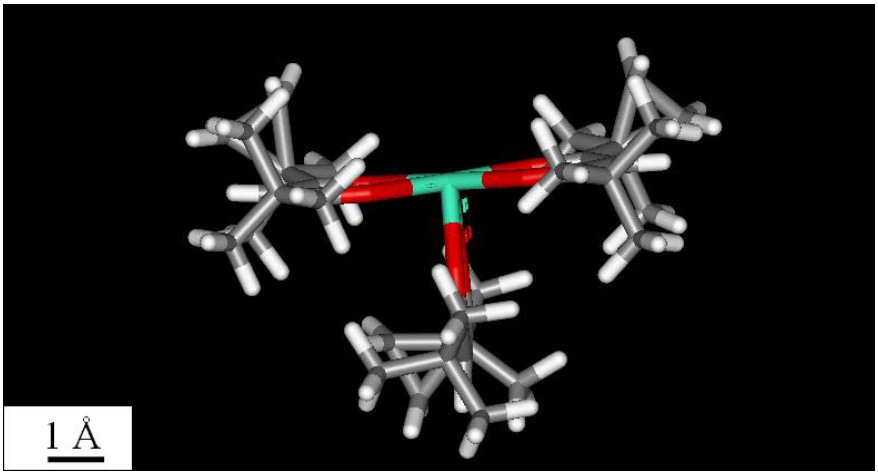

Fig. 2.7: Structure of the complex gadolinium tris(2,2,6,6-tetramethyl-3,5-heptanedionate) ($Gd(tmhd)_3$)

Due to the very large coordination sphere of lanthanides, those inert inner shell complexes however can bind to additional ligands and polarizable components (e.g. Gd (III) typically another three), which defines their use as shift reagents. That way, it should however be possible to mediate compatibility with a second organic phase and activate additional energy contributions to allow self-organization and the related formation of nanocomposites.

2.5.2 Nanostructured materials

One of the proposes of the nanotechnology is to fabricate nanoparticles of desired shape and chemical, physical and mechanical properties. With regard to polymer nanocomposites, one of the techniques to fabricate nanoparticles is based on templating single molecules, several

molecules, colloids, crystals, gels, etc. Templating is classified in direct and indirect form. Direct templating is called when the structure of the templating is still recognized in the final material such as casting, coating, curing. When the original template is changed during the templating process, the templating is called indirect.[122] Inorganic-organic nanocomposites can commonly be obtained by templating techniques such as layered-silicate based polymer nanocomposites.[123] Two types of hybrids were found. One is called intercalated in which a polymer chain is intercalated between the silicate layers. The other one is called exfoliated in which the silicate layers are dispersed in a polymer matrix.

2.5.3 Spin-lattice relaxation time (T_1) on NMR imaging application

Nuclear magnetic resonance imaging techniques has been developed and widely used for the diagnostic medicine application. Reviews in this topic can be found elsewhere.[124-126] In NMR imaging technique, paramagnetic contrast agents are used to enhance the image contrast between normal and diseased tissue, but they are not measured directly. Instead, they are detected indirectly on the basis of changes in proton relaxation. Those protons are mainly from water, which is the most composition of tissue. In principle, when a paramagnetic compound is added, it shortens the relaxation time of neighbouring proton nuclei, resulting in the image contrast enhancement.

The history of NMR imaging technique began in 1946 when Bloch and coworkers has first reported the shortening of spin-lattice relaxation time or longitudinal relaxation time (T_1) of ^{1}H water when ferric nitrate as a paramagnetic solute is added. [127] However, the mathematic formulation of paramagnetic-enhanced solvent relaxation is first described by Solomon[128] in 1955 and later modified by Bloembergen in 1957. [129] The equation is represented as follows:

$$\frac{1}{T_1} = \frac{2}{15}\frac{S(S+1)\gamma^2 g^2 \beta^2}{r_{in}^6}\left(\frac{3\tau_c}{1+\omega_I^2\tau_c^2}+\frac{7\tau_c}{1+\omega_S^2\tau_c^2}\right)+\frac{2}{3}S(S+1)\left(\frac{A}{\hbar}\right)^2\left(\frac{\tau_e}{1+\omega_S^2\tau_e^2}\right) \quad \text{Eq. 10}$$

where S is electron spin quantum number, γ is the proton gyromagnetic ratio, g is electronic g factor, β is the Bohr magneton, ω_I and ω_S are Larmor frequencies for nuclear and electron spins, r_{in} is ion-nucleus distance, $A/\hbar$ is the electron-nuclear hyperfine coupling constant, and τ_c and τ_e are correlation times for dipolar and scalar interactions.

In general, the relaxation rates observed in the presence of a paramagnetic molecule are the sum of the proton relaxation rate caused by the paramagnetic and the proton relaxation rate that would exist without the paramagnetic (diamagnetic) relaxation rate.

$$\frac{1}{T_{1\,\text{observed}}} = \frac{1}{T_{1\,\text{paramagnetic}}} + \frac{1}{T_{1\,\text{diamagnetic}}} \qquad \text{Eq. 11}$$

In principle, the solvent relaxation rates are linearly dependent on the concentration of the paramagnetic species, [M], in the absence of solute-solute interaction. In other words, the paramagnetic concentration has an influence on nuclear relaxation rate, i.e. T_1 is proportional to the paramagnetic concentration

$$\frac{1}{T_{1\,\text{observed}}} = R_1[M] + \frac{1}{T_{1\,\text{diamagnetic}}} \qquad \text{Eq. 12}$$

The relaxivity, R_1, can be then defined as the slope of this dependence in units of $M^{-1}\cdot s^{-1}$ or $mM^{-1}\cdot s^{-1}$. Nevertheless, the Solomon-Bloembergen equation as mentioned above is based on the relaxation of water proton in the proximity of metal complexes. Therefore the interactions of water molecules to the paramagnetic species (either binding to the metal ion or coordination with metal ligands) as well as translational diffusion of water molecules have to be considered.

Generally, the magnitude of relaxation enhancement depends on the proximity of the nuclear and electronic spins and on the correlation time of their interaction. The Solomon-Bloembergen theory classifies contributions for the water proton relaxivity due to three distinct types of interactions as indicated schematically in Fig. 2.8.[130] The first type involves the primary coordination of water molecules with the metal ion (Fig. 2.8a). This type of coordination is

known as inner-sphere relaxation. The second type of interaction is the hydrogen bonding of water molecules in the second coordination sphere (Fig. 2.8b). The third type involves translational diffusion of water molecule past the chelate (Fig. 2.8c). Due to the lack of understanding of second coordination sphere interactions, type b and c are included and referred simply to outer-sphere relaxation.

In the case of inner-sphere relaxation, a following equation is applied

$$\left[\frac{1}{T_1}\right]_{\text{inner sphere}} = \frac{P_M q_w}{T_{1M} + \tau_M} \qquad \text{Eq. 13}$$

where P_M is the mole fraction of metal ion, q_w is the number of water molecules bound per metal ion, T_{1M} is the relaxation time of the bound water protons and τ_M is the residence lifetime of the bound water. The value of T_{1M} is given by the Solomon-Bloembergen equation (Eq. 10).

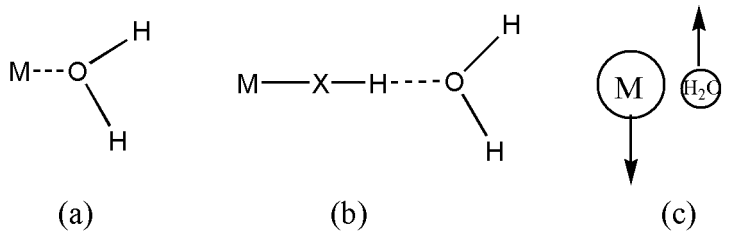

Fig. 2.8: Schematic representation of three types of interaction between water molecules and metal ion

The outer sphere contribution plays are more important role with the use of multidentate ligands that reduce the number of the coordinated water molecules.[ ] In addition, the use of hydrophobic paramagnetic materials reduce the possibility of interaction with the water and the contribution of the diffusion coefficient. Contrarily to the inner phase, the outer-sphere is a more complex problem involving diffusion and no chemical interaction between water and the metal complex.

The most general equation for outer-sphere relaxivity have some similarities with the Solomon-Bloembergen equation and is given in the Eq.14.

$$\left[\frac{1}{T_1}\right]_{\text{outer sphere}} = \frac{C\pi N_S \gamma_I^2 \gamma_S^2 \hbar^2 S(S+1)}{d_a^3 \tau_D}\left[7\, j(\omega_S) + 3\, j(\omega_S)\right] \qquad \text{Eq. 14}$$

where C is a numeral constant, N_S is the number of metal ions per cubic centimeter, d_a is the distance of closest approach of the solvent molecule to the metal complex, $\hbar$ is the Dirac constant, and τ_D, the relative translational diffusion , $\tau_D = d_a^2 / 3(D_I + D_S)$, where D_I and D_S are the diffusional coefficients of water and the metal complex, respectively. The spectral density functions, j in the Eq. 14, are mathematically complex and depend on the frequencies.[99]

3 Relevant Methods

In this section of the thesis, the relevant methods, which are used in the next section, are briefly described.

3.1 Transmission electron microscopy

Transmission electron microscope (TEM) enables, through the interaction of the electron beam with the sample, the direct production of an image. The main components of the TEM are shown in the Fig. 3.1. TEM is based on the principles of the light microscope but is capable of magnifications of 100,000 times and a high resolution of approximately 0.1 nm. As the name indicates, TEM uses a high energy electron beam passing through (transmission) a very thin slice of the specimen (sample) in a vacuum environment. The electrons in the microscope, are accelerated with an electric voltage between 80 and 200 keV, which is used as "light". Electrostatic or magnetic "lenses" focus the electron beam, and project the highly-magnified image onto a phosphor screen, special photographic film or a computer. The sample has to be placed on an electron-transparent support that has to be extremely thin (50-200 nm) for allowing the transmission of the electrons through it and to create an image. A thin carbon –film is usually used for TEM, but its non-complete transparency contributes to the presence of the noise in the final image.

The illumination source (or electron gun) is the thermo-ionic emission. A filament (cathode) is the source of the electrons, usually a tungsten wire. The condenser has the function of gathering the electrons of the first crossover image and focus them onto the specimen to illuminate only the area being examined. The objective lens is used to focus an initial magnification of the image. Intermediated lenses magnify the image coming from the objective lens. Finally, projector lenses magnify the image coming from the intermediate lens and projects it onto the fluorescent screen. The final image can be seen in the camera or computer localized under the fluorescent screen.

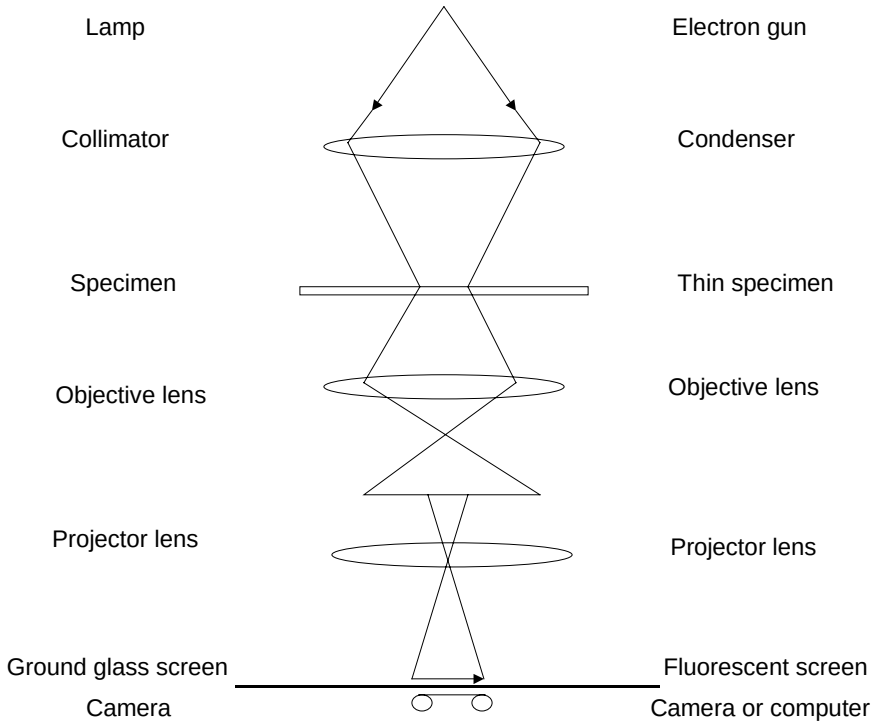

Fig. 3.1: The major components of the TEM (right side) in comparison with the light microscopy (left side) (based on the ref.[[131]])

The resolution ρ of a microscope is defined as the distance at which two points or objects can be distinguished. The resolution can be calculate using the Abbe Theory:

$$\rho = \frac{0.61\,\lambda}{\sin\alpha} \qquad \text{Eq. 15}$$

where λ is the wavelength of the light, and α is the angle of the incoming beam. One of the advantages of using TEM is the high resolution. The Abbe theory can be modified and applied to TEM by the DeBroglie's equation:

$$\lambda = \frac{h}{m_e v_e} \qquad \text{Eq. 16}$$

where h is the Planck constant, m_e is the mass of an electron and v_e is the electron velocity. DeBroglie showed that the wavelength of an electron beam is a function of the accelerating

voltage. The bigger the accelerating voltage, the shorter the wavelength. Applying the Abbe equation, it can be seen that a shorter wavelength leads to the better resolution.

TEM is typically used to examine the internal structure of materials both in biological and non-biological precedence.

3.2 X-ray diffraction

X-rays were discovered by Wilhelm Konrad Röntgen in 1895. X-rays are produced by bombarding a metal anode at high energy (grater than 20 eV) and can penetrate several atomic layers of the materials and produce interference between the X-rays scattering from different planes (Fig. 3.2). The Bragg's law considers a crystal as a number of planes that can reflect the light. The separation between the planes is *d*. The angle of incidence is θ which is equal to the angle of reflection and from trigonometry the path difference is $2d\sin\theta$.

Constructive interference is described by Bragg's law:

$$2d\sin\theta = n\lambda \qquad \text{Eq. 17}$$

where λ is the wavelength of the X-rays s, and *n* is the order of the reflection (*n*= 1, 2,…). Constructive interference means that the X-rays must have a path difference that is equal to the wavelength.

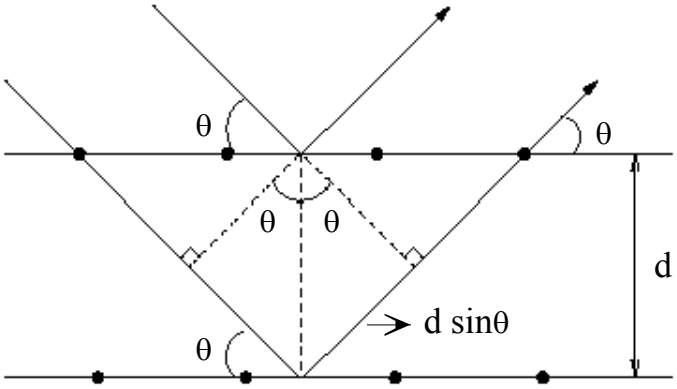

Fig. 3.2: Scheme of the principle of the X-ray diffraction

The arrangement of atoms in materials can be determined by two different X-ray diffraction techniques, Wide Angle X-ray Scattering (WAXS) and Small Angle X-ray scattering (SAXS). The analysis of the WAXS diffraction spectra provides the information about the atomic distribution in the length scale of 1 to 0.1 nm. SAXS is very useful for particles up to a diameter of about 50 nm and allows the determination of the structure of colloids and polymer particles such as lamellar, hexagonal, etc. The thickness of lamellar structures in a polymer is bigger than the spacing between atoms in a crystal and therefore the scattering angle in lamellar phases is smaller, according with the Bragg's law. Hence the structure of the lamellae is determined by SAXS, and the crystalline part is studied by WAXS.

3.3 Dynamic light scattering

Light is scattered by the interaction of electrons with the incident radiation. In the dynamic light scattering the fluctuations of the scattering intensity are due to Brownian motion of the particles correlated by means of an intensity-time correlator $g_2(t)$:

$$g_2(t) = \langle I_{t'} \cdot I_{t'+t} \rangle \qquad \text{Eq. 18}$$

where $I_{t'}$ is the number of photos arriving at the detector at the time interval t', t is the delay time and the brackets $\langle\ \rangle$ denote an average over typically 10^6 – 10^8 correlations. The correlation function is calculated multiplying the number of photons from two successive time intervals and storing the results in the first instrumental channel.

At the limits, it is found

$$\lim_{t\to 0} g_2(t) = \left\langle I_{t'}^2 \right\rangle \qquad \text{Eq. 19}$$

and

$$\lim_{t\to \infty} g_2(t) = \left\langle I_{t'} \right\rangle^2 \qquad \text{Eq. 20}$$

because correlation is maximal for close instants and does not exist for very distant instants.

For small monodisperse particles and homogeneous spheres the normalized scattered electric field autocorrelation function is

$$g_1(t) = e^{-\Gamma t} \qquad \text{Eq. 21}$$

with

$$\Gamma = \frac{D}{q^2} \qquad \text{Eq. 22}$$

where D is the diffusion coefficient, q is the norm of the scattering vector:

$$q = \frac{4n_0\pi}{\lambda}\sin\frac{\theta}{2} \qquad \text{Eq. 23}$$

where n_0 is the refraction index, λ is the wavelength and θ is the angle of incidence.

$g_1(t)$ is related to the intensity correlation function by the Siegert relation

$$g_2(t) = \left\langle I_{t'}^2 \right\rangle \cdot b \cdot g_1^2(t) + \left\langle I_{t'} \right\rangle^2 \qquad \text{Eq. 24}$$

where b is an instrumental constant that reflects the deviations from ideal correlation.

The fluctuations of the intensity of the scattered light depend on the diffusion coefficient and therefore on the particle size and shape. From the parameter Γ the diffusion coefficient can be calculated, and hence by applying the Stokes-Einstein equation the hydrodynamic radius can be evaluated:

$$R_h = \frac{kT}{6\pi\eta D} \qquad \text{Eq. 25}$$

In colloid chemistry a polydisperse system is more common. In this case, $g_1(t)$ has to be integrated over all the possible sizes:

$$g_1(t) = \int_0^\infty G(\Gamma)\, e^{-\Gamma t}\, d\Gamma \qquad \text{Eq. 26}$$

where $G(\Gamma)$ is a cumulant distribution function and can be evaluated by inverse Laplace transform techniques. In order to calculate the hydrodynamic radius, a so-called *z*-average diffusion coefficient has to be calculated.

$$D_z = \langle D \rangle = \sum_i m_i M_i D_i \,/\, \sum_i m_i M_i \qquad \text{Eq. 27}$$

where m_i, M_i, and D_i represent the total mass, molecular weight, and diffusion coefficient of kind *i* particles, respectively.

3.4 Preparative ultracentrifugation

The two types of the centrifugation techniques are the analytical and the preparative. The analytical techniques involve the measurement of the sedimentation coefficient and the molecular weight and use optical systems to analyze the sample during the process. On the other hand, the preparative techniques refer to the isolation of particles for size or density in the majority of the cases for posterior reuse. The term “ultra” means that centrifugation is carried out at speed faster than 20,000 rpm.

Preparative centrifugation techniques can be classified in two main methods: differential pelleting and density gradient centrifugation. In the differential pelleting, as its name indicates, the particles, which are distributed in a solution, are centrifuged to obtain a pellet containing the heaviest particles and a supernatant containing unsedimented particles. Purification of the sample can be achieved with successive re-suspensions and centrifugations. This differential pelleting is carried out in the so-called "velocity way", and it means that the separation is because of the centrifugal forces and no equilibrium or approach equilibrium is reached.

Separations involving the density gradient centrifugation may be due to differences in size or differences in density between the particles. The rate-zonal centrifugation separates molecules based on size, and the isopycnic centrifugation based on density. The isopycnic centrifugation involves the sedimentation of particles in a density gradient column. Under centrifugal force, the gradient redistributes and the particles will move to the position at which the gradient density is equal to its own density. If there is not a gradient density in the sample the particles will show only a Brownian motion in a layer corresponding to its density. Isopycnic centrifugation works in the "approach equilibrium" where the concentration of the molecules will be determined by a balance of the external centrifugal force with diffusion. It is an "approach equilibrium" since to reach the true equilibrium an infinite time is necessary.

A particle under a centrifugal field will experiment three forces:

the centrifugal force,

$$G = \omega^2 r \qquad \text{Eq. 28}$$

the buoyant force,

$$F_b = -m_p \bar{v} \rho_s \omega^2 r \qquad \text{Eq. 29}$$

and the frictional force

$$F_f = -N_A f \frac{dr}{dt} \qquad \text{Eq. 30}$$

where ω is the angular velocity (rad·s^{-1}), r is the centrifugal radius (cm), m_p is the mass of the particle, $\bar{v}$ is the partial specific volume of the particle (the solvated volume of a unit mass of particle), ρ_s is the density of solvent, N_A is the Avogadro's number, f is the frictional coefficient of a single particle ($f = 6\pi\eta a$ which is the Stokes equation for spherical particles of radius a in a solution of viscosity η), and $\frac{dr}{dt}$ is the velocity of the particles.

The particles will move when the total of forces equal zero. After equating the total forces to zero and solving $\frac{dr}{dt}$, the following equation is obtained:

$$\frac{dr}{dt} = \frac{\omega^2 rm(1-\bar{v}\rho_s)}{Nf} \qquad \text{Eq. 31}$$

Very few theoretical considerations are involved in the isopycnic centrifugation however the shape of a zone at equilibrium for a homogeneous zone can be expressed of the following way:

$$c_r = c_{(r,\Theta)} \exp\left[-\omega^2 r_\Theta m \bar{v} \left(d\rho_s / dr\right)_r \left(r - r_\Theta\right)^2 \Big/ 2RT \right] \qquad \text{Eq. 32}$$

Here r_Θ is the radial coordinate of the isopycnic point of the zone which corresponds to the maximal concentration $\left(c_r, \Theta\right)$ of the particles and c_r is the concentration at radius r.[132] This equation resembles a Gaussian shape.

3.5 Magnetometry

The propose of the magnetometry is to measure the magnetization of a material either intrinsic or induced by application of an external magnetic field.

The most common technique employed for magnetization measurements at room temperature is the Vibrating Sample Magnetometer (VSM). VSM measures the magnetic properties of a

sample as a function of applied magnetic field, temperature and time. The principle of operation is shown in the Fig. 3.3.

A VSM operates based on Faraday's law of induction which gives the value of the induced voltage in a coil with n_c turns and area *A*. The electro-motive force across the coil will be proportional to the rate of change of magnetic flux through it:

$$Emf = -n_c \frac{d\phi}{dt} \qquad \text{Eq. 33}$$

where ϕ is the magnetic flux through the loop.

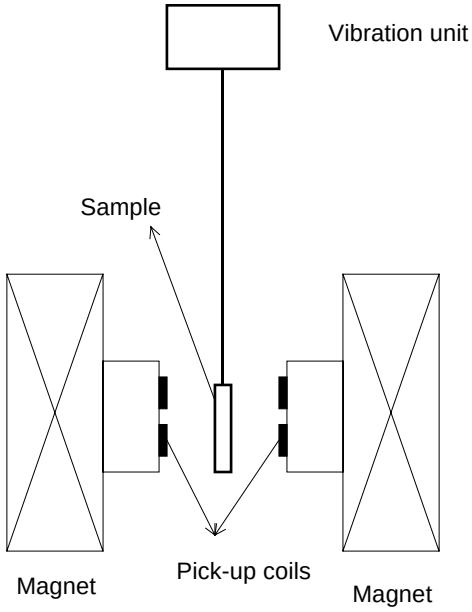

Fig. 3.3: Schematic setup of the vibrating sample magnetometer

In a VSM, a sample is subjected to vibrations nearby a set of pick–up coils under an external magnetic field. The magnetic flux change due to the movement of a magnetic sample causes an induction voltage across the pick-up coils that is proportional to magnetization of the sample. The greater the magnetization, the greater the induced current.

4 Results and Discussion

4.1 Water-based ferrofluids containing magnetite polystyrene nanoparticles

This section deals with the developing of a new route which is based on miniemulsion processes for the production of aqueous ferrofluids consisting of uniform and stable magnetic polystyrene nanoparticles, which are highly homogeneous and possess high magnetite contents up to 40 wt.-%. The first step follows the classical procedure. Here, oleic acid coated magnetite particles are dispersed in octane and combined with an aqueous surfactant solution. This mixture is then miniemulsified and subsequently carefully heated to evaporate the octane which leads to aqueous ferrofluid containing magnetite aggregates. To obtain an aqueous ferrofluid consisting of polystyrene encapsulated magnetite particles, a second miniemulsion process is used. Here, a mixture of the magnetite aggregate dispersion and a styrene miniemulsion are co-sonicated, followed by a polymerization process. The final hybrid particles are characterized by thermogravimetry, preparative ultracentrifugation, transmission electron microscopy and magnetometry measurements.

In previous experiments,[ ] encapsulated magnetite particles were obtained by first mixing oleoyl sarcosine acid coated magnetite into the monomer and then formulating a miniemulsion of the monomer/magnetite dispersion in water. Due to aggregation of magnetite and the coupled viscosity problems, the amount of magnetite in the monomer was limited to about 15 wt.-%.[66] This reaction however still showed some imperfections since the distribution of magnetite between the particles and within each particle was still rather heterogeneous, which was presumably due to the interaction between the magnetite moieties and a related size- and content-specific destabilization of the miniemulsion droplets. Also the influence of pH seemed to be crucial, which was attributed to both the pH dependence of the surface charge of magnetite and the protonation of the oleoyl sarcosine acid and the coupled interface energy.

In order to obtain homogeneous encapsulation with a high magnetite content, a three-step process was intended to develop. In the first step, hydrophobized magnetite particles with a diameter of about 10 nm were synthesized in a classical coprecipitation procedure. In a second step, these magnetite particles were transformed to magnetite aggregates of about 40 to 200 nm in water by using a miniemulsion process. In a third step, the magnetite aggregates were encapsulated with a monomer by an ad-miniemulsification process and after polymerization, polymer highly magnetite loaded particles were obtained.

The first step is already well known from the literature. It is the scope of this paper to develop the second and the third step of the synthesis route.

The importance of the second step could be shown previously. If the small hydrophobized magnetite particles obtained in the first step were dispersed in water as separate magnetite particles, in the following fusion/fission process, only a very low number of these small magnetite particles can collide with the monomer droplets resulting in a very low encapsulation efficiency. Therefore, for a successful fusion/fission process larger magnetite aggregates are necessary which could be obtained in the second step of the synthesis route by using the miniemulsion process. The influence of reaction parameters on the magnetite aggregate size will be discussed in detail.

The third step, the influence of the aggregate size and the presence of acrylic acid on the encapsulation of the aggregates will be described. The three-step synthesis route is shown in Fig. 4.1.

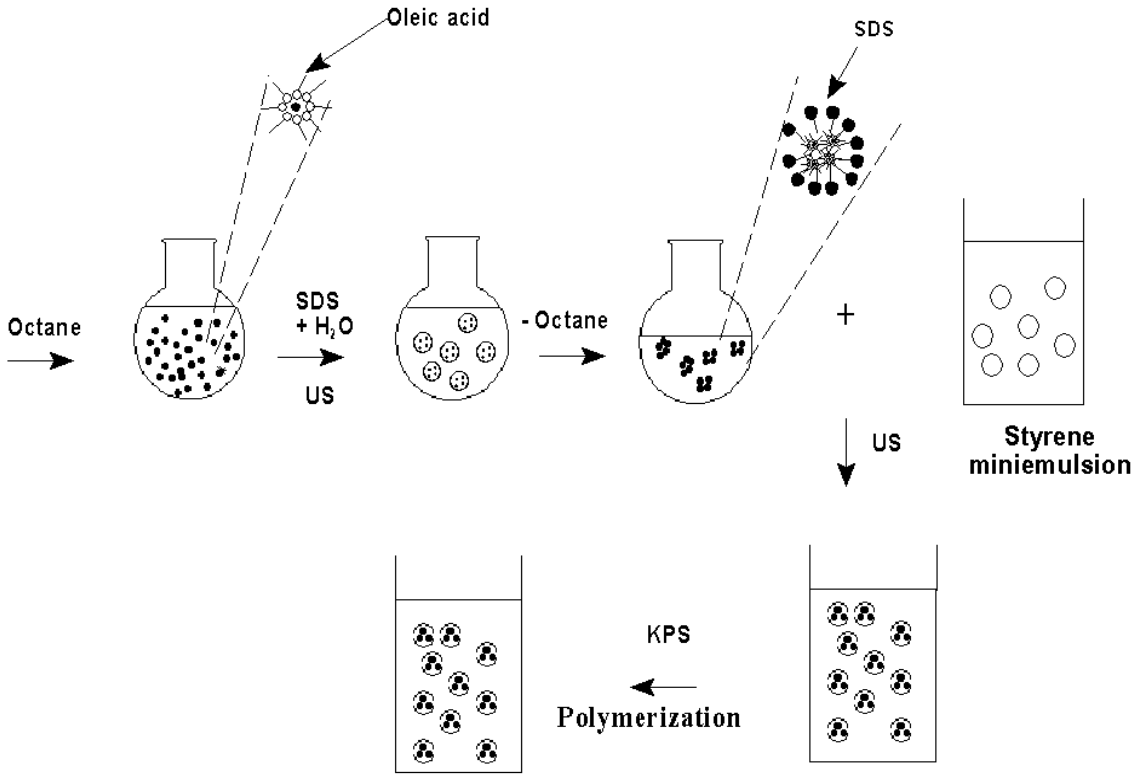

Fig. 4.1: Formulation of polymer coated magnetite particles with a high magnetite ratio.
In the first step, hydrophobized magnetite particles are produced and in a second step transferred to magnetite aggregates in water by using the miniemulsion process. In a third step, the principle of co-miniemulsion is used. The controlled fusion/fission process in the miniemulsification realized by high energy ultrasound or high pressure homogenization destroys all aggregates and liquid droplets, and only hybrid particles being composed of magnetite and monomer remain due to their higher stability

4.1.1 Hydrophobic magnetite nanoparticles

Magnetite particles with a mean diameter of 10 nm were obtained in a coprecipitation process[] by quickly adding a concentrated ammonium solution to a solution of Fe^{2+} / Fe^{3+} with a molar ratio of 3:2 which allows the compensation of the oxidation of some iron II to iron III during the coprecipitation in an open vessel.[]

By adding oleic acid (22.2 or 44.4 wt.-% with respect to the magnetite, see Table 4.1) at temperatures above its melting temperature, the magnetic particles were hydrophobized. After evaporation of the water and washing out the non-adsorbed oleic acid, a dry powder was obtained. The oleic acid content was determined by thermogravimetric measurements of the powder as shown in Fig. 4.2. In the case that 22.2 wt.-% oleic acid was added for

hydrophobization, between 200 and 400 °C a one-step mass loss of about 20 % is detected indicating that most of the oleic acid is indeed adsorbed on the particles and could not be washed out. A calculation with a mean diameter of 10 nm and a magnetite density of 5.16 $g \cdot cm^{-3}$ leads to an area occupied by one oleic acid molecule of 0.27 nm^2. When 44.4 wt.-% oleic acid was added for hydrophobization, a two-step mass loss was detected. The first mass loss of 15 % was obtained between a temperature of 200 and 280 °C, the second mass loss of about 18 % was observed between a temperature of 380 and 480 °C. The two-step decay indicates that different species of oleic acid are present in such a sample. The area which could at maximum be occupied by one oleic acid molecule was calculated to be about 0.16 nm^2 which suggests that a multi-layer arrangement is presumably realized.

The hydrophobized magnetite particles could be easily dispersed in octane, the particle size of the oleic acid coated particles in octane was about 20 nm. A stable dispersion with a magnetite content of 14 wt.-% was prepared for further use.

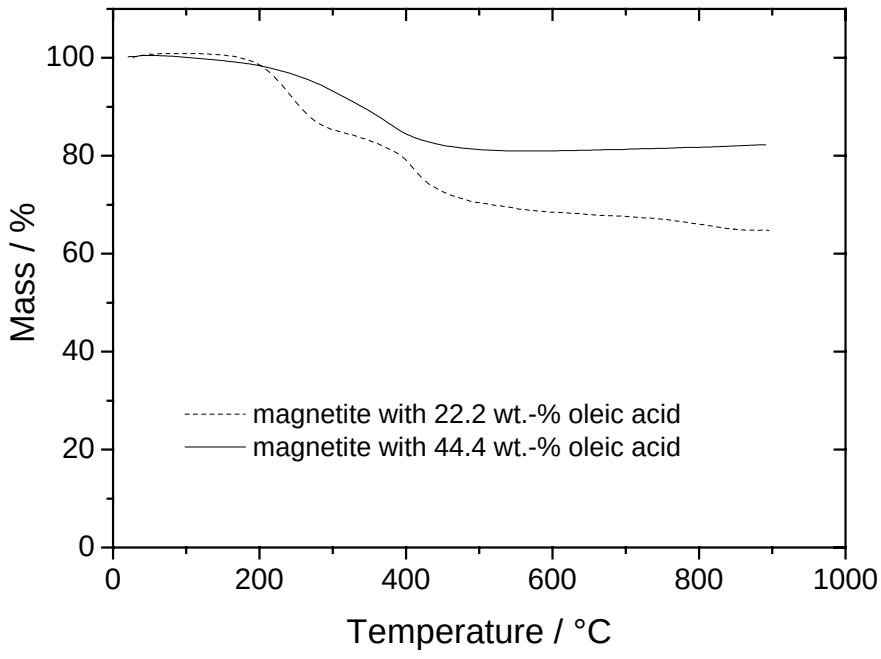

Fig. 4.2: Thermogravimetric curves of magnetite particles coated with oleic acid

4.1.2 Aqueous magnetite aggregate dispersion

In a next step, the hydrophobic magnetite particles in octane as dispersion medium are reformulated to stable water-based ferrofluids for the encapsulation process. For that, a miniemulsion process was carried out to produce magnetite/octane-in-water dispersions. Stable aqueous miniemulsions with droplets consisting of the magnetite/octane dispersions (as obtained above) were obtained by using as low as 1.0 wt.-% of the anionic surfactant SDS (Mag-1 to Mag-3). For the formulation of stable miniemulsions, the addition of a hydrophobic agent is required to provide an osmotic stabilization. However, the magnetite/octane-in-water miniemulsions with hexadecane and without hexadecane show both a high stability indicating that oleic acid does not only act as coating agent, but can also replace the osmotic pressure agent.

After evaporation of the octane, a water-based ferrofluid consisting of oleic acid coated aggregated magnetite dispersed in a water phase is obtained (for an example see Fig. 4.3). In other words: the magnetite aggregates must have a surfactant double layer, the first layer is oleic acid which provides a hydrophobicity of the particles for later encapsulation, the second layer being SDS promotes the stabilization in water. The characteristics of the dispersions are summarized in Table 4.1. The size of these aggregates depends on both the oleic acid (introduced in the first step) and the SDS concentration and can be adjusted to be between 40 and 200 nm. The higher the SDS concentration is, the smaller the magnetite aggregate sizes are. Doubling of the amount of oleic acid in the magnetite particles leads to smaller magnetite aggregates. If hexadecane was used additionally as hydrophobic agent, the particle size was larger since hexadecane does not evaporate and contributes also to the particles size (the wt.-ratio of magnetite/oleic acid to hexadecane in the samples Mag-1 and Mag-4 is 4 : 1).

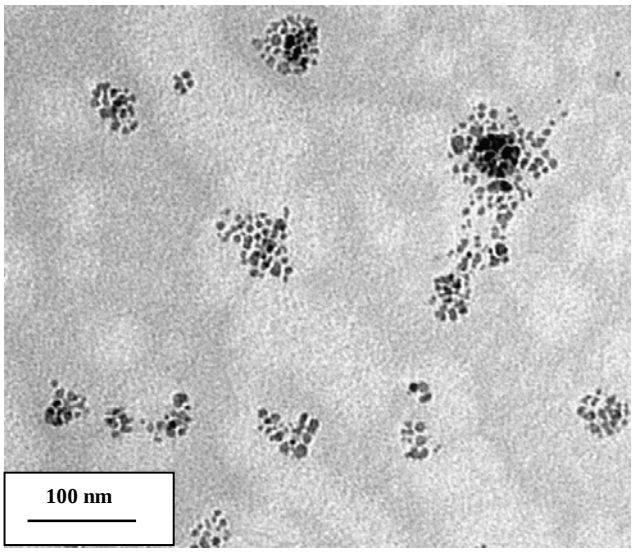

Fig. 4.3: Magnetite aggregates obtained after a miniemulsion process in water

Table 4.1: Preparation conditions and influence of the concentration of surfactants on the water based ferrofluid particle size

Sample	Added oleic acid [a)]	Hexadecane [b)]	SDS [b)]	Solid content	Particle size [c)]
	wt.-%	wt.-%	wt.-%	%	nm
Mag-1	22.2	3.6	1.0	3.6	198
Mag-2	22.2	0	1.0	2.5	178
Mag-3	44.4	0	1.0	4.0	103
Mag-4	22.2	3.6	4.1	4.9	141
Mag-5	22.2	0	4.1	4.0	109
Mag-6	44.4	0	4.1	4.6	89
Mag-7	22.2	0	8.2	2.5	63
Mag-8	44.4	0	8.2	5.2	61
Mag-9	22.2	0	10.3	3.5	60
Mag-10	44.4	0	10.3	5.7	41

[a)] Related to magnetite

[b)] Related to dispersed phase. The dispersed phase consists of octane, magnetite and oleic acid.

[c)] After evaporation of the octane

4.1.3 Encapsulation of the magnetite particles in polymer

In the third step of the synthesis route, a monomer miniemulsion with 20 wt.-% dispersed phase is prepared and added to the water-based ferrofluid containing the magnetite aggregates as obtained above. Then, this mixture was cosonicated, and the controlled fusion/fission process which is characteristic for miniemulsification is expected to destroy all aggregates and liquid droplets. After this step, only hybrid particles being composed of magnetite and monomer are expected to remain, presumably since this species shows the highest stability as it was already shown for the encapsulation of carbon black in styrene.[45] The idea is to obtain another stable miniemulsion from two stable miniemulsions by cosonication and to take advantage of the possibility to use different magnetite and styrene concentration.

Then, polymerization of the monomer was started for all the samples presented here by adding the initiator KPS at 80 °C. The use of the hydrophobic initiators 2,2'-azobis(isobutyronitrile) (AIBN) or 2,2'-azobis(2-methylbutyronitrile) (V59) turned out to be less efficient for the encapsulation process, and therefore these initiators were not studied any further. Whereas in a typical styrene miniemulsion polymerization, the polymerization using KPS at 80 °C is usually completed after 2 h, in the case of the magnetite/styrene miniemulsion, between 18 to 24 h were required for a full conversion of the styrene. Then stable dispersions without the formation of any coagulum were obtained, the characteristics of them are summarized in Table 4.2.

For the synthesis of Latex-1, the aqueous dispersion with the smallest magnetite aggregates of 41 nm, Mag-10, and a styrene miniemulsion were mixed in a ratio of the two dispersed phases of 1:1. This means that the particles consist of 50 % of styrene and 50 % of magnetite/oleic acid/SDS which results in a theoretical magnetite content of 19.4 %. After 40 min of the reaction, acrylic acid was added in order to functionalize the particles for further possible reactions (e.g. for binding of antibodies onto the particle surface). After completion of the polymerization, the latex particles have a particle size of about 80 nm (see Fig. 4.4). The weight-average molecular weight of the polymer formed in the particles was determined to be

about 210,000 $g \cdot mol^{-1}$ which indicates that the presence of magnetite in the polystyrene does not have any effect on the final weight-average molecular weight of the polymer. However, the amount of oleic acid is not negligible in the particles and also contributes to the polymer since also double bonds of the oleic acid are converted. In the control miniemulsion polymerization of styrene/oleic acid without magnetite, about 50 % of the double bonds have been converted. However, the determination is more difficult in the presence of magnetite. After extraction of the polymer with THF or chloroform, no unpolymerized oleic acid could be detected by NMR.

TGA measurements show a two-step decay, between 250 and 350 °C a mass loss of about 20 % is detected, then a second mass loss between 400 and 450 °C is observed resulting in a remaining mass of 20 % which is attributed to the magnetite, a value corresponding well to the expected value.

The structural homogeneity of the encapsulation process is characterized by sedimentation experiments in a preparative ultracentrifuge. In a density gradient, it is simple to differentiate between the low density polymer phase, the high density magnetite phase and all intermediates which are the encapsulated species with different layer thickness and layer perfection. For the experiment, sucrose solutions of different densities were layered, building up a density gradient from 1.0 to 1.3 $g \cdot cm^{-3}$.

In the case of Latex-1, only one particle fraction with a narrow density distribution (1.2 $g \cdot cm^{-3}$) is detected (see Fig. 4.5a), indicating that all formed particles do show a very similar magnetite/polymer composition or degree of encapsulation. At the same time, the absence of pure polystyrene particles or pure magnetite aggregates is clearly proven.

The corresponding Latex-2 without acrylic acid shows a rather similar density distribution of the particles. This means that the encapsulation of the small size magnetite aggregates is not very much influenced by the presence of acrylic acid.

Table 4.2: Characteristics of the latexes consisting of the magnetite/polymer particles

Latex	Magnetite	Acrylic acid	Styrene	Magnetite (theoretical)	Magnetite (determined by TGA)
			wt.-%	wt.-%	wt.-%
Latex-1	Mag-10	+	50	19.4	20.7
Latex-2	Mag-10	-	50	19.4	32.5
Latex-3	Mag-8	+	50	21.2	32.9
Latex-4	Mag-8	-	50	21.2	33.5
Latex-5	Mag-1	+	50	37.2	34.9
Latex-6	Mag-1	-	50	37.2	39.1
Latex-7	Mag-10	+	40	23.3	25.4
Latex-8	Mag-10	+	33	25.9	29.5
Latex-9	Mag-10	+	20	31.1	34.7

This structural or composition homogeneity is also observed by TEM. As shown in Fig. 4.4, full encapsulation of the magnetite particles is obtained. It is found that the small magnetite particles are well separated, what means that each is presumably completely coated with a thin layer oleic acid, and then, the entire aggregate is covered with a layer of polymer. Due to the oleic acid, the formed polymer is rather soft.

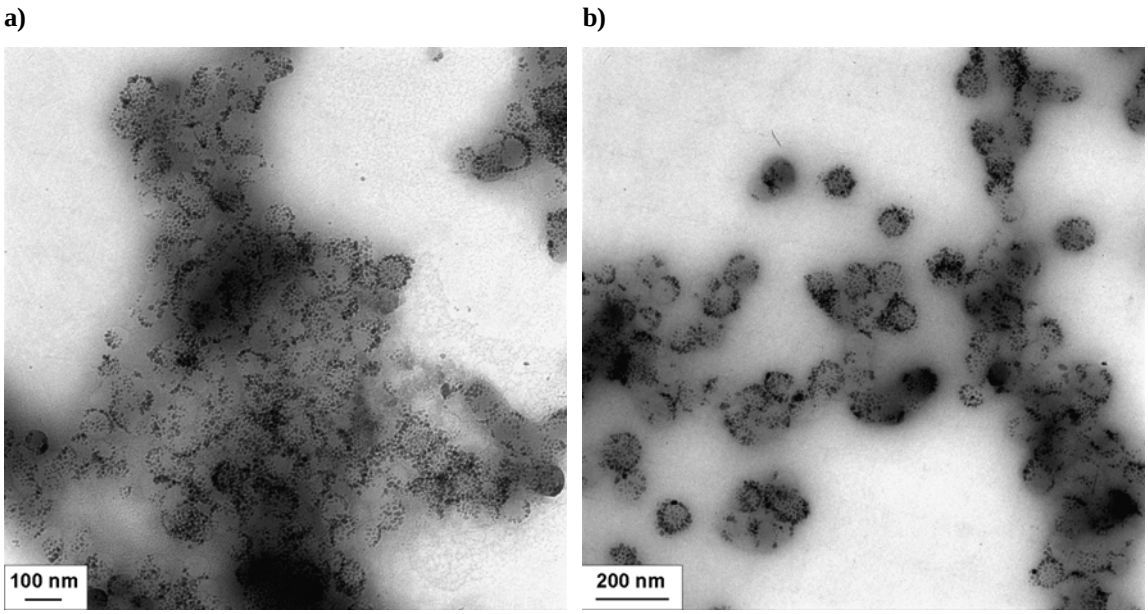

Fig. 4.4: Transmission electron micrograph (TEM) for magnetite polystyrene particles (Latex-1) at different magnifications.

Both decrease of acrylic acid content as well as increase of the primary magnetite aggregate size leads to less efficient encapsulation of the magnetite. For the experiments, magnetite dispersions with different aggregate sizes, Mag-8 and Mag-1, were combined with the same styrene miniemulsion. The following polymerization was carried out with and without the presence of acrylic acid. The density distributions of the latexes obtained by ultracentrifuge experiment are shown in Fig. 4.5.

In Latex-3 and Latex-4, medium sized aggregates were encapsulated with a magnetite content of about 33 % as determined by TGA. This is a much higher amount than expected and can partly be attributed to the fact that some of the magnetite Fe_3O_4 is converted to Fe_2O_3. In the case of Latex-5 and Latex-6, the largest aggregates were encapsulated by styrene. In this case a high magnetite content of about 40 % was obtained.

With increasing the aggregate size, the density distribution is larger, indicating that homogeneous encapsulation of larger particles is more difficult. This is due to statistical reasons during the fusion/fission process: the magnetite aggregates should not be too large because then

only few large aggregates are faced to many styrene droplets. Please also note that the magnetite particles of 10 nm are too small to be efficiently encapsulated. A situation where a similar number of magnetite aggregates and styrene droplets exists is obviously favored for a homogeneous encapsulation process.

The use of acrylic acid has also a large influence on the encapsulation efficiency. For the encapsulation of size aggregates synthesized without any acrylic acid (Latex-4 and Latex-6), in the ultracentrifuge experiment, particles of different densities were detected indicating that the particles are less homogeneous. There are still no free polystyrene particles detected, but particles with a high density which could be attributed to free magnetite particles. However, when small amounts of acryl acid are added during the synthesis (Latex-3 and Latex-5), the encapsulation is favored leading to a hybrid particles with a higher homogeneity in their density, free magnetite particles are not found indicating that acryl acid acts at the interface between the magnetite and the polymer and therefore supports the oleic acid to increase the wetting and therefore the compatibility between the phases.

Using the ferrofluid with the smallest magnetite aggregate particles, Mag-10, for encapsulation, the magnetite content could easily be varied between 20 and 34 % (Latex-1 and Latex-7 to Latex-9) as determined by TGA, the densities were rather homogeneous (Fig. 4.5). Note that the average density (see arrows) is increasing with increasing magnetite load.

a)

Latex-1	Latex-2	Latex-3	Latex-4	Latex-5	Latex-6
Mag-10		Mag-8		Mag-1	
with AA	without AA	with AA	without AA	with AA	without AA

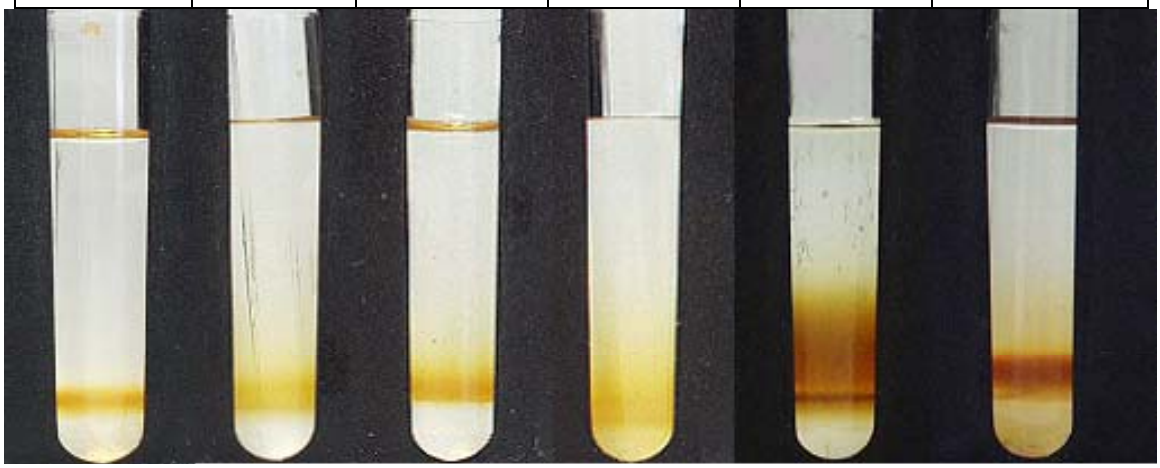

b)

Latex-7	Latex-8	Latex-9
with AA	with AA	with AA
25.4 % magnetite	29.5 % magnetite	34.7 % magnetite

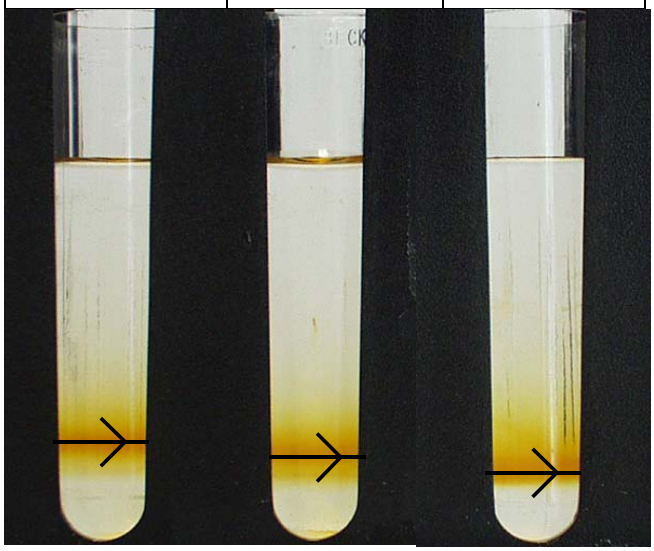

Fig. 4.5: Encapsulation of polystyrene/magnetite particles studied by ultracentrifuge experiments in a density gradient: a) samples with different magnetite aggregates and with or without acrylic acid; b) Mag-10 as magnetite aggregates were used at different magnetite contents, the latexes were prepared with acrylic acid. Note that the average density (arrows) is increasing with increasing magnetite load

4.1.4 Magnetic properties

The magnetic properties of the synthesized ferrofluids with the polymer encapsulated magnetite particles are of high interest for all further applications. The magnetic properties including the saturation magnetization (M_s), the mass magnetic susceptibility (χ), the specific saturation magnetization (σ, values extrapolated to $H \rightarrow \infty$), the relative saturation remanence ($m_r = M_r/M_s$) and the intrinsic coercivity (H_{ci}) of some of the ferrofluids presented in this paper are presented in Table 4.3 and Fig. 4.6. All of the ferrofluids show a typical superparamagnetic behavior at room temperature without any hysteresis loop. The superparamagnetic behavior is also reflected in the low M_r/M_s ratio and in the small H_{ci} values. This clearly indicates that the magnetite primary particles with a diameter of approximately 10 nm are still well separated in the polymer particles (see diameter values, d_p, Table 4.3).

In Fig. 4.6a, the magnetization curves for the samples at different stages of the synthesis are compared, namely a) the oleic acid coated magnetite particles dispersed in octane (magnetite particles in octane), b) the water-based ferrofluid containing the magnetite aggregates after octane evaporation (Mag-10) and c) the polymer encapsulated magnetite aggregates (Latex-1). For the oleic acid coated magnetite particles in octane, a saturation magnetization value of 87 emu·g^{-1} magnetite is obtained which is close to the saturation magnetization of the bulk material (89 emu·g^{-1} magnetite). The magnetite aggregates in water, Mag-10, have a saturation magnetization of 68 emu·g^{-1} magnetite, the loss of magnetization may be due to oxidation processes during the sonication which leads to the formation of some non-magnetic iron oxide (Fe_2O_3). For the polystyrene magnetite particles Latex-1, the saturation magnetization is still as high as 53 emu·g^{-1} magnetite which is about 60 % of the magnetization of the bulk material. It means that during the polymerization, probably again some of the magnetite converts to Fe_2O_3 due to the presence of the oxidizing initiator fragments.

Fig. 4.6b shows that the amount of magnetite in the particles does not influence the saturation magnetization. In all cases (Latex-7, -8, and -9), the saturation magnetization was between 51 and 54 emu·g^{-1} magnetite indicating that the magnetization is quite constant after the polymerization process.

a)

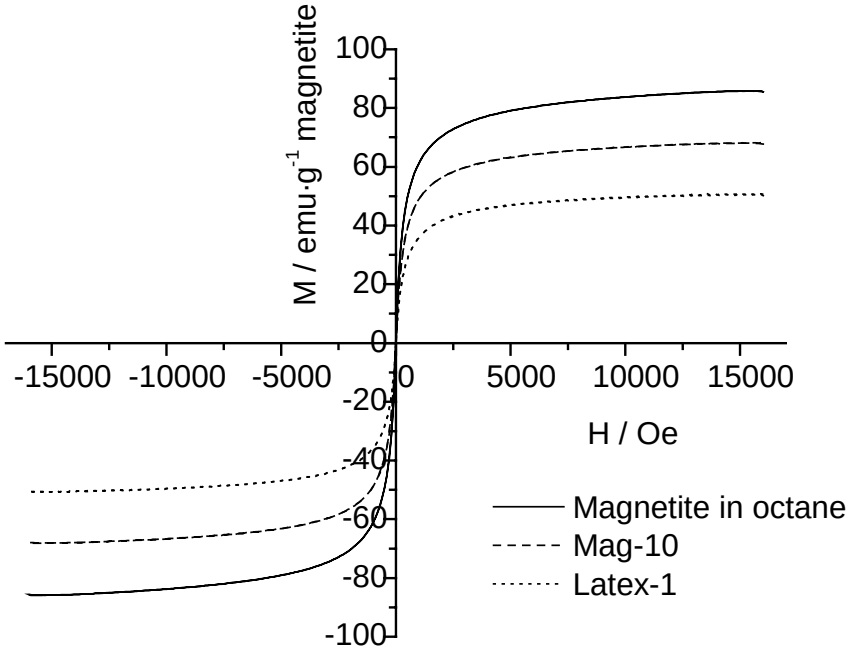

b)

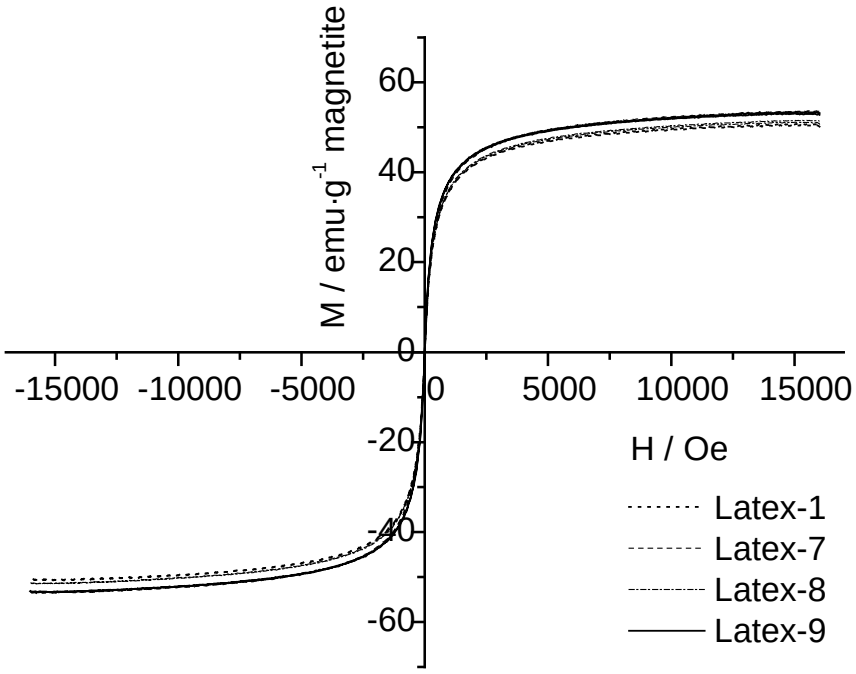

Fig. 4.6: The magnetic field dependence of magnetization a) of magnetite in octane, the magnetite aggregates in water (Mag-10) and the encapsulated magnetite particles (Latex-1); b) of different encapsulated magnetite particles (Latexes-1, -7, -8, and -9)

Table 4.3: Magnetic properties of the ferrofluids.

Sample	M_s	χ	$\sigma_{H\to\infty}$	M_r/M_s	H_{ci}	d_p [b)]
	emu·g^{-1} magnetite	emu·Oe^{-1}	emu·g^{-1} latex		Oe	nm
Magnetite particles in octane[a)]	~85.707	$5.60\cdot10^{-4}$	6.620	0.0026	1.12	2.20
Mag-10	67.939	$1.03\cdot10^{-4}$	1.108	0.0032	1.46	9.09
Latex-1	53.958	$8.98\cdot10^{-5}$	0.787	0.0034	1.54	9.77
Latex-7	52.910	$1.71\cdot10^{-3}$	0.764	0.0082	3.17	10.3
Latex-8	51.034	$2.00\cdot10^{-3}$	0.865	0.0059	2.28	10.59
Latex-9	52.81	$2.40\cdot10^{-3}$	0.909	0.0040	1.46	10.89

a) Little evaporation might have taken place during the measurement

b) Values obtained from Eq. 9

4.1.5 Using biosurfactants

The sodium salt of the cholic acid ($3\alpha,7\alpha,12\alpha$ trihydroxy-5β-cholan-24 acid) was used instead of SDS with the same conditions of the sample Mag-10 for the stabilization of the magnetite particles in water. No stabilization of the magnetite particles was achieved with the use of lecithin and Tween 80 due to probably to the absence of the carboxylic group. Cholic acid sodium salt can excellently be used for the stabilization of magnetic aggregates in water (see Fig. 4.7).

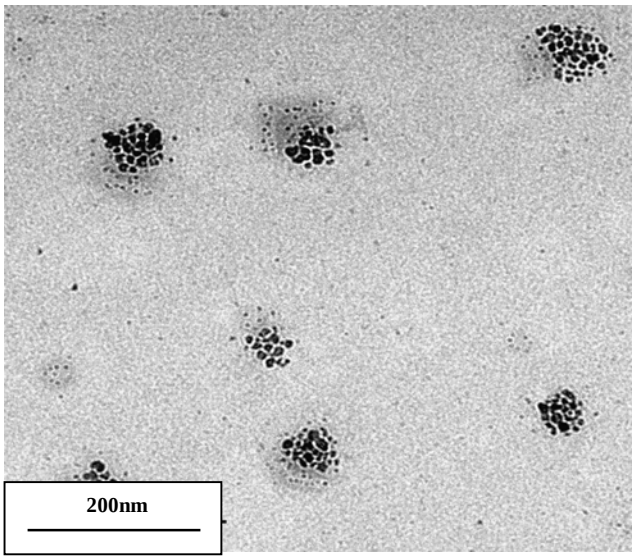

Fig. 4.7: Magnetite aggregates in water with cholic acid as surfactant.

4.2 Nanostructured composites from the iron pentacarbonyl decomposition

This section deals with the results and discussions of the approach for the production of new confined paramagnetic nanocomposites directly from the thermal decomposition of iron pentacarbonyl within the monomer phase containing oleic acid. Subsequently, a miniemulsion polymerization process, using the iron containing monomer dispersion as dispersed phase, was carried out. This two-step process enables the confinement of iron oxide nanoparticles in poly(butyl methacrylate) and their high order structure. The first step consists of the thermal decomposition of the iron pentacarbonyl containing in the monomer phase using oleic acid as stabilizer without any solvent. In the second step this iron containing monomer dispersion was used for making a miniemulsion polymerization thereof. The two-step process enables the immediately polymerization of the monomer phase containing iron particles for the production of nanostructured composites with paramagnetic properties.

The final high structured nanocomposites are mainly characterized by transmission electron microscopy, thermogravimetry, small- and wide angle X-ray, measurements, preparative ultracentrifugation, infrared spectroscopy and magnetization measurements.

The potential of the paramagnetic nanocomposite colloids as contrast agents for magnetic resonance imaging can be shown by first relaxation NMR measurements.

4.2.1 Thermal decomposition in the monomer phase

Butyl methacrylate (BMA), with a boiling point of 163 °C, is very apt to be used first as solvent for the decomposition of iron pentacarbonyl at 110°C and then as monomer for the subsequent miniemulsion polymerization. Besides, the presence of carbonyl group in the monomer can be very effective to allow the encapsulation process of the iron oxide. The thermal decomposition of iron pentacarbonyl was carried out in BMA using oleic acid in the range between 0.0 and 25.0 % (related to iron pentacarbonyl) as surfactant for either 9 or 24 h (see Table 4.4), at 110 °C and at 250 rpm (for more details, see Table 4.4).

Table 4.4: Dispersion of iron in monomer using oleic acid as surfactant

Sample	Oleic acid[b)]	Time of decomposition	Solid content After freeze drying	Inorganic content after TGA
	wt.-%	h	wt.-%	wt.-%
BMA-D1[a)]	0.0	9	-	-
BMA-D2	1.2	9	1.7	42.0
BMA-D3	12.5	24	15.6	15.3
BMA-D4	25.0	24	34.8	13.3

[a)] The dispersion is not stable against sedimentation
[b)] Related to iron pentacarbonyl

In absence of oleic acid (sample BMA-D1) and with only 1.2 % of oleic acid (sample BMA-D2), polymerization of the monomer phase occurred during the thermal decomposition for 24 h. Therefore, the decomposition time was decreased to 9 h in order to hinder the polymerization of butyl methacrylate. It is known from the literature that iron pentacarbonyl acts as polymerization initiator in the case of olefins[133] when the thermal decomposition is carried out without or with small quantities of oleic acid. Without or with negligible amounts of oleic acid

the contact area between the iron pentacarbonyl molecules and the monomer is bigger and this increases the possibility of radical formation for the initiation of the polymerization.

The conversion of the iron pentacarbonyl can be detected by FTIR measurements. The peak at 2000 cm^{-1} in the FTIR spectrum from iron pentacarbonyl corresponds to the carbonyl group. The FTIR spectrum from the sample BMA-D4 dispersion does not present any peak at 2000 cm^{-1}, providing the absence of C=O from monoxide in the sample (see Table 4.4).

The reduction of the decomposition time to 9 h in the sample BMA-D1 and BMA-D2 leads to rests of non-reacted iron pentacarbonyl in the final dispersion as they are detected by the FTIR measurements (for the sample BMA-D2, see Fig. 4.8a) Therefore, in order to enhance the stabilization of the iron containing monomer dispersion and to allow the further use for the miniemulsion polymerization, after the decomposition of iron pentacarbonyl a 110 °C in all the samples, the non-reacted iron pentacarbonyl is removed by agitation in a open flask at room temperature for 4 h in an extractor hood.

From the FTIR spectra it is difficult to affirm the presence of butyl methacrylate in the sample because the peak from C=O of the carboxylic acid from the oleic acid, and the acrylate are overlapping (1705-1750 cm^{-1}).

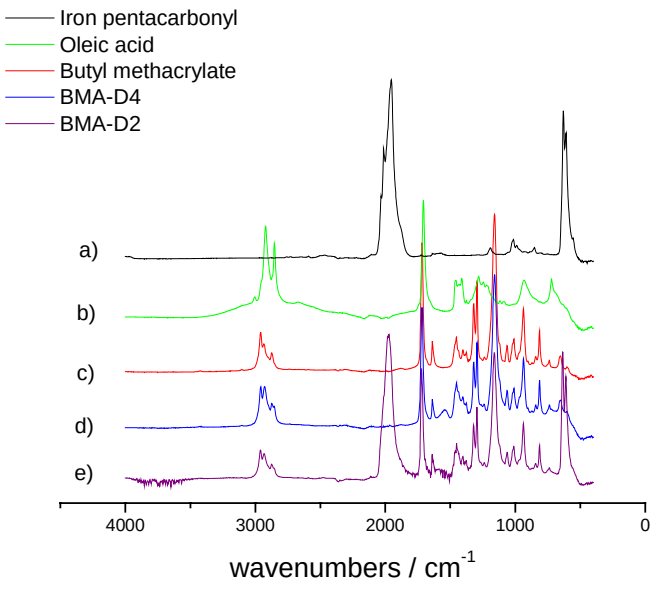

Fig. 4.8: FTIR spectra with air as background

As it can be detected by TEM measurements, the formed nanoparticles are polydisperse in size and between 5 and 15 nm as shown in Fig. 4.9 for the sample BMA-D2.

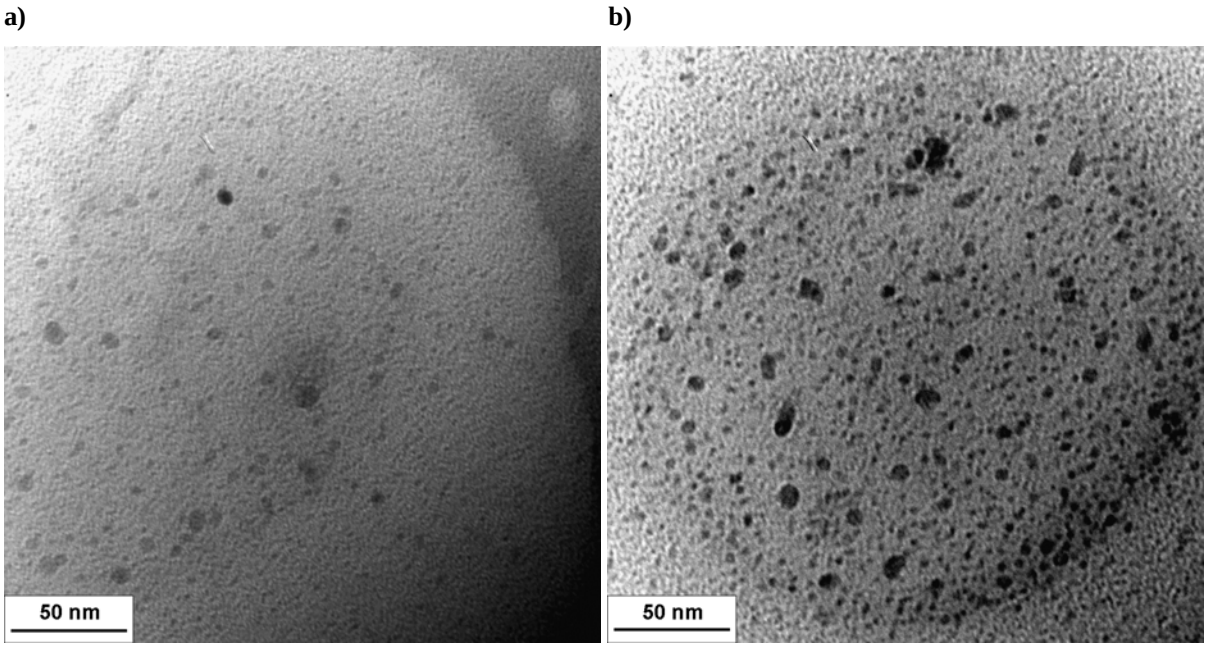

Fig. 4.9: TEM pictures of the sample BMA-D2

In order to determinate the inorganic content produced during the decomposition, the samples were freeze dried, and the amount of iron or iron oxide was determinated by TGA (see Table 4.4). Already from the solid content, it can be seen that in the case of using 1.2 % oleic acid, the inorganic content was determined to be 42 %. It is assumed that this is iron oxide (since a further oxidation in O_2 atmosphere in the TGA measurement at higher temperatures is not observed (see Fig. 4.10)). The 58 % can be attributed to a mixture of poly(butyl methacrylate), poly(oleic acid) and oleic acid indicating that during the decomposition, some polymerization takes place. In future experiments, Mössbauer spectroscopy has to be used in order to determine which kind of iron derivative is contained in the monomer after the decomposition of iron pentacarbonyl.

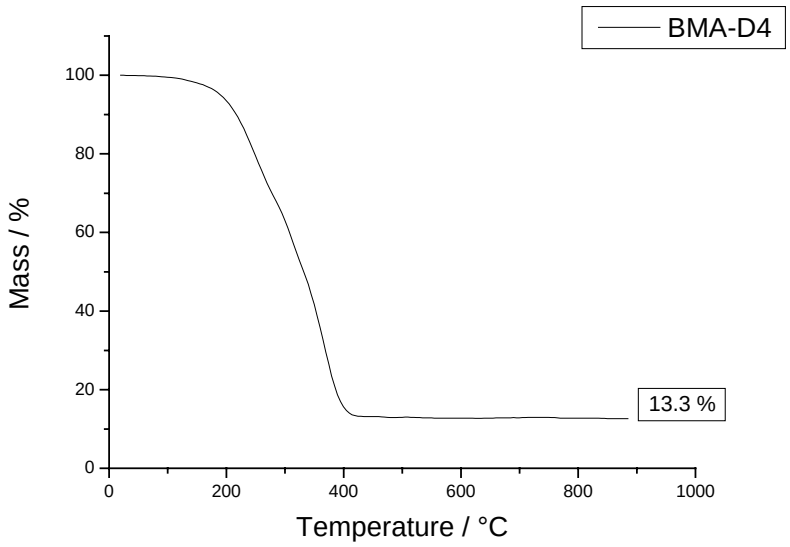

Fig. 4.10: TGA measurements of the sample BMA-D4 under oxygen atmosphere

The TGA measurements at higher oleic acid contents show the presence of approximately 85 % of the organic mixture. The NMR spectrum from the freeze dried sample BMA-D4 in Fig. 4.11a proves the presence of the acrylic group and the double bonds, indicating that un-reacted BMA is present. The broadening of the peaks may be attributed to a strong interaction to the inorganic particles.

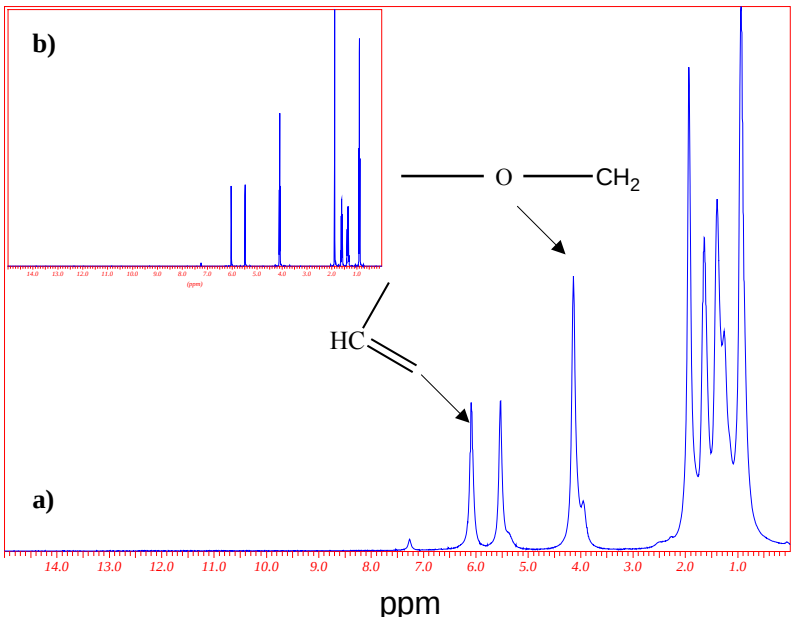

Fig. 4.11: ^{1}H NMR in $CDCl_3$ for a) the sample BMA-D4 and b) Butyl methacrylate

In order to obtain information about the structure of the sample, WAXS and SAXS measurements were carried out. From the WAXS measurements of sample BMA-D4 (Fig. 4.12a), only one sharp peak at low scattering angle is detected, otherwise the material does not show any long range structuring, that means no crystallinity. The SAXS measurements show more in detail the tendency to form a structured material. The peak in SAXS (Fig. 4.12b) corresponds to the first peak in the Fig. 4.12a and reveals possibly a tendency to form a structured system.

a)

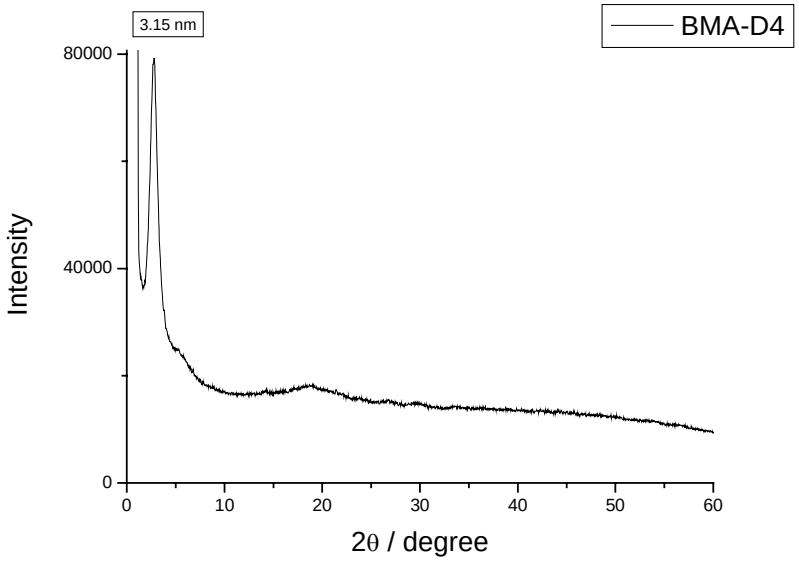

b)

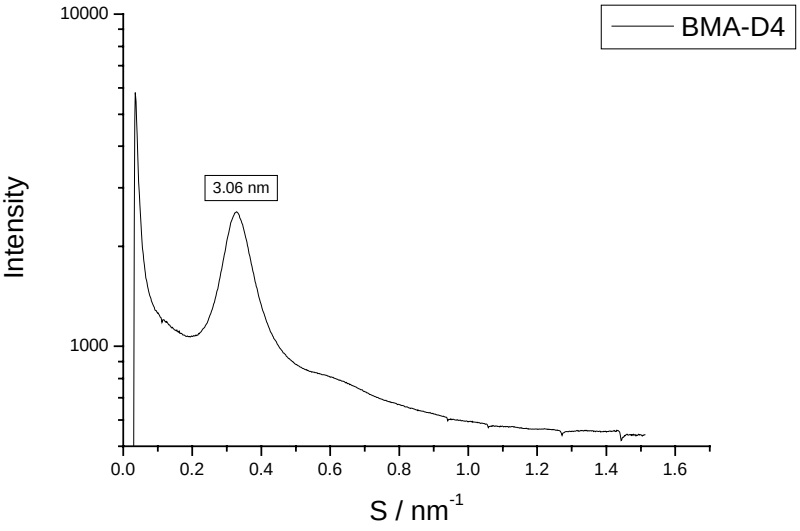

Fig. 4.12: a) WAXS and b) SAXS measurements of sample BMA-D4

4.2.2 Nanocomposite particles after miniemulsion polymerization

In the second step of the procedure, the polymeric nanoparticles in aqueous dispersion were obtained.

From the as-obtained iron-containing monomer dispersion (Table 4.4), stable miniemulsions (before polymerization) and stable dispersions (after polymerization) were obtained with 4.2 and 11.7 % of the surfactant SDS (related to disperse phase) (for more details see Table 4.5). The particle size of the final dispersions was determined from DLS. It is seen that with decreasing the surfactant amount, usually the diameter of the particle size increases as expected and is in the range between 300 and 140 nm. A typical molecular weight of the polymer was determined by GPC to be 100,000 $g \cdot mol^{-1}$, indicating that the presence of the iron does not negatively influence the molecular weight compared to usual miniemulsion polymerization polymers.

With a decrease of the SDS and the oleic acid concentration, also a decrease in the iron oxide content can be observed as determined by TGA, possibly due to small coagulation of the iron oxide. In the best case, an iron oxide content of 14.1 % could be obtained.

Table 4.5: Miniemulsion polymerization latexes based on 0.5 g monomer containing iron nanoparticles.

Name	Iron oxide - monomer dispersion	SDS[a)]	Diameter	Solid content	Iron oxide content
		wt.-%	nm	wt.-%	wt.-%
PI1a	BMA-D1	11.7	160	9.9	2.2
PI1b	BMA-D1	4.2	188	10.1	3.6
PI2a	BMA-D2	11.7	137	9.5	8.9
PI2b	BMA-D2	4.2	214	7.9	7.2
PI3a	BMA-D3	11.7	213	10.6	10.3
PI3b	BMA-D3	4.2	278	8.0	6.0
PI4a	BMA-D4	11.7	304	11.0	14.1
PI4b	BMA-D4	4.2	222	11.3	7.6

[a)] Related to disperse phase

TEM pictures of the sample PI3a-latex obtained after the miniemulsion polymerization from sample BMA-D3-24 h decomposition are shown in the Fig. 4.13 and Fig. 4.14 at low and high magnifications, respectively. In Fig. 4.13, iron containing aggregates can be observed which are engulfed by the poly(butyl methacrylate) in an eye-like assembly. The size of the particles is between 500 nm and 1 μm which is not in agreement with the size observed in the TEM pictures, but can be explained by the low Tg of the polymer leading to pancake-like structures while TEM-preparation. The iron containing aggregates consist of discrete iron oxide particles, which are presumably oleic acid coated. Because of the oleic acid, strongly hydrophobic iron oxide aggregates are demixed from the polymer phase. The polarity of the two phases is presumably very different. At higher magnifications of this sample PI3a (see Fig. 4.14a, and b), a highly ordered structure consisting of needles or bars which are presumably formed for the assembly of iron containing nanoparticles which in turn are coated with a layer of oleic acid can be observed. The SAXS measurement (Fig. 4.15a) reveals a lamellar structure with a repeat period of 3.9 nm. Presumably, in the highly reductive presence of elemental iron, oleic acid is reduced to stearic acid or to iron stearate. The stearic acid then can crystallize and is not able to stabilize the iron particles in the polymer particles and therefore a very strong demixing is obtained in the final composite nanoparticles. The WAXS spectrum (Fig. 4.15b) reveals rather amorphous material as already seen in the first part of this section.

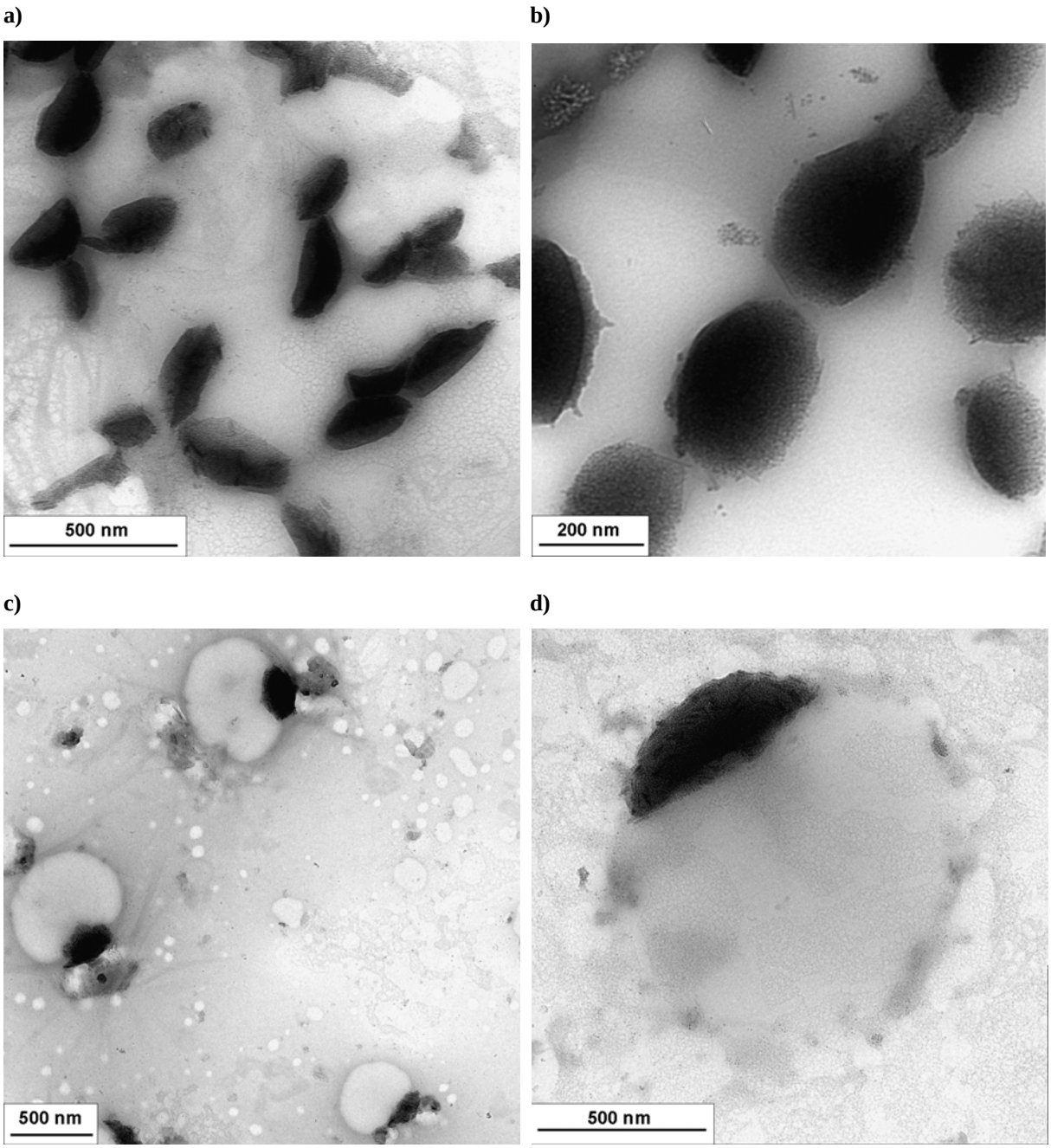

Fig. 4.13: TEM picture of sample PI3a (11.7 % SDS, 12.5 % oleic acid related to ipc) at low magnifications

a) **b)**

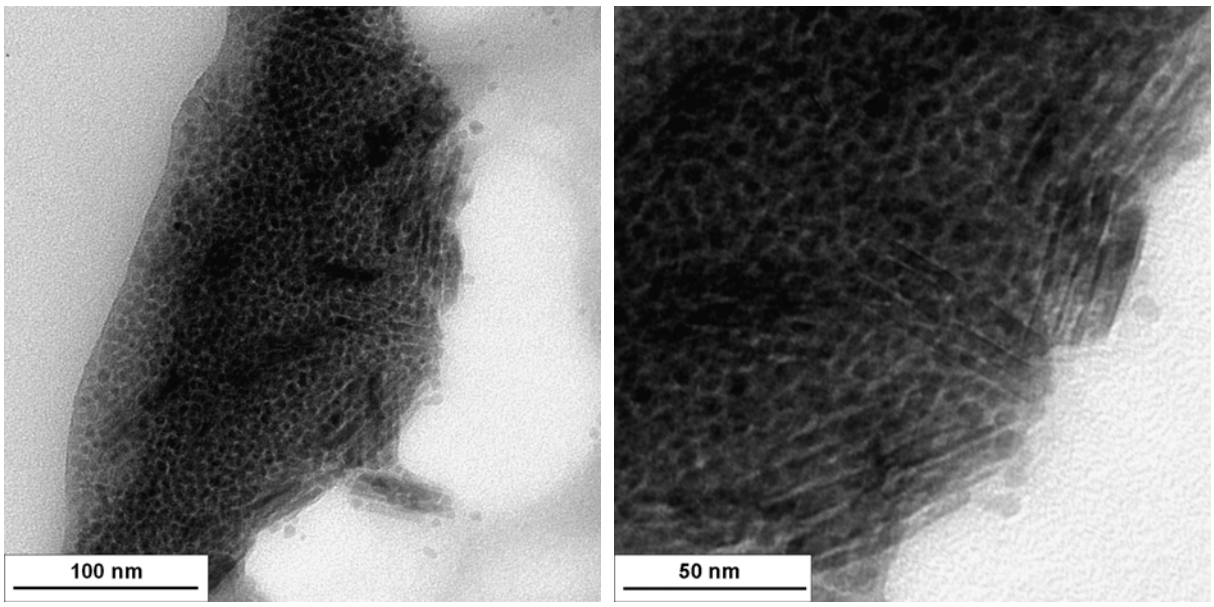

Fig. 4.14: TEM picture of sample PI3a (11.7 % SDS, 12.5 % oleic acid related to ipc) at high magnifications

a)

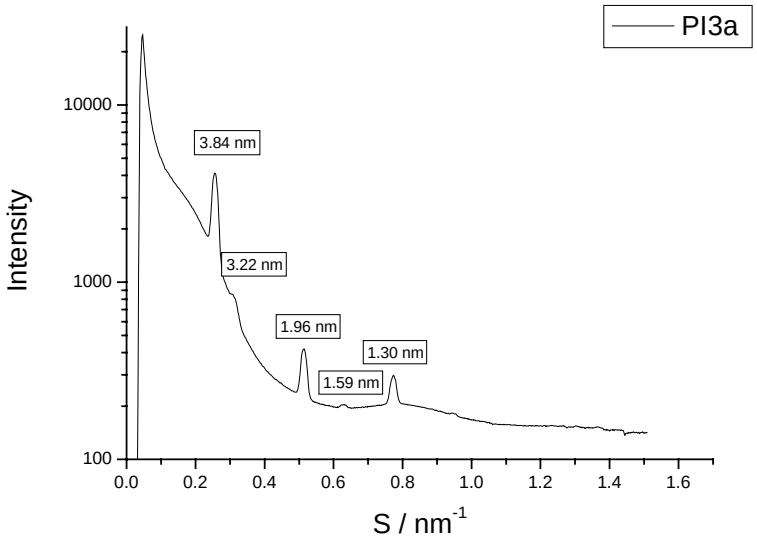

b)

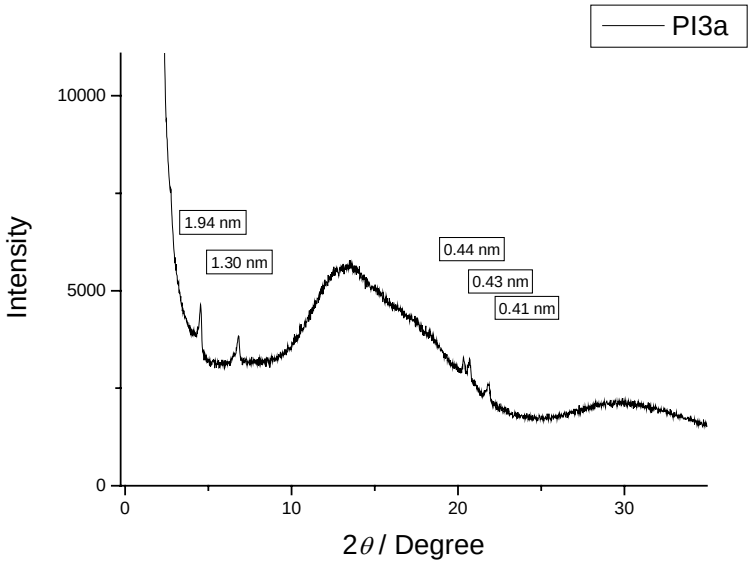

Fig. 4.15: a) SAXS and b) WAXS measurements from sample PI3a (11.7 % SDS, 12.5 % of oleic acid related to ipc)

Very similar results in the TEM image and in the SAXS and WAXS measurements were obtained for sample PI3b. This means, reducing the SDS amount from 11.7 to 4.2 % does not lead to any change in the inner structure of the material. The only change is in the iron oxide content, which, according to the TGA measurements, was decreased. This change in the iron

oxide content can possibly be explained because of some instabilization during the miniemulsion process when the SDS amount is decreased.

Increasing the amount of oleic acid, sample PI4a, which is a latex produced from iron containing monomer dispersion BMA-D4 (25.0 % oleic acid) shows a similar structure as sample PI3a, which is produced from the iron containing monomer dispersion BMA-D3 (12.5 % oleic acid). So, any change in the images is due to the increase of the oleic acid percentage (related to ipc) from 12.5 to 25.0 %. The SAXS measurement (data no shown) also reveals a lamellar structure with a repeat period of 3.9 nm if the latex was produced by a monomer dispersion where the Fe $(CO)_5$ has been decomposed for 24 h.

Totally different structures are obtained if a monomer dispersion is used which is obtained by only 2 h decomposition but not 24 h. In this case, the non-reacted iron pentacarbonyl is also removed. Sample PI3a-2hd was produced from the miniemulsion polymerization of the iron containing monomer dispersion, sample BMA-D3, that only was subjected at thermal decomposition for 2 h. The pictures in Fig. 4.16 reveal a film containing iron oxide aggregates. Therefore it can be concluded that there is a strong influence of the thermal decomposition time onto the final structure.

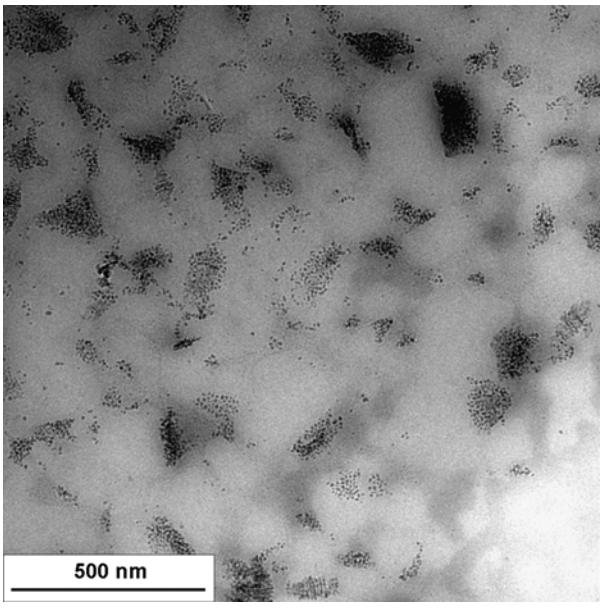

Fig. 4.16: TEM micrographs of sample PI3a-2hd after 2 h of thermal decomposition in the monomer BMA-D3 (11.7 % SDS, 12.5% oleic acid related to ipc)

When the amount of oleic acid was drastically reduced from 12.5 to 1.2 % based on ipc, as in the case of the sample PI2a, a better distribution of iron oxide was achieved and/or no crystallization was taken place throughout the thermal decomposition (Fig. 4.17). However, any affirmation can be made due to the impossibility to keep the same conditions during the thermal decomposition since decomposition time was changed from 24 to 9 h.

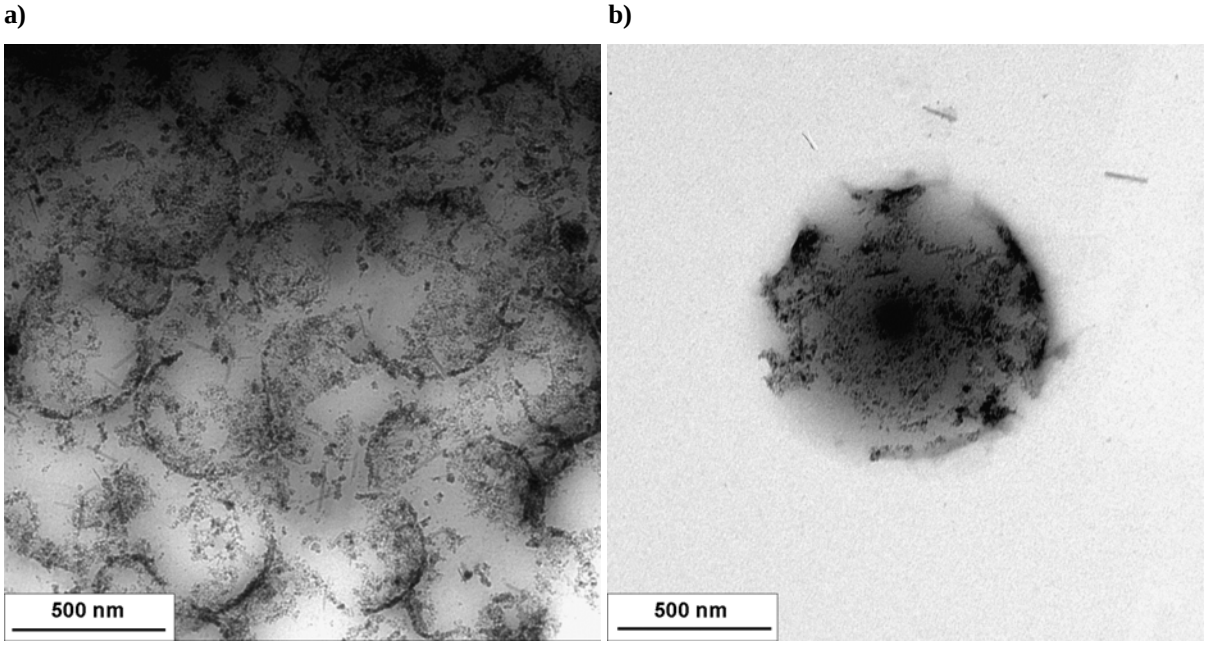

Fig. 4.17: TEM pictures of the sample PI2a (11.7 % SDS, 1.2 % oleic acid related to ipc)

In order to prove if the found mesostructure is caused by the presence of oleic acid, a miniemulsion based on a monomer-dispersion without oleic acid (BMA-D1-24h decomposition) was prepared (sample PI1a). It has to be stressed that even though the monomer dispersion shows some instability, for comparison the miniemulsion was carried out.

The SAXS measurement for the sample PI1a (Fig. 4.18a), based in iron-monomer dispersion without oleic acid, reveals again the presence of a lamellar structure with the same repeat period of 3.9 nm as shown for the other samples. However in the TEM measurements as shown in Fig. 4.19 no clear evidence of this structure was found. The WAXS measurement in Fig. 4.18b shows an amorphous material with some crystallinity. Thus, the role of oleic acid in the sample is still unclear, but potentially it is not needed at all for the formation of the lamellar structure.

a)

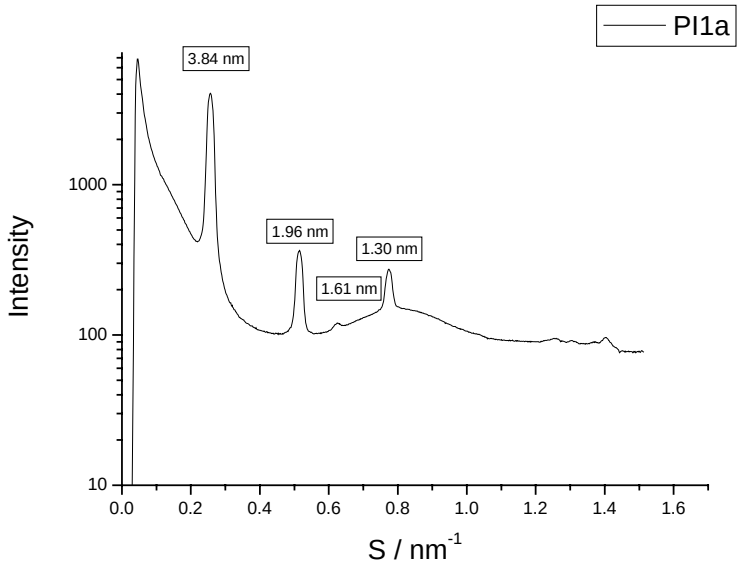

b)

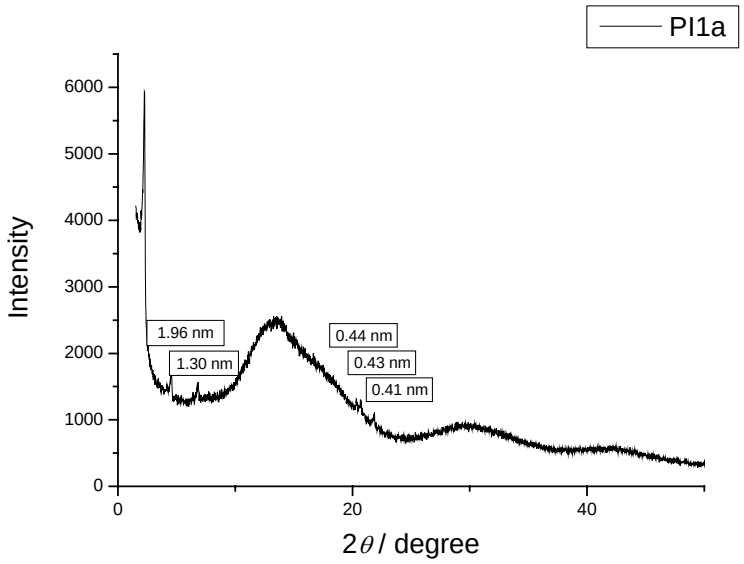

Fig. 4.18: a) SAXS and b) WAXS measurements of the sample PI1a (from BMA-D1, without oleic acid)

a) **b)**

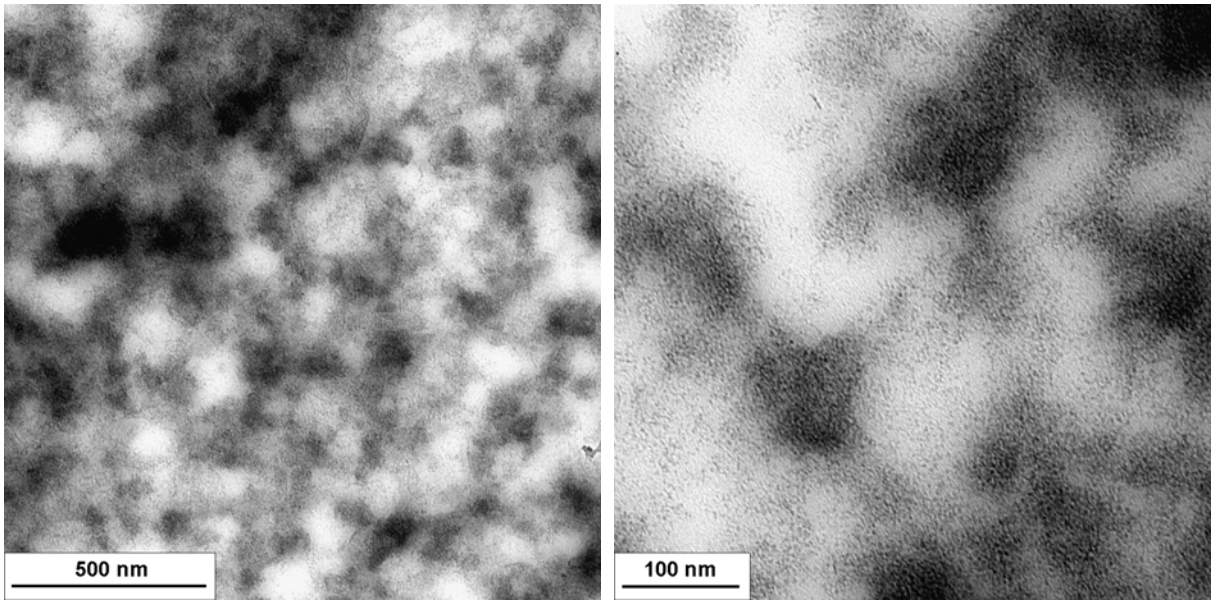

Fig. 4.19: TEM pictures of sample PI1a

As a further point, it is of importance to analyze the homogeneity of the particles after the encapsulation process. In order to visualize this homogeneity, measurements with the preparative ultracentrifugation were carried out. Through the preparative ultracentrifugation is easy to differentiate between the low density polymer phase and the high density inorganic phase. For the experiment, sucrose solutions of different densities were layered, forming a density gradient from 1.0 to 1.3 $g \cdot cm^{-3}$. The results are shown in Fig. 4.20.

Samples PI1a and PI1b are not homogeneous due to the absence of hydrophobic oleic acid molecules in the iron oxide particles which could enable the compatibility with the monomer phase. Samples PI3a and PI3b as well as samples PI4a and PI4b show very high homogeneity in the encapsulation process. These latexes shown a narrow density distribution that is adjusted to the 1.1 $g \cdot cm^{-3}$ density layer. No free iron oxide and no free poly(butyl methacrylate) nanoparticles can be seen observed.

For all of the samples in Fig. 4.20, no strong influence on the encapsulation homogeneity with the decrease of surfactant was found which corresponds nicely with the TEM pictures.

PI1a	PI1b	PI3a	PI3b	PI4a	PI4b
11.7 % SDS	4.2 % SDS	11.7 % SDS	4.2% SDS	11.7 % SDS	4.2% SDS
Without oleic acid		12.5 % oleic acid related to ipc		25.0 % oleic acid related to ipc	

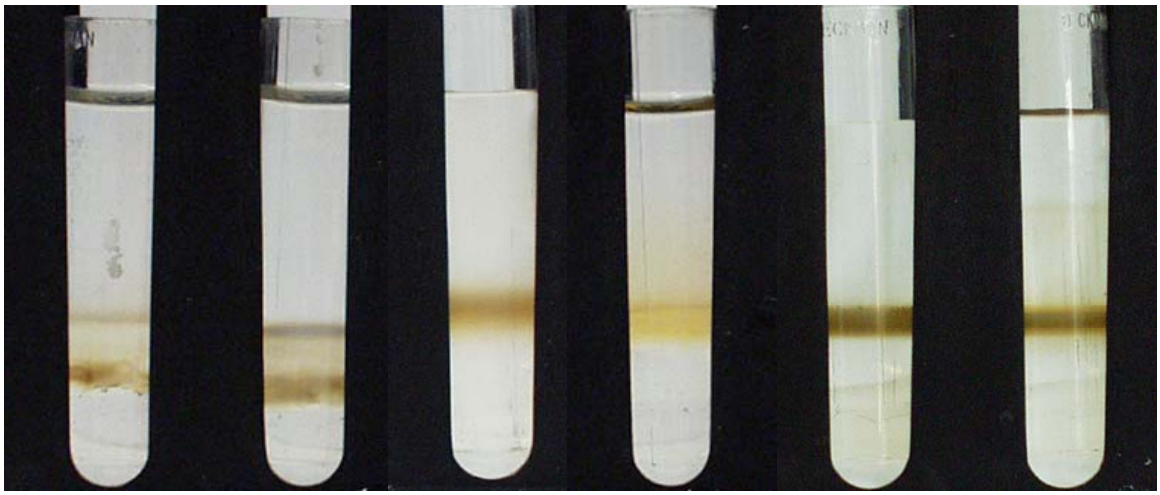

Fig. 4.20: Ultracentrifuge experiments in a density gradient

4.2.3 Magnetic properties

The magnetic measurements of the latex after the miniemulsion polymerization show in all of the samples a diamagnetic behavior which is possibly due to the fact that the diamagnetism both of the water phase and the poly(butyl methacrylate) is bigger than the paramagnetism of the iron oxide. Therefore, to avoid this diamagnetism influence, the magnetic properties were measured on dried samples. The magnetization curve is shown in Fig. 4.21. The sample PI1a with only 2.2 % of iron oxide is diamagnetic. In this case the diamagnetic polymer contributes preferentially in the behavior of the iron containing nanocomposites. Sample PI3a and PI4a, with 10.3 and 14.1 % of iron oxide respectively, show paramagnetic behavior under an external magnetic field. In spite of the presence of iron oxide nanoparticles, the magnetic dipole within the iron oxide nanoparticles is very weak. From the magnetization measurements, the existence of magnetic iron oxide into the nanocomposites is proven.

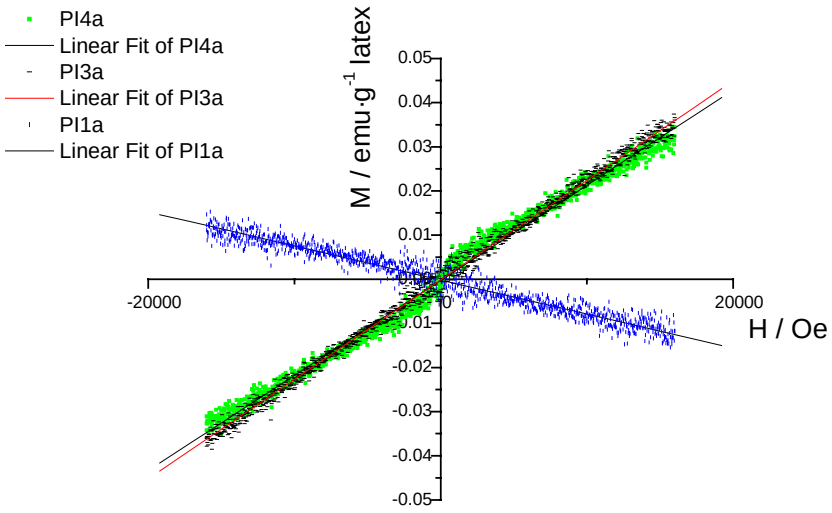

Fig. 4.21: Magnetic measurements of the samples PI1a, PI3a and PI4a

The specific magnetization and the mass magnetic susceptibility are shown in Table 4.6. The small negative value of mass magnetic susceptibility reveals again the diamagnetic of the samples PI1a and the positive ones the paramagnetic behavior of the samples PI3a and PI4a.

Table 4.6: Magnetic properties of the iron containing nanocomposites

Sample	Specific magnetization _____ $emu \cdot g^{-1}$ dried sample	Mass susceptibility magnetic χ _____ $emu \cdot Oe^{-1}\ g^{-1}$ dried sample
PI1a	-0.012	-7.72×10^{-7}
PI3a	0.035	2.25×10^{-6}
PI4a	0.032	2.15×10^{-6}

4.3 Gadolinium-based nanoparticles

This section presents the results and discussion concerning with the research approach used for the preparation of new nanolayered composites consisting of poly(butyl acrylate) (PBA) and organic-soluble lanthanide chelates by miniemulsion process. Just by the miniemulsion process and in a very simple way, nanolayered composites are formed. It should be stressed that the most common way to produce nanolayered composites consisting of inorganic and polymer is by templating process (see section 2.5.2). These layered nanocomposites present paramagnetic behavior and a very high relaxivity, as shown in the magnetization and NMR relaxation measurements, respectively. The term "layered nanocomposites" and "nanolayered composites" are used synonymously.

4.3.1 Nanostructured composites

Here, we describe the polymerization of butyl acrylate in presence of different lanthanide complexes and analyze the resulting structures mainly with transmission electron microscopy (TEM), small angle X-ray scattering (SAXS), and thermogravimetry analysis (TGA). It will turn out that all systems form highly organized lamellar nanocomposites with a spin rich lanthanide subphase where the repeat period is of the order of 3-4 nm.

The composition of the samples discussed in this section is summarized in Table 4.7. All polymerization reactions occur analogous to those of the pure monomer; especially, no destabilization or macroscopic demixing throughout polymerization is obtained.

Table 4.7: Characteristics of the prepared samples in miniemulsion after polymerization.

Sample	Mol-ratio mmol BA / mmol $Gd(tmhd)_3$	Diameter nm	Solid content %
PGd-4	55.2	184	14.9
PGd-5	27.9	164	8.6
PGd-1	9.3	256	9.3
PGd-Lu-1	9.3	219	14.3
PGd-2	6.1	363	1.8
PGd-3	3.2	a)	a)
PAl	15	190	18
PSm	9.1	330	6.0
PEu	9.1	203	7.3
PHo	9.3	203	12.1
PLa	8.9	a)	a)
PNd	9.1	250	7.3

a) Aggregation during the polymerization

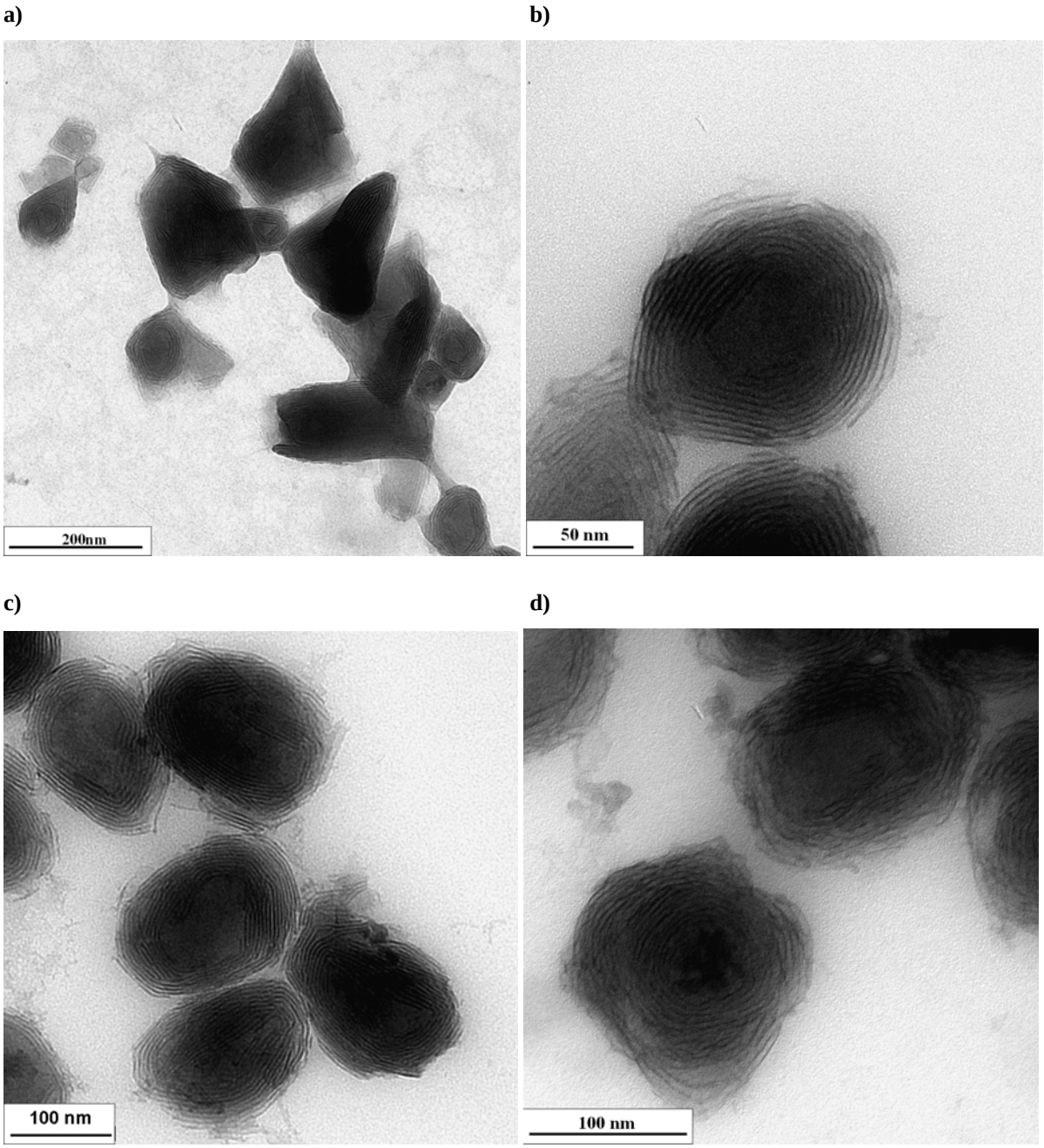

Fig. 4.22: TEM of the resulting nanocomposites a), b),and c) PGd-1 with 15 min preheating and d) PGd-1 without preheating)

Fig. 4.22 shows typical TEM picture of sample PGd-1. One can clearly identify the onion-like and/or tart-like structure of a layered nanocomposite in the case of the preheated sample. If no preheating of the monomer/Gd-chelate was performed the structure is less defined as depicted in Fig. 4.22c). As the apparent layer distance depends on the direction of projection, one cannot determine quantitatively the lamellar repeat period from such pictures. Due to the stiffness and

lacking bendability of the layers, the otherwise spherical nanoparticles deform to polyhedral objects.

To quantify the overall order, SAXS measurements were performed both on the starting mixture as well as on the final nanoparticles (Fig. 4.23). At least four of the peaks of the reaction mixture prior to polymerization can be attributed to a highly ordered lamellar phase with a repeat period of 3.46 nm. The peak at 1.45 nm cannot be attributed to the lamellar arrangement and characterizes presumably the in- plane order between different electron rich Gd-centers.

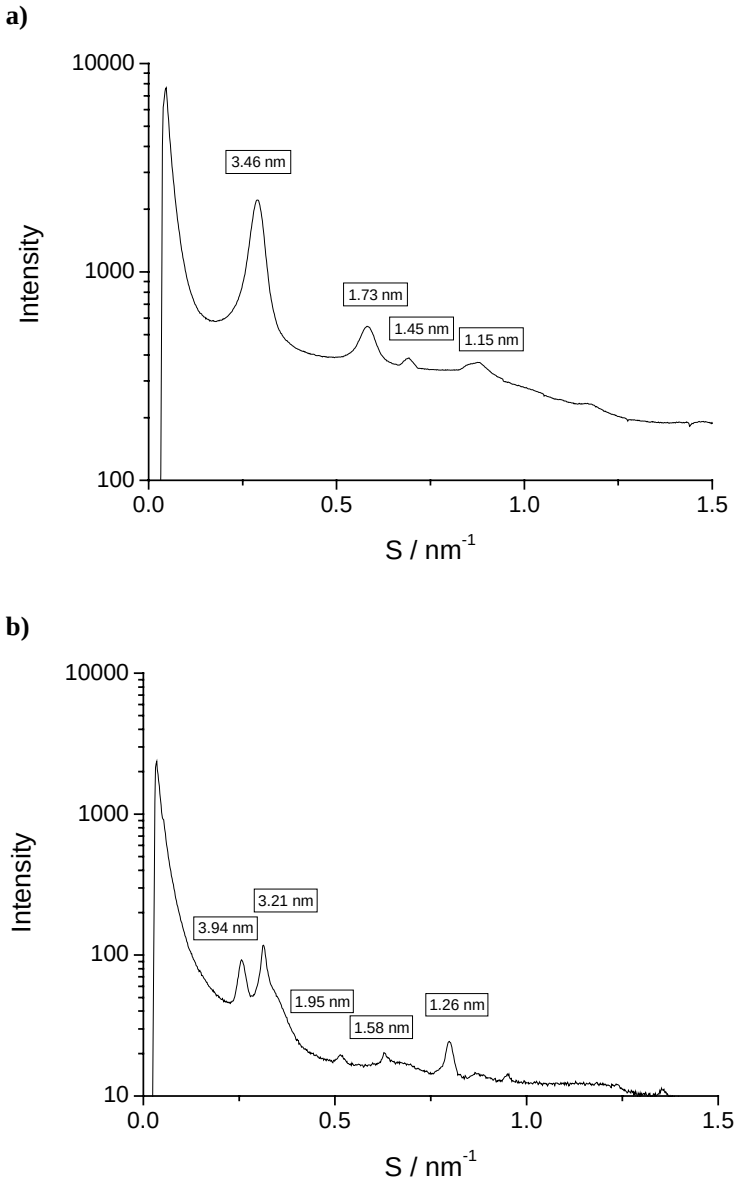

Fig. 4.23: SAXS measurement of PGd-1 a) before; and b) after polymerization.

If we vary the composition of the mixture, (series PGd-1 to PGd-5), the scattering curves of the reaction mixtures change, but the primary peak is essentially not moved (Fig. 4.24). This clearly underlines that the observed order it is not due to a continuously swellable lyotropic phase, but due to a well defined complex between lanthanide complex and butyl acrylate. As the SAXS order is maximal for PGd-1, we can assort its composition to be close to the optimal composition of the complex phase (9 mmoles of BA to 1 mmole of the lanthanide complex).

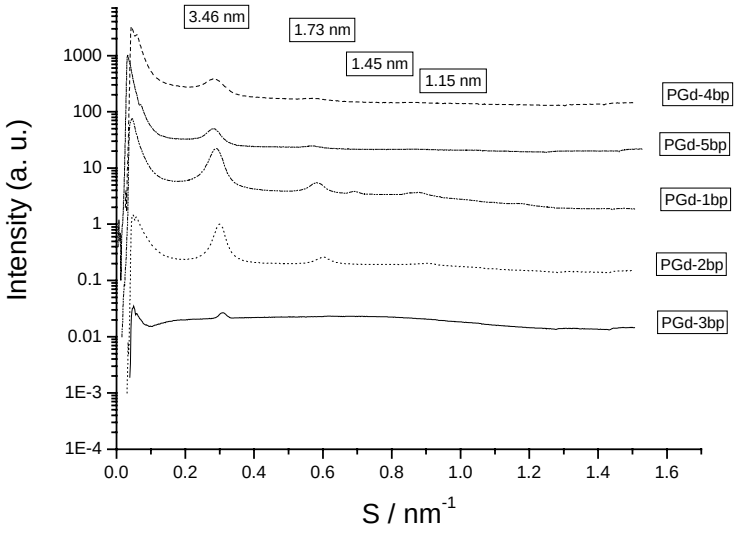

Fig. 4.24: SAXS measurements of the samples before polymerization (the abbreviation *bp* denotes "before polymerization")

Cerius modeling of the complex structure (Fig. 2.7) reveals that the three bidentate ions are located on one side of the complex, keeping the other half-space open for the secondary binding. This would back up a bilayer structure of the Gd-complexes, with a calculated thickness of the Gd phase of around 1.25 nm. With a relative weight ratio of 0.37 for the Gd-phase (from stoichiometry), an overall repeat period of ca. 3 - 4 nm is calculated (depending on the density), indicating that the local structure indeed reflects the outer reaction stoichiometry. For other compositions, the system decomposes to pure nanocomposite and pure polymer particles.

The scattering of the system after polymerization (Fig. 4.23) is more complicated and can be interpreted as the coexistence of two lamellar phases in different nanoparticles with lamellar repeat periods of 3.94 nm and 3.21 nm, respectively. This is speculatively attributed to the destabilization of the complex by polymerization, which however is kept trapped close to its original state.

WAXS indicates the absence of any crystallinity in the nanocomposites, but also shows a sequence of three broadened peaks, which indicate the mutual 2d-order between the electron-rich Gd-centers. From the peak position, we can calculate a distance of 0.65 nm, which goes well with the estimated diameter of the inert inner shell Gd-complex. This means that the Gd-centers are indeed organized within the visible layers, presumably in a bilayer-like-square-planar fashion.

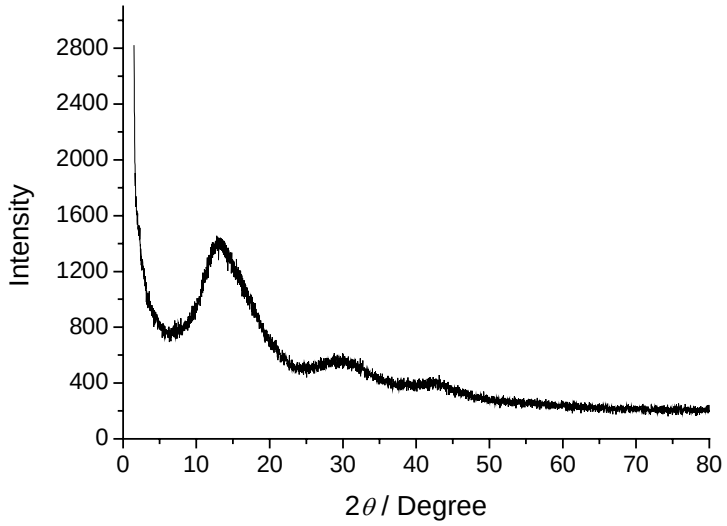

Fig. 4.25: WAXS of sample PGd-1

The fact that this special type of order is indeed typical also for other lanthanides beside Gd is proven with the samples listed in Table 4.7 where at fixed, near optimal concentration the metal center was varied. For Al (with no accessible f-Orbitals), formation of a nanocomposite fails. The complex dissolves in the monomer at elevated temperatures beyond 70 °C, but also polymerization at 95 °C only results in demixing throughout polymerization and consecutive

aggregation. Also lanthanum (III), with no outer electrons, does form a stable monomer mixture at higher temperatures, but forms unstable precipitates throughout polymerization.

All the other metal centers show similar layered nanocomposite morphologies as the Gd complex, as presented in Fig. 4.26. The europium-based poly(butyl acrylate) nanoparticles have an elongated layer-by-layer structure (Fig. 4.26a). The europium complex is fluorescent, and this property is still found for the final Europium-based poly(butyl acrylate) latex. Opposite to most other systems, the Eu-nanohybrid particles do spontaneously transfer to form a coloured, but transparent film, indicating a weaker binding between polymer and complex layers.

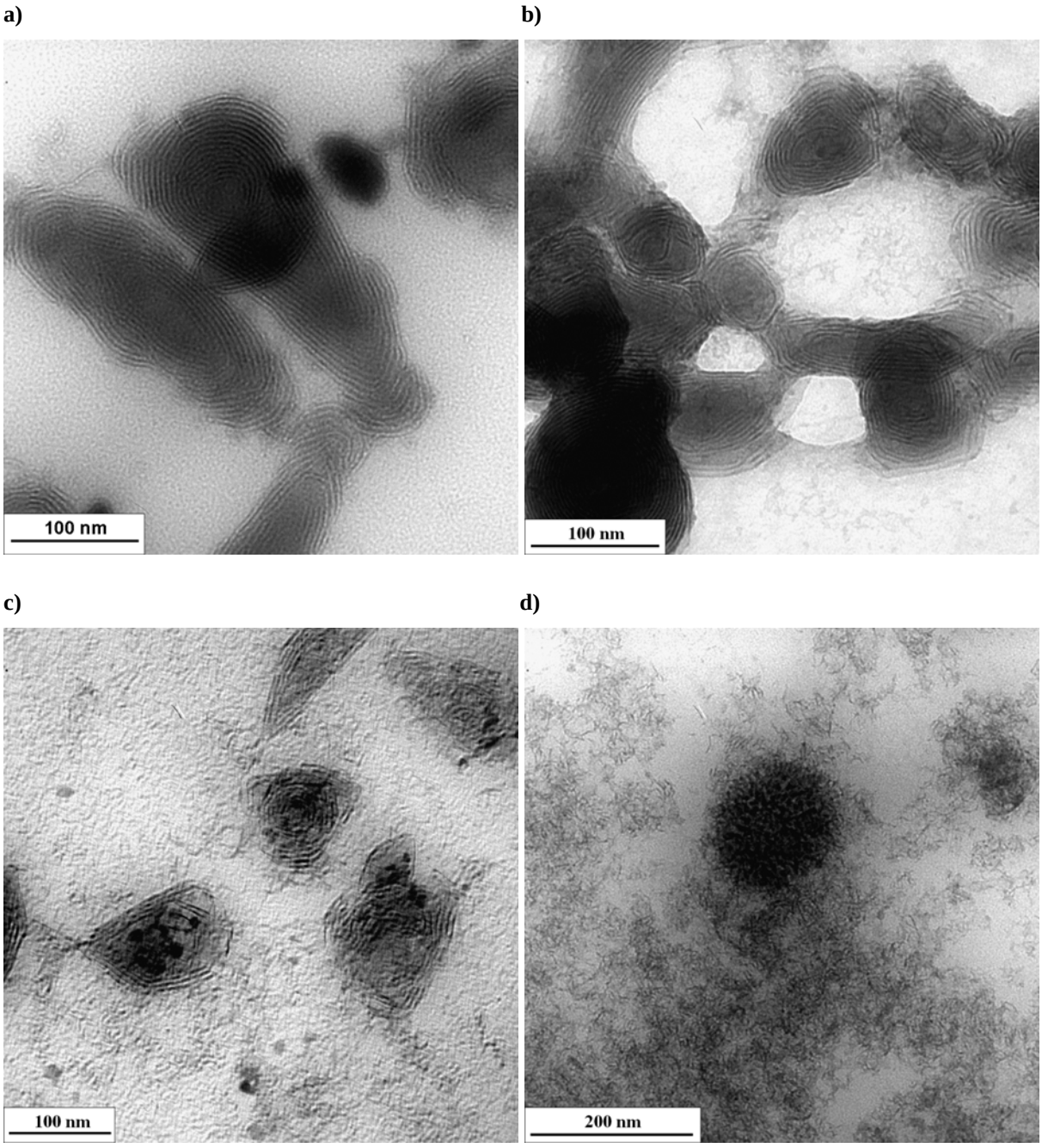

Fig. 4.26: TEM pictures of different lanthanide nanocomposites: a) $Eu(thmd)_3$@PBA; b) $Sm(thmd)_3$@PBA; c) $Nd(thmd)_3$@PBA; d) $Ho(thmd)_3$@PBA.

In addition, the Eu-complex with poly(butyl acrylate) is soluble in THF, and GPC reveals a molecular weight of 586,000 $g \cdot mol^{-1}$, in good agreement with an unperturbed radical polymerization process for the butyl acrylate monomers. The samarium (Fig. 4.26b) and the neodymium (Fig. 4.26c) structures are very similar to the gadolinium structure; no transparent

film is formed from their nanoparticles (and no dissolution found), as the polymer layers are obviously highly cross-linked by the complexes. The holmium-structure (Fig. 4.26d) is different: the nanoparticles are easily coalesce towards transparent films, and in the film, regular pattern with smaller dimensions and lower correlation lengths are found. Microphase separation and nanocomposite formation still occurs, but the complex layers exhibit lower stability and persistence.

Variation of the monomer leads to a better understanding of the underlying organization process: employment of the long chain analogue lauryl methacrylate (Fig. 4.27) reveals very similar structures indicating that binding towards the lanthanide centers occurs via the ester carbonyls. Styrene, on the other hand, allows easy dissolution of the complexes (by metal-π-interactions) and the fabrication of latexes with very high spin and nuclear momentums, but the structure stays molecularly mixed and does not self-organize, presumably due to missing amphiphilic contrast.

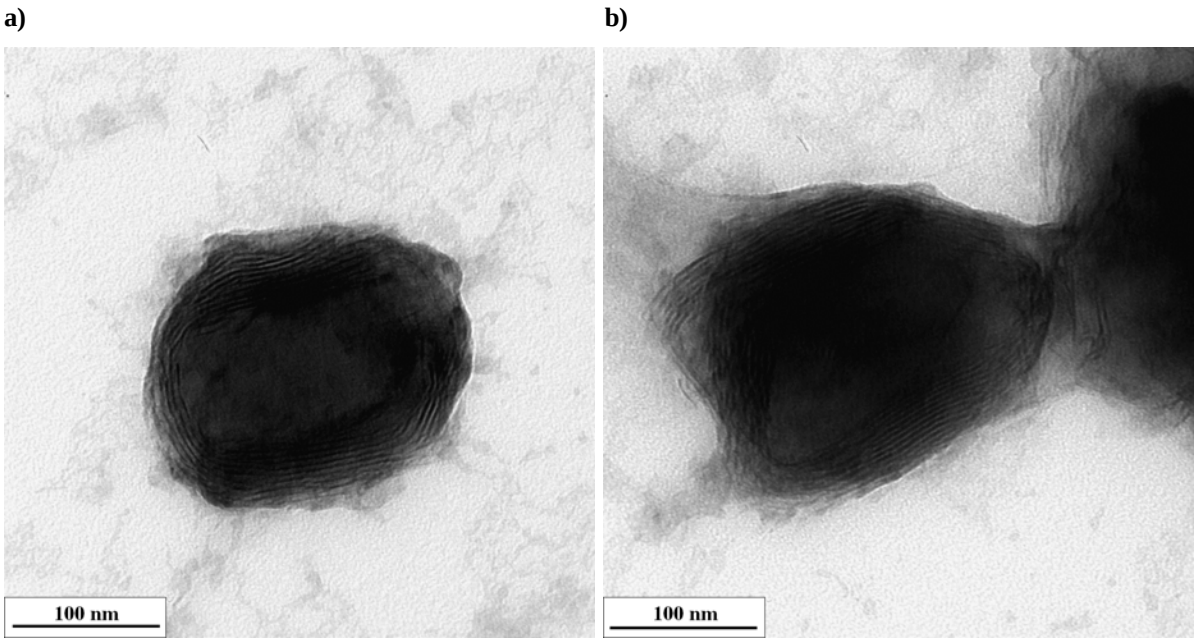

Fig. 4.27: TEM micrographs of the LMA sample.

It is important to note that using a non-ionic surfactant (in this case Lutensol AT50) in the miniemulsion process does not effect the final polymer structure. No layered nanocomposites

were found after the miniemulsion polymerization as reflected in the SAXS measurements (data no shown) and in the TEM pictures of the sample PGd-Lu-1 (Fig. 4.28). The use of a steric surfactant which acts preferential in the water polymer interface do no enable the formation of layered materials and on the contrary favors the aggregation of the Gd-chelate in the interface without having no negative effect in the stabilization of the final particles.

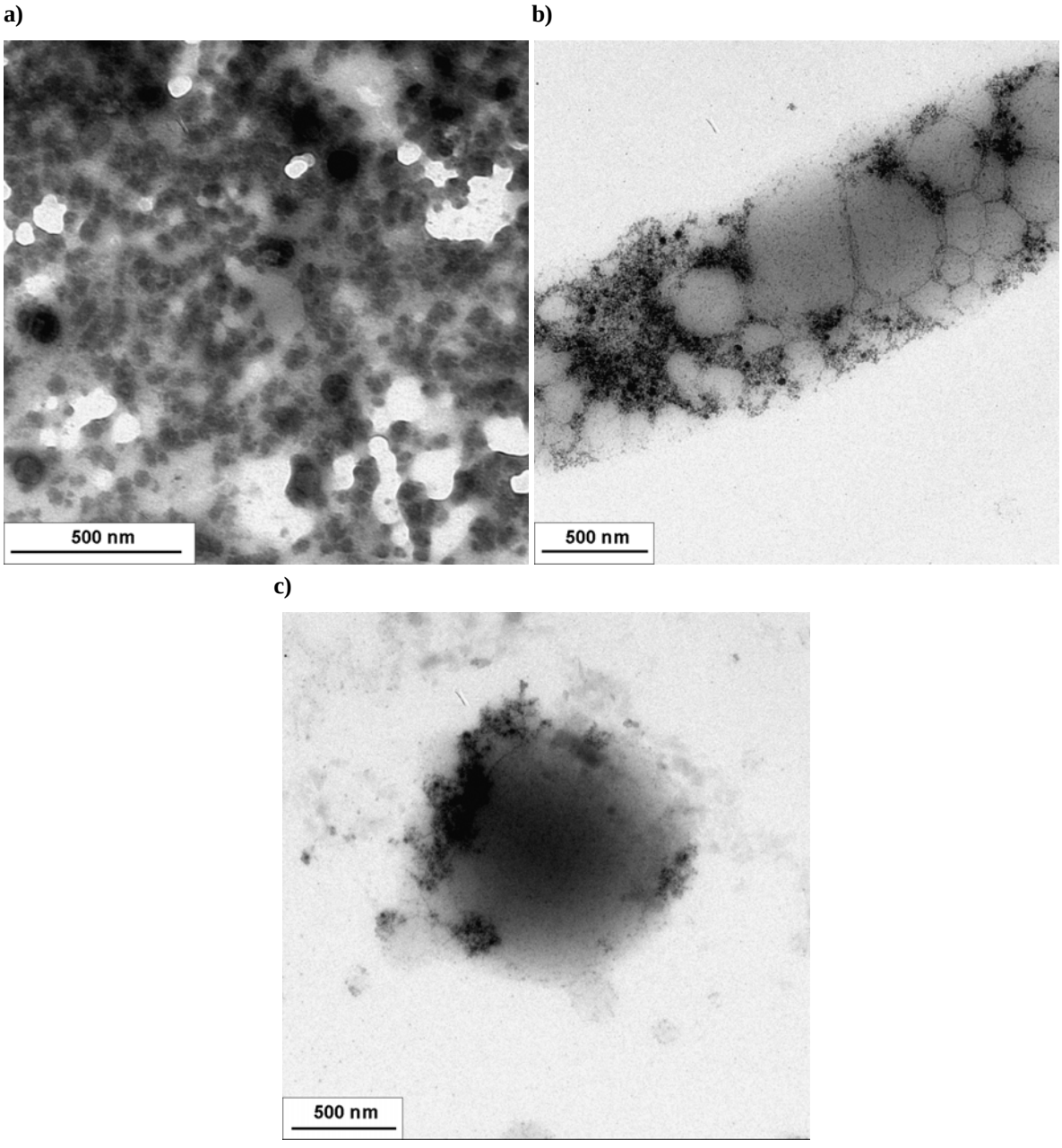

Fig. 4.28: TEM micrographs of the sample PGd-Lu-1

4.3.2 Magnetic properties

The sample PGd-1 and PGd-5 (latexes) show paramagnetic behavior in the magnetic measurements at room temperature, it means, linear increase of the magnetization with the increase of the magnetic field and without hysteresis loop (Fig. 4.29).

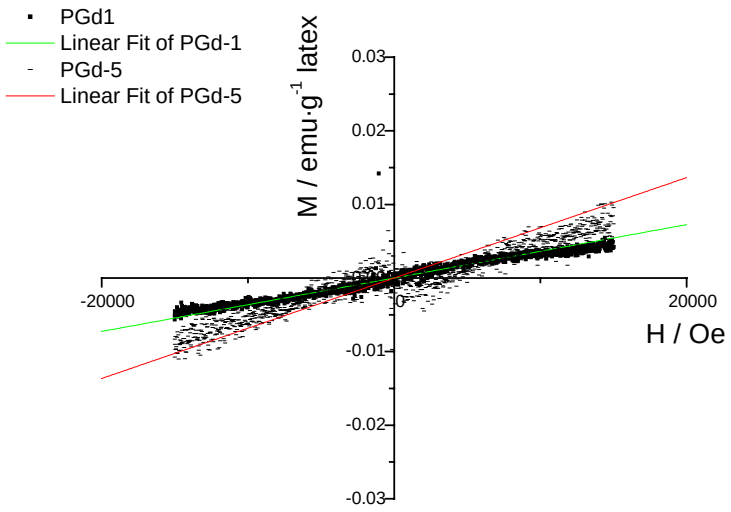

Fig. 4.29: Magnetization curve of the layered nanocomposites

The samples show small and positive mass magnetic susceptibility (see Table 4.8). In spite of the presence of poly(butyl acrylate) in the nanocomposites, the sample carrier for the VSM measurements and the small magnetic moments, the layered nanocomposites is "positively susceptible" to magnetization by a external magnetic field because the strong effect of the unpaired electron spins of the Gadolinium. The paramagnetic behavior allows the future use of these nanocomposites as magnetic resonance imaging contrast agent.

Table 4.8: Magnetic properties of the layered nanocomposites

Sample	Specific magnetization	Mass magnetic susceptibility χ
	$emu \cdot g^{-1}$ latex	$emu \cdot Oe^{-1}\ g^{-1}$ latex
PGd-1	0.0045	$3.63\ 10^{-7}$
PGd-5	0.0050	$2.66\ 10^{-7}$

4.3.3 Relaxation measurements

Paramagnetic properties are a necessary but no sufficient condition for using a compound as contrast agent in the magnetic resonance imaging. Relaxation effects depend on the proximity of nucleus and the paramagnetic molecule, among other parameters. Spin-lattice relaxation time of the water protons is always carried out in order to verify the possibility of using water-soluble paramagnetic compounds in the magnetic resonance imaging. However, it would be more interesting to investigate the proton relaxation of the water nearby the hydrophobic paramagnetic material, in this case the layered nanocomposites consisting of poly(butyl acrylate) and $Gd(tmhd)_3$. In this section for first time the spin-lattice relaxation of water protons in the presence of hydrophobic paramagnetic species which are encapsulated in polymer is presented.

As mentioned before, the addition of paramagnetic compounds such as Gd^{3+} complex can reduce the spin-lattice relaxation. In this section, the effect of $Gd(tmhd)_3$ on the T_1 relaxation of water protons of the polymer latexes using SDS as surfactant for stabilization of the miniemulsions is studied.

In the Table 4.9, the T_1 relaxation time for the sample PGd-1 at two different dilutions are shown.

Table 4.9: T_1 relaxation time of the water protons of the sample PGd-1 at different dilutions

Sample	Dilution	T_1 / ms
PGd-1	1:10	23
PGd-1	1:100	76
Pure water	-	1000

For a 1:10 dilution of the sample PGd-1 a T_1 relaxation time of 23ms was found. For the same mole mass for a water soluble gadolinium complex in 1:10 dilution a value of 120 ms is obtained. A stronger relaxation of the water protons occurs in the nanolayered nanocomposites containing hydrophobic Gadolinium chelate. When the this latex was again 10-fold diluted, a 3-fold increase in the relaxation time was measured. From the relaxation measurements, no significant influence of the water environmental in the latexes is found. This phenomenon can be due to the localization of the gadolinium within the polymer particles, without substantial contact with the water. The contact with the water is presumably at the particle.

Based on the mentioned theories, the small increase in water relaxation time with the dilution is explained in term of the chemical and/or physical interactions between the gadolinium nuclei within the polymer and the water molecules. There is no doubt that the monomer has very strong influence in the formation of the high structured nanocomposites. Coordination of carbonyl group and Gd nuclei is possible (Fig. 4.30).

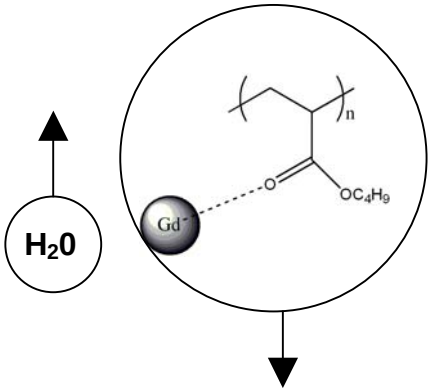

Fig. 4.30: Schematic representation of the quasi-inner-sphere coordination between carbonyl group of poly(butyl acrylate) and Gd nuclei. At the same time, this quasi-inner-sphere complex interacts with the water in the so-called outer-sphere mechanism

In our system, the quasi-inner-sphere mechanism consists in the chemical interaction between gadolinium nuclei and the polymer. There is no direct interaction of the gadolinium with the water because of the hydrophobicity of the chelate. The outer-sphere mechanism consists in the interaction of the nanolayered composites with the water (Fig. 4.30). From NMR relaxation measurements of the nanolayered latexes at different dilutions, a small influence of the amount of water on the water relaxation time has been observed, showing that the quasi-inner-sphere mechanism is likely to be the strongest.

5 Conclusions and Outlook

In the first work presented in this thesis, it was shown that the encapsulation of high amounts of magnetite particles into polystyrene particles can efficiently be achieved by a new three-step preparation route including two miniemulsion processes. In the first step, oleic acid coated magnetite particles in octane are prepared. In the second step, a dispersion of the magnetite in octane is miniemulsified in water by using SDS as surfactant. After evaporation of the octane, the magnetite aggregates which are covered by a oleic acid/SDS bilayer were mixed with a monomer miniemulsion and in the third step of the synthesis route, a ad-miniemulsification process is used to obtain final and full encapsulation. Here, a fusion/fission process induced by ultrasound is just effective for the monomer droplets, whereas the monomer coated magnetite aggregates stay intact. That way, all monomer droplet are split and heteronucleated onto the magnetite aggregates to form a monomer film. After polymerization, polymer encapsulated magnetite aggregates were obtained. Characterization by thermogravimetry, preparative ultracentrifugation, and transmission electron microscopy showed that up to 40 % magnetite could be encapsulated, resulting in particles with a high homogeneity of the magnetite content. Magnetometry measurements reveal that the magnetite aggregates still consist of separated superparamagnetic magnetite particles which is due to the coverage by the oleic acid. During the encapsulation process, 60 % of the magnetization compared to bulk magnetite is still preserved.

Secondly, it was shown the approach to fabricate novel iron oxide containing nanocomposites with lamellar structure and by a two-step process including miniemulsion polymerization. The first step consisting of the decomposition of iron pentacarbonyl using oleic acid as stabilizer was used to obtain an iron containing monomer dispersion which is used in the second step for the miniemulsion polymerization. The miniemulsion polymerization of the iron oxide

containing monomer-dispersion with different concentration of oleic acid enables the production of either nanocomposites which have discrete iron oxide nanoparticles throughout distributed in the polymer particle or eye-like nanocomposites which contain demixing phases, one consisting of discrete iron oxide nanoparticles in a lamellar arrangement and the other one the poly(butyl methacrylate), depending on the amount of oleic acid used for the thermal decomposition. Magnetic measurements showed the paramagnetic behavior of the final nanocomposites and the potential used as contrast agent for magnetic resonance imaging.[124]

Finally, the spontaneous formation of nanohybrid materials made from a ligating monomer and closed-shell lanthanide complexes is presented. The resulting structures seem to be well defined with respect to stoichiometry, and are highly organized towards lamellar structures due to a combination of amphiphilic contrast and -potentially- spin coupling. Relaxations as well as magnetometry results shown that these new layered nanocomposites are paramagnetic and possesses a very high relaxivity of the water protons. The as-synthesized particles can have direct applications as magnetic and X-ray contrasting agents,[134] or for radioembolization therapy.[135]

The influence of the temperature and composition on the magnetic behavior of these systems as well as the T_1 relaxation time depending on the composition at different dilutions has to be explored in future work

6 Experimental Section

6.1 Water based-ferrofluid containing magnetite polystyrene nanoparticles

Materials

Ferric chloride anhydrous ($FeCl_3$) and ferrous chloride tetrahydrate ($FeCl_2 \cdot 4H_2O$) were purchased from Fluka. Ammonium hydroxide (28-30 % NH_3), octane (98 %), hexadecane (99 %), sodium dodecyl sulfate (SDS), cholic acid sodium salt, potassium peroxodisulfate (KPS), lecithin, Tween 80, and oleic acid (90 %) were purchased from Aldrich and used as received.

The monomers acrylic acid and styrene from Aldrich were distilled under reduced pressure before use.

Synthesis of hydrophobized magnetite nanoparticles

According to ref. [], the magnetite particles were produced by coprecipitation from an aqueous Fe^{3+} / Fe^{2+} solution (ratio 3:2) using concentrated ammonium hydroxide in excess. The particles were subsequently coated with oleic acid:

14.6 g of $FeCl_3$ and 12.0 g of $FeCl_2 \cdot 4\,H_2O$ were dissolved in 50 ml distilled water. 40 ml of ammonium hydroxide were added rapidly. After coprecipitation of magnetite particles, oleic acid (for quantities see Table 4.1) was added, and the suspension was heated to 70 °C for 30 min. Then, the temperature was increased to 110 °C in order to evaporate water and excess of ammonium. The black lump-like residuum was cooled to room temperature and washed several times with distilled water. After drying, a powder was obtained.

Octane / magnetite dispersion and water-based ferrofluid

1.0 g of oleic acid containing magnetite powder as received above was added to 6.0 g of octane with or without hexadecane (for details see Table 4.1) to form a dispersion of hydrophobized

magnetite in octane as carrier medium. This dispersion was added to a solution consisting of 24 g water and SDS (for quantities see Table 4.1). After mixing for 1 h at 500 rpm, the mixture was subjected to sonication twice for 2 min at 90 % amplitude with a Branson sonifier W450 digital in an ice-cooled bath. After carefully evaporating the octane at 80 °C for 6 h while adding every 30 min approximately 2 ml of water to compensate the evaporation of water, a stable water-based ferrofluid is obtained. For the use of biosurfactant, it was choice the conditions of the sample Mag-10 but using sodium salt of cholic acid, lecithin and Tween 80.

Polymer encapsulation

A styrene miniemulsion was prepared using the following recipe: 6.0 g of styrene and 250 mg of the hydrophobic agent hexadecane were added to a surfactant solution consisting of 72 mg of SDS dissolved in 24 g of water. After stirring 1 h for pre-emulsification, the miniemulsion was obtained by sonication for 2 min at 90 % amplitude in an ice-cooled bath.

For the encapsulation, the styrene miniemulsion and the water-based magnetite dispersions as obtained above were combined and co-sonified twice for 1 min at 50 % amplitude in an ice-cooled bath. Magnetite powder to monomer ratios of 4:1, 2:1, 3:2, 1:1, 7:8, 3:4, 1:2, 1:4, and 1:8 (for details see Table 4.1) were employed. To start the polymerization, 20 mg of KPS were added, and the temperature was increased to 80 °C; after 40 min 30 mg of acryl acid were added. The polymerization time was between 18 and 24 h.

6.2 Nanostructured composites from iron pentacarbonyl decomposition

Materials

Iron pentacarbonyl (ipc), $Fe(CO)_5$ (purum, >> 97% (Fe)), was purchased from Aldrich and filtered before used. Sodium dodecyl sulfate (SDS) oleic acid (90%), and butyl methacrylate (BMA) (99%), hexadecane (99%), 2,2'-azo(2-methylbutyronitrile) (V59) were purchased from Aldrich and used as received. Distilled water was used in all the experiments.

Thermal decomposition in the monomer phase

2 g of iron pentacarbonyl and the quantity of oleic acid (for quantities see Table 4.4) and 4 g of butyl methacrylate were mixed and subjected in a three-neck flask to agitation at 250 rpm, at a temperature of 110 °C under atmospheric pressure. After 9 h or 24 h (for details see Table 4.4), depending on the oleic acid concentration, an iron containing monomer dispersion was obtained.

Nanocomposite particles after miniemulsion polymerization

A miniemulsion polymerization was performed from the iron monomer dispersion that was obtained before. The organic phase consisting of 0.5 g of iron containing monomer dispersion as received above, 0.030 g of hexadecane and 0.040 g of V59 were mixed with the water phase consisting of a solution of 4.5 g of water and either 11.7 or 4.2 % of SDS (for more details see Table 4.5). After stirring 1 h for pre-emulsification, the miniemulsion was obtained by microsonication using a microtip for 2 min (each 5 s a pause of 10 s) at 70 % amplitude with a branson sonifier W450 digital in an ice-cooled bath. For the polymerization, the temperature was increased to 80 °C. The polymerization was carried out for 24 h.

6.3 Gadolinium-based nanocomposites

Materials

Gadolinium tris(2,2,6,6-tetramethyl-3,5-heptanedionate) ($Gd(tmhd)_3$), europium tris(2,2,6,6-tetramethyl-3,5-heptanedionate) ($Eu(tmhd)_3$), samarium tris(2,2,6,6-tetramethyl-3,5-heptanedionate) ($Sm(tmhd)_3$), holmium tris(2,2,6,6-tetramethyl-3,5-heptanedionate) ($Ho(tmhd)_3$), and lanthanium tris(2,2,6,6-tetramethyl-3,5-heptanedionate) ($LA(tmhd)_3$) were purchased from Strem. Hexadecane (99 %), sodium dodecyl sulfate (SDS), V59 (2,2'-azo(2-methylbutyronitrile)) were purchased from Aldrich and used as received. The monomers butyl

acrylate (BA) and lauryl methacrylate (LMA) and methyl methacrylate (MMA) from Aldrich were distilled under reduced pressure before use. Distilled water was used for all experiments. Lutensol AT50 (C_{16}-C_{18}-fatty alcohol with a ethylene oxide block length of about 50 units) was purchased from BASF AG.

Synthesis of the nanoparticles

For polymerization, the technique of miniemulsion polymerization was employed to result in nanoparticles which are easier to analyze. A monomer miniemulsion was prepared using the following recipe: the amount of lanthanide chelate given in Table 4.7 were dissolved in 0.5 g of monomer (butyl acrylate or lauryl methyl acrylate) at 72 °C and subjected to a preheat at the same temperature for 15 min. Then the 0.030 g of hexadecane, and 0.040 g of V59 were added at room temperature to a surfactant solution consisting of surfactant dissolved in 4.5 g of water and 0.066 g of SDS (or Lutensol AT50). After stirring 1 h for pre-emulsification, the miniemulsion was obtained by microsonication for 2 min (each 5 s a pause of 10 s) at 70 % amplitude with a Branson sonifier W450 digital in an ice-cooled bath. To start the polymerization, the temperature was increased to 72 °C. The polymerization time was between 10 and 12 h.

7 Methods

DynamicLlight Scattering (DLS)

The particle size was determined using a Nicomp particle sizer (Model 370, PSS Santa Barbara, CA) at a fixed scattering angle of 90°.

Gel Permeation Chromatography (GPC)

Gel permeation chromatography was used to obtain the weight-average molecular weight of the polystyrene in the magnetite/polymer nanoparticles. A thermo-separation products' GPC equipment with a polyester without reactive functional groups as column packing (PSS GRAM column) was used. The GPC separation was carried out at 70 °C, with a flow rate of 0.7 $ml \cdot min^{-1}$, with *N*-methylpyrrolidone as mobile phase and with a UV detector operating at 270 nm. To obtain the weight-average molecular weight of the poly(butyl methacrylate) in the iron containing poly(butyl methacrylate) latex, a column consisting of polystyrene divinylbencene packing (MZ-Analysentechnik) was used. The GPC separation was carried out at 70 °C, with a flow rate of 0.7 $ml \cdot min^{-1}$, with tetrahydrofuran (THF) as mobile phase and with a UV detector operating at 260 nm.

Nuclear Magnetic Resonance(NMR)

^{1}H NMR spectroscopy was performed on a Bruker DPX 400 operating a magnetic field strength of 9.395 T and using deuterated chloroform as the solvent at room temperature. Win-NMR (Bruker) program was used to work on the spectra.

Relaxation measurements

The spin-lattice or longitudinal relaxation time (T_1) of the gadolinium polymer latexes was measured on a Bruker DPX 400 spectrometer, operating a magnetic field strength of 9.395 T. All *T*1 relaxation measurements were recorded with the combination of standard inversion-

recovery technique and magic angle spinning (MAS) technique. The latexes were sealed in 5 ml glass tube. The inversion-recovery pulse programme can be written as $(d_1\text{-}180°_x\text{-}d_2\text{-}90_x\text{-FID})_n$. The observed transverse relaxation rates were calculated from either the intensity at half height or the area under the peak.

Preparative Ultracentrifugation

The preparative ultracentrifugation was used to obtain information about the encapsulation distribution. A drop of the final dispersion consisting of inorganic/polymer particles was added to a tube containing sucrose density gradients ranging between 1.00 to 1.30 $g \cdot cm^{-3}$ and centrifugated at 4 °C for 120 min at 37,000 rpm in a Beckmann L-70 centrifuge.

Thermogravimetric Analysis (TGA)

The magnetite or iron oxide content of the dried samples was measured by thermogravimetry. The thermogravimetric analysis (TGA) measurements were performed with a Netzsch-Gerätebau TG 209 under nitrogen atmosphere at 20 $ml \cdot min^{-1}$. The temperature range is between 30 and 900 °C with a heating rate of 20 $K \cdot min^{-1}$.

Transmission Electron Microscopy (TEM)

The samples were characterized by a Zeiss 912 Omega Electron Microscope operating at 120 kV. The samples were diluted and mounted on carbon coated copper grids.

Vibrating Sample Magnetometer (VSM)

The magnetic properties of the particles were determinated by a PAR (Princeton Applied Research) vibrating sample magnetometer (H_{max} =1200 $kA \cdot m^{-1}$).

Small Angle X-ray (SAXS)

SAXS patterns were recorded employing a Kratky camera or using a rotating anode with pinhole collimation. A Nonius rotating anode (P = 4 kW, CuK_α) and an image-plate detector system was used.

Wide Angle X-ray (WAXS)

WAXS diffraction was measured with a Nonius CP-120 diffractometer using a Cu-K_α radiation (λ = 0.154 nm) on the dried samples at room temperature.

Fourier Transform Infrared (FTIR) spectroscopy

For infrared measurements a BIORAD 6000 FTIR spectrometer was used. A Golden Gate arrangement, single reflection diamond ATR, was used for the measurements of the liquid samples.

8 References

[1] A. Kross, *Geschichte des Magnetismus*, vde- verlag, Berlin 1994.

[2] R. Blakemore, *Science* **1975**, *190*, 377-379.

[3] J. L. Gould, J. L. Kirschvink, K. S. Deffeyes, *Science* **1978**, *201*, 1026-1028.

[4] C. Walcott, R.P. Green, *Science* **1974**, *184*, 180-182.

[5] M. M. Walker, J. L. Kirschvink, S.-B. R. Chang, A. E. Dizon, *Science* **1984**, *224*, 751-753.

[6] J. L. Kirschvink, A. Kobayashi-Kirschvink, B. J. Woodford, *Proc. Natl. Acd. Sci. USA* **1992**, *89*, 7683-7687.

[7] http://www.iupac.org/reports/2001/colloid_2001/manual_of_s_and_t.pdf

[8] [a] K. Landfester, *Miniemulsions for polymerizations processes and materials science*, Habilitationsschrift, Universitat Potsdam, 2002; [b] K. Landfester, *Macromol. Rapid. Comm.* **2001**, *22*, 896-936.

[9] M. Antonietti, K. Landfester, *Prog. Polym. Sci.* **2002**, *27*, 689-757.

[10] P. Tartaj, M. Morales, S. Veintemillas-Verdaguer, T. González-Carreno, C. J. Serna, *J. Phys. D: Appl. Phys*. **2003**, *36*, R182-R197.

[11] C. C. Berry, A. S. G. Curtis, *J. Phys. D: Appl. Phys*. **2003**, *36*, R198-R206.

[12] J. V. Dawkins, *Aqueous Suspension Polymerization* in *Comprehensive Polymer Science*, Ed. Allen, Bevington, Pergamon Press, Oxford, 1989, 231-241.

[13] Y. J. Chou, M.S. El-Aasser, J.W. Vanderhoff, *J. Dispers. Sci. Technol.* **1980**, *1*, 129-150.

[14] H. Köhler, *Geofysiske Publikasjoner* **1922**, *2*, 3-15.

[15] W. I. Higuchi, J. Misra, *J. Pharmaceutical Sci* **1962**, *51*, 459-466.

[16] A. J. Webster, M. E. Cates, Langmuir **1998**, *14*, 2068-2079.

[17] I. M. Lifshitz, V. V. Slyozov. *Phys. Chem. Solids* **1961**, *19*, 35-50.

[18] A. S. Kalbalnov, A. V. Pertzov, E. D. Shchukin, *J. Colloid Intef. Sci*. **1987**, *118*, 590-597.

[19] M. Postel, J. G. Riess, J. G. Weers, *Artif. Cells, Blood Substitutes, Immobilization Biotechnol*. **1994**, *22*, 991-1005.

[20] K. C. Lowe, Artif. Cells, Blood Substitutes, Immobilization Biotechnol. **2000**, 28, 25-38.

[21] S. S. Davis, H. P. Round, T. S. Purewal *J. Colloid Interf. Sci.* **1981**, *80*, 508-511.

[22] B. Abismail, J. P. Canselier, A. M. Wilhelm, H. Delmas, C. Gourdon, *Ultrason. Sonochem*. **1999**, *6*, 75-83.

[23] P. Walstra, *Chem. Eng. Sci.* **1993**, *48*, 333-349.

[24] S. E. Friberg, S. Jones, in: Kirk-Othmer, *Encyclopedia of Chemical Technology*, 4 ed., J. I. Kroschwitz, Ed., Wiley, New York 1994, Vol. 9, pp. 393-413.

[25] R. W. Wood, A. L. Loomis, *Phil. Mag*. **1927**, *4*, 417-433.

[26] V. I. Sorokin, *Soviet Phys./Acoust.* **1957**, *3*, 281-291.

[27] M. K. Li, H. S. Fogler, *J. Fluid Mech*. **1978**, *88*, 499-511.

[28] M. K. Li, H. S. Fogler, *J. Fluid Mech.* **1978**, *88*, 513-528.

[29] K. S. Suslick, *Science* **1990**, *247*, 1439-1445.

[30] W. Lauterborn, *Ultrason. Sonochem.* **1997**, *4*, 65-75.

[31] O. Behrend, K. Ax, H. Schubert, *Ultrason. Sonochem.* **2000**, *7*, 77-85.

[32] K. Fontenot, F. J. Schork, *Ind. Eng. Chem. Res.* **1993**, *32*, 373-385.

[33] K. Landfester, N. Bechthold, F. Tiarks, M. Antonietti, *Macromolecules* **1999**, *32*, 5222-5228.

[34] Y. J. Chou, M. S. El-Aasser, J. W. Vanderhoff, *J. Dispers. Sci. Technol.* **1980**, *1*, 129-150.

[35] A. R. M. Azad, J. Ugelstad, R. M. Fitch, F. K. Hansen In *Emulsion Polymerization*; I. Piirma, Gardon, J.L., Ed.; ACS: Washington, D.C., 1976; Vol. 24, pp 1-23.

[36] K. Landfester, N. Bechthold, F. Tiarks, M. Antonietti, *Macromolecules* **1999**, *32*, 2679-2683.

[37] S. Lang, Curr. Opin. Colloid Interface Sci. **2002**, 7, 12-20.

[38] I. M. Banat, R. S. Makkar, S. S. Cameotra, *Appl. Microbiol. Biotechnol.* **2000**, *53*, 495-508.

[39] J. L. Reimers, F. J. Schork, *Ind. Eng. Chem. Res.* **1997**, *36*, 1085-1087.

[40] J. Ugelstad, M. S. EL Aasser, J. W. Vanderhoff, *J. Polym. Sci. , Polym. Lett. Ed.* **1973**, *11*, 503-513.

[41] J. Ugelstad, F. K. Hansen, S. Lange, *Makromol. Chem.* **1974**, *175*, 507-521.

[42] K. Landfester, N. Bechthold, S. Förster, M. Antonietti, *Macromol. Rapid Comm.* **1999**, *20*, 81-84.

[43] N. Bechthold, F. Tiarks, M. Willert, K. Landfester, M. Antonietti, *Macromol. Symp.* **2000**, *151*, 549-555.

[44] B. Erdem, E. D. Sudol, V. L. Dimonie, M.S. El-Aasser. *Macromol. Symp*. **2000**, *155*, 181-198.

[45] F. Tiarks, K. Landfester, M. Antonietti, *Macromol. Chem. Phys.* **2001**, *202*, 51-60.

[46] B. D. Cullity, *Introduction to Magnetic Materials*, Adisson-Wesley, reading, 1972.

[47] R. W. Chantrell, J. Popplewell, S.W. Charles, *IEEE T Magn.* **1978**, *Mag-14*, 975-977.

[48] S. S. Papell, US Patent No. 3215572 (1965).

[49] G. W. Reimers, S. E. Khalafalla, US Patent No. 3843540 (1976).

[50] J. R. Kelley, U.S. Patent No. 4019994 (1977).

[51] J. Shimoiizaka, K. Nakatsuka, T. Fujita, A. Kounosu, *Fine particles Processing, Proceedings of the international symposium on fine particles processing*, P. Somasundaran (ed.), 2nd vol., New York (1980).

[52] R. S. Molday, US Patent No. 4452773 (1984).

[53] A. Rembaum, U. S. Patent No. 4267234 (1981).

[54] J. Lee, T. Isobe, M. Senna, *Colloid Surface A* **1996**, *109*, 121-127.

[55] M. Suzuki, M. Shinkai, M. Kamihira, T. Kobayashi, *Biotechnol. Appl. Bioc*. **1995**, *21*, 335-345.

[56] I. Dumazet-Bonnamour, I., P. Le Perchec, *Colloid Surface A* **2000**, *173*, 61-71.

[57] V. Veiga, D.H. Ryan, E. Sourty, F. Llanes, R.H. Marchessault, *Carbohyd. Polym.* **2000**, *42*, 353-357.

[58] F. Sauzedde, A. Elaïssari, C. Pichot, *Colloid Polym. Sci.* **1999**, *277*, 846-855.

[59] V. S. Zaitsev, D. S. Filimonov, I. A. Presnyakov, R. J. Gambino, B. Chu, *J. Colloid Interf. Sci.* **1999**, *212*, 49-57.

[60] P. A. Dresco, V.S. Zaitsev, R.J. Gambino, B. Chu, *Langmuir* **1999**, *15*, 1945-1951.

[61] J. -C. Daniel, J.-L. Schuppiser, M. Tricot, U. S. Patent No. 4358388 (1982).

[62] D. Charmot, C. Vidil, U. S. Patent No. 5356713 (1994).

[63] [a] US Patent No. 4,654,267 (1987), invs.: J. Ugelstad, T.Ellingsen, A. Berge, O. B. Helgee; [b] J. Ugelstad, A. Berge, T. Ellingsen, R. Schmid, T.-N. Nilsen, P. C. Mørk, P. Stenstad, E. Hornes, Ø. Olsvik, *Prog. Polym. Sci.* **1992**, *17*, 87-161; [c] J. Ugelstad, P.

Stenstad, L. Kilaas, W. S. Prestvik, R. Herje, A. Berge, E. Hornes, *Blood Purif*. **1993**, *11*, 349-369.

[64] K. Wormuth, *J. Colloid Interf. Sci.* **2001**, *241*, 366-377.

[65] K. Landfester, M. Willert, M. Antonietti, *Macromolecules* **2000**, *33*, 2370-2376.

[66] D. Hoffmann, K. Landfester, M. Antonietti, *Magnetohydrodynamics* **2001**, *37*, 217-221.

[67] J. Roger, J. N. Pons, R. Massart, A. Halbreich, J. C. Bacri, *Eur. Phys. J. – Appl. Phys.* **1999**, *5*, 321-325.

[68] C. Bergemann, D. Müller-Schulte, J. Oster, L.A. Brassard, A.S. Lübbe, *J. Magn. Magn. Mater.* **1999**, *194*, 45-52.

[69] A. S. Lübbe, C. Bergemann, W. Huhnt, T. Fricke, H. Riess, J.W. Brock, D. Huhn, *Cancer Res.* **1996**, *56*, 4694-4701.

[70] E. Viroonchatapan, M. Ueno, H. Sato, I. Adachi, H. Nagae, K. Tazawa, I. Horikoshi, *Pharmaceut. Res.* **1995**, *12*, 1176-1182.

[71] J. Dobson, A. Keramane, A. J. El Haj, *European Cells and Materials* **2002**, *4*, 42-44.

[72] D. K. Kim, Y. Zhang, W. Voit, K. V. Rao, J. Kehr, B. Bjelke, M. Muhammed, *Scripta Mater.* **2001**, *44*, 1713-1717.

[73] M. Mitsumori, M. Hiraoka, T. Shibata, Y. Okuno, Y. Nagata, Y. Nishimura, M. Abe, M. Hasegawa, H. Nagae and Y. Ebisawa. *Hepato-gastroenterol.* **1996**, *43*,1431-1437.

[74] K. Raj, B. Moskowitz, R. Casciari, *J. Magn. Magn. Mater.* **1995**, *149*, 174-180.

[75] M. Zahn, *J. Nanopart. Res.* **2001**, *3*, 73-78.

[76] A. Nethe, T. Scholz, H.-D. Stahlman, *Magnetohydrodynamics* **2001**, *3*, 312-317.

[77] C. Abel-Keilhack, J. Hesselbach, *J. Appl. Phys.* **2003**, *93*, 8441-8443.

[78] Ch. Alexiou, A. Schmidt, R. J. Klein, P. Hulin, Ch. Bergemann, W. Arnold, *J. Magn. Magn. Mater.* **2002**, *252*, 363-366.

[79] A. Jordan, R. Scholz, P. Wust, H. Fähling, R. Felix, *J. Magn. Magn. Mater.* **1999**; *201*, 413-419.

[80] R. Hiergeist, W. Andra, N. Buske, R. Hergt, I. Hilger, U. Richter, W. Kaiser, *J. Magn. Magn. Mater.* **1999**, *201*, 420-422.

[81] M. Mitsumori, M. Hiraoka, T. Shibata, Y. Okuno, Y. Nagata, Y. Nishimura, M. Abe, M. Hasegawa, H. Nagae, Y. Ebisawa, *Hepato-gastroenterol.* **1996**, *43*,1431-1437.

[82] J. M. Singer, NATO ASI Series E, No. 138, M. S. El- Aasser and R.M. Fitch (Eds.), p. 371, N. Nijhoff Publ., Dordrecht, The Netherlands (1987).

[83] C. Petit, A. Taleb, M.P. Pileni, *J. Phys. Chem. B* **1999,** *103*, 1805-1810.

[84] C. Petit, A. Taleb, M. P. Pileni, *Adv. Mater.***1998**, *10*, 259-261.

[85] D. P. Dinega, M. G. Bawendi, *Angew. Chem. Int. Ed. Engl*. **1999**, *38*, 1788-1791.

[86] Ullmann's encyclopedia of industrial chemistry, Wiley, 2003 http://www.mrw.interscience.wiley.com/ueic/articles/a18_215/frame.html#

[87] T. W. Smith, D. Wychick, *J. Phys. Chem.* **1980**, *84,* 1621-1629.

[88] K. S. Suslick, M. Fang, T. Hyeon*, J. Am. Chem. Soc.* **1996**, *118*, 11960-11961.

[89] V. F. Puntes, K.M. Krishnan, P. Alivisatos, *Appl. Phys. Lett.* **2001**, *78,* 2187-2189.

[90] K.S. Suslick, S-B. Choe, A.A. Cichowlas, M. W. Grinstaff, *Nature* **1991**, *353,* 414-416.

[91] Y. Koltypin, G. Kataby, X. Cao, R. Prozorov, A. Gedanken, *J. Non-Cryst. Solids* **1996**, *201*, 159-162.

[92] G. Kataby, A. Ulman, R. Prozorov, A. Gedanken, *Langmuir* **1998**, *14,* 1512-1515.

[93] C. H. Griffiths, M. P. O'Horo, T. W. Smith, *J. Appl. Phys*. **1979**, *50*, 7108-7115.

[94] N. A. D. Burke, H. D. H. Stöver, F. P. Dawso, J. D. Lavers, P. K. Jain, H. Oka, *IEEE Trans. Magn.* **2001**, *37*, 2660-2662.

[95] C. Pathmamanoharan, N. L. Zuiverloon, A. P. Philipse, *Prog. Colloid Polym. Sci.* **2000**, *115*, 141-145.

[96] T. Hyeon, S. S. Lee, J. Park, Y. Chung, H. B. Na, *J. Am. Chem. Soc.* **2001**, *123*, 12798-12801.

[97] R. Tannenbaum, S. Reich, C. L. Flenniken, E. P. Goldberg, *Adv. Mater.* **2002**, *14*, 1402-1405.

[98] A. F. Cockerill, G. L. O. Davies, R.C: Harden, D. M. Rackham, *Chem. Rev.* **1973**, *73*, 553-588.

[99] P. Caravan, J. J. Ellison, T. J. McMurry, R. B. Lauffer *Chem. Rew*, **1999**, *99*, 2293-2352.

[100] G. De Stasio, P. Casalbore, R. Pallini et al. *Cancer Res.* **2001**, *61*, 4272-4277.

[101] D. H. Carr, J. Brown, G. M. Bydder, R. E. Steiner, H.-J. Weinmann, U. Speck, A. S. Hall, I. R. Young, *Am. J. Roentgenol.* **1984**, *143*, 215-224.

[102] K. Micskei, L. Helm, E. Brücher, A. E. Meherbach, *Inorg. Chem.* **1993**, *32*, 3844-3850.

[103] D. L. Ladd, R. Holisster, X. Peng, et. al., *Bioconjugate Chem.* **1999**, *10*, 361-370.

[104] P. Ronved, B. Lindberg, J. Klaveness, *Carbohyd. Res.* **1991**, *214*, 325-330.

[105] F. E. Armitage, D.E. Richardson, K.C.P. Li, *Bioconjugate Chem.* **1990**, *1*, 365-374.

[106] D. Meyer, M. Schaeffer, A. Bouillot, S. Beauté, C. Chambom, *Invest. Radiol.* **1991**, 25, s50-s52.

[107] H. Tokumitsu, H. Ichikawa, T.K. Saha, Y. Fukumori, L. H. Block., S. T. P. *Pharma Sciences* **2000**, *10*, 39-49.

[108] U. Schmiedl, M. Ogan, H. Paajanen, M. Marotti, L. E. Crooks, A. C. Brito, R. C. Brasch *Radiology* **1987**, *162*, 205-210.

[109] L. Lattuada, G.Lux, *Tetrahedron Lett.* **2003,** *44*, 3893-3895.

[110] R. C. Brasch, Y. Berthezene, V.S Vexler, M. Moseley, O. Clément, A. Muehler, D. Price, H. Jeome, *Invest. Radiol*. **1991**, 26, s42-s45

[111] F. Cavagna, C. Luchinat, A. Scozzafava, Z. Xia, *Magnet. Reson. Med.* **1994**, *31*, 58-60.

[112] E. C. Wiener, M.W. Brechbiel, H. Brothers, R.L. Magin, O. A. Gansow, D. A. Tomalia, P. C. Lauterbur, *Magnet. Reson. Med.* **1994**, *31*, 1-8.

[113] D. Roberts, W.L. Zhu, C. M. Frommen, Z. Rosenzweig, *J. Appl. Phys*. **2000**, *87*, 6208-6210.

[114] J. Guo, X. Jiang, C-Z Yang, *J., Appl. Polm. Sci.* **2003**, *87*,1358-1364.

[115] K-C. Yu, H-B Hu, M-L Liu, H-Z Yuan, C-H Ye, R-X Zhuo, *Chinese J. Polym. Sc.* **1999**, *17*, 471-475.

[116] E. Tóth, F Connac, L. Helm, K. Adzamli, A.E. Merbach, *J Biol. Inorg. Chem.* **1998**, *3*, 606-613.

[117] K. M. Johnson, L.Z. Tao, R.P. Kennan, J. C. Gore, *Magnet. Reson. Med.* **1998**, *40*, 133-142.

[118] J. H. Braybrook, D. H. Laurance, *Polym. Inter.* **1991**, *26*, 251-259.

[119] C. H. Reynolds, N. Annan, K. Beshah, J.H. Huber, S.H. Shaber, R.R. Lenkiski,J. A. Wortman, *J. Am. Chem. Soc.* **2000**, *122*, 8940-8945.

[120] M. Miyamoto, K. Hirano, H. Ichikawa, Y. Fukumori, Y. Akine, K. Tokuuye, *Chem. Pharm. Bull.* **1999**, *47*, 203-208.

[121] H. Tournier, R. Hyacinthe, M. Schneider, *Acad. Radiol.* **2002**, *9 (suppl 1)*:s20-s28.

[122] J. H. Schattka, *Synthese pöroser Metalloxidstrukturen durch Template Nanocoating*, Dissertation, Universität Potsdam, 2002.

[123] E. P. Giannelis, R. Krishnamoorti, E. Manias, *Adv. Polym. Sci.* **1999**, *38*, 107-147.

[124] P. Caravan, J. J. Ellison, T. J. McMurry , R.B. Lauffer, *Chem. Rev.* **1999**, *99*, 2293-2352.

[125] T. L. James, *Nuclear magnetic resonance in biochemistry*, Academic Press, Inc., New York, 1975.

[126] D. D. Stark and W.G. Bradley *Magnetic resonance imaging*, The C.V. Mosby Company, Missouri, 1988.

[127] F. Bloch, W.W. Hansen, P. Packard, *Physiol. Rev.* **1946**, *70*, 474-485.

[128] I. Solomon, *Physiol. Rev.* **1955**, *99*, 559-565.

[129] N. Bloembergen, *J. Chem. Phys.* **1957**, *27*, 572-573.

[130] R. B. Lauffer*, Chem. Rev.* **1987**, *87*, 901-927.

[131] D. Chescoe, P. J. Goodhew, *The operation of transmission and scanning electron microscopes*, Oxford University Press, New York, 1990.

[132] S. P. Spragg, J. Steensgaard, Theoretical aspects of practical centrifugation. In Preparative centrifugation. A practical Approach, (Ed. D. Rickwood), Oxford University, New York, 1992.

[133] US patent 845,903, Improvements relating to the polymerization of olefins.

[134] K. Rupp, K. Handreke, G. Schuhmann-Giampieri, *Invest. Radio*. **2002**, *37*, 241-247.

[135] J. F. W. Nijsen, M. J. van Steenbergern, H. Kooijman, H. Talsma, L. M. J. Kroon-Batenburg, M. van de Weert, P. P. van Rijk, A. de Witte, A. D. V. Schip, *Biomaterials* **2001**, *22*, 3073.

Acknowledgments

This thesis was carried out from October 2001 to February 2004 in the Max Planck Institute of Colloids and Interfaces in Golm, with the financial support of the Deutsche Forschungsgemeinschaft and Max Planck Society.

I would like to express my enormous gratitude to my two supervisors: Prof. Dr. Markus Antonietti, for giving me the opportunity to work in the colloid department with its unique research infrastructure, for his open-mind scientific ideas and his encouragement, and to Prof. Dr. Katharina Landfester for her constant readiness to assist me with helpful discussions and her continuous interest in my work. I have learned a great deal from you.

My warmest thanks go to Regina Rothe for her being present and accessible at all times and for helping me with the preparation of my talks in German.

Furthermore, I am deeply indebted to Dr. Hartmann and Rona Pietschke for introducing me in the Transmission Electron Microscopy which allowed me to observe by myself the amazing nanoworld.

My sincere gratitude also goes to Dr. Robert Müller of the Institute for Physical High Technology in Jena for the magnetization measurements and training.

I would like to thank Dr. habil. Klaus Tauer for providing assistance with the FTIR measurements and Dr. habil. Helmut Cölfen for teaching me the Cerius molecular modeling software.

I still want to thank Dr. Oychai Tongcher for the kind cooperation in the relaxation part of this thesis.

I would like to thank all the technicians of the department, in particular Ingrid Zenke for all WAXS and SAXS measurements, Antje Völkel for the preparative ultracentrifugation

measurements, Olaf Niemeyer for the NMR measurements and Marlies Gräwert for the GPC measurements.

I want to thank Samira Nozari for her friendship and moral support.

I would also like to thank the miniemulsion group that I had the chance to know and to share experiences with: Dr. Mirjam Willert, Dr. Emmanuelle Marie, Dr. Matthieu Barrère, Dr. Ufuk Yildiz, Dr. Oychai Tongcher, Dr. Rivelino Montenegro, Andreas Taden, Christian Holze. Thank you for being the excellent colleagues you were.

Finally acknowledgement of my gratitude goes, in particular, to my family in Colombia: Doña Lilia, Don Hernando, Miryam, Lady, Francisco, Albeiro, Sandra, Camilo, Claudia, Franklin, Juan Esteban, Andrés, David and Uriel; and to my family in Germany: Astrid, Andreas, Dirk, Elke, Holger, Dorothèe, Paul Jonas, Timo and Isabelle. Muchas gracias por su valioso apoyo en la distancia.

I am very grateful to my husband, Gunnar Jochen Weimann, who enriches me with his diplomatic personality, and who always supports me with his love. Mijo, te agradezco porque siempre me reconfortas espiritualmente. I would also like to thank you for the final correction of this thesis.

Last but not least, I thank colleagues and friends who contributed of whatever way to the culmination of this thesis. It has been a pleasure to have had the opportunity to immerse myself in such a good research and multicultural environment.